2021

Wave farms and coastal protection on gravel dominated beaches

Rodriguez-Delgado, Cristobal

UNIVERSITY OF
PLYMOUTH

Wave farms and coastal protection on gravel dominated beaches

by

Cristóbal Rodríguez Delgado

A thesis submitted to the University of Plymouth

in partial fulfilment for the degree of

DOCTOR OF PHILOSOPHY

School of Engineering, Computing and Mathematics

September 2021

To my father, thank you for making me the person I am today.

Acknowledgements

First of all, to Irene, who was brave enough to join me in this adventure. Without you, this thesis would not have been possible. Thank you for your support during these three years, especially in the darkest days. Thank you for making Plymouth a home for us.

I would like to acknowledge Prof. Gregorio Iglesias for his trust and also for giving me the opportunity to work with him during this PhD. I am really thankful for his guide, his continuous support and advice, and the moments we have shared in Plymouth.

Thank you also to Dr Dave Simmonds for his support during the final stage of the PhD, whose comments have really improved the quality of this thesis.

Thank you to the COAST research group members for support me in the day-to-day work. I would like to acknowledge especially to Alessandro Antonini for his help with the different numerical models and to Carlos, for his unforgettable welcome to Plymouth, his invaluable help and all the non-work moments we have shared.

And last but not least, I would like to thank my family and friends in Granada. Thank you for supporting me in the distance and for all your love. Thank you all for making easier this significant Step of my life.

AUTHOR'S DECLARATION

At no time during the registration for the degree of Doctor of Philosophy has the author been registered for any other University award without prior agreement of the Doctoral College Quality Sub-Committee.

Work submitted for this research degree at the University of Plymouth has not formed part of any other degree either at the University of Plymouth or at another establishment.

This study was financed with the aid of a studentship from the School of Marine Science and Engineering of the University of Plymouth.

The material presented in this thesis has been published in three journal papers.

Journal Papers:

- Rodriguez-Delgado, C., Bergillos, R.J., Ortega-Sánchez, M., Iglesias, G., 2018. Protection of gravel-dominated coasts through wave farms: Layout and shoreline evolution, Science of The Total Environment 636, 1541-1552.

- Rodriguez-Delgado, C., Bergillos, R.J., Ortega-Sánchez, M., Iglesias, G., 2018. Wave farm effects on the coast: The alongshore position, Science of The Total Environment 640, 1176-1186.

- Rodriguez-Delgado, C., Bergillos, R.J., Iglesias, G., 2019. Dual wave farms and coastline dynamics: The role of inter-device spacing, Science of The Total Environment 646, 1241-1252.

Word count of main body of thesis: 26.062

Signed.....

Date.....September 2021

Abstract

The repercussions produced by the use of fossil fuels, e.g. climate change and sea level rise, have increased attention on the development of renewable energies. The European Commission has adopted the replacement of carbon fuels by renewable energy sources as one of the main objectives for the XXI century. Among these, wave energy is poised to become one of the most important due to the extensive worldwide resource and comparatively low environmental impacts. Although this renewable energy is yet in an early stage of its development and further research is required, the global resource, including the Mediterranean Sea, provides a promising future for wave energy which can enhance the presence of renewable energies in the global energy mix.

However, for wave energy to become a fully fledge carbon-free energy source, the repercussions for nearshore hydro- and morphodynamics must be fully understood prior to undertaking any wave farm installation. In fact, wave farms (i.e. arrays of wave energy converters) have been recently proposed to fulfil a dual function as renewable energy producers and coastal defence elements countering erosion. Although these impacts have been previously studied on sandy beaches, gravel dominated coasts have not been addressed so far. These coasts are common in high latitudes and steep hinterlands and they are growing due to the use of coarse sediments for nourishment works on sandy beaches. They are common in the UK, the Mediterranean coast, Canada, New Zealand and Denmark among other areas.

The research investigates the impacts of wave farms on gravel dominated beaches. To this end, changes produced by the presence of a wave farm on the shoreline evolution of a gravel dominated beach (Playa Granada, southern Spain) have been studied. This beach has suffered erosion problems since the discharge of the Guadalfeo river, the main source of sediments for the beach, was regulated in 2004 by the construction of Rules'

Reservoir. With the construction of this river damn, 85% of the discharge was regulated which altered system's dynamics. Approximately 0.3 hm^3 of sediments have been lost which have produced a maximum retreat of the shoreline of 87 m since the construction of the reservoir. The impact on the wave field of different wave farm scenarios and designs has been studied by means of a third-generation spectral wave propagation model (SWAN). Different parameters of the wave field at the breaking line have been extracted from the results of the wave propagation model. To this end, the fraction of breaking waves in each cell was obtained, and the breaking line was fixed in those cells with a 5% of waves breaking. These results were used to apply a longshore sediment transport (LST) formulation on the study site. Finally, LST rates computed were implemented in a one-line model to address changes on the shoreline position. This model, which is based on the continuity equation, relates the advance (or retreat) of the shoreline to the volume gradient, calculated as the sediment balance by means of LST rates. The selected WEC to form the modelled wave farms was WaveCat, an overtopping-type device, which has shown promising results in terms of coastal protection in recent research. This WEC is formed by two hulls, similar to those found in a catamaran, with a total diameter of D = 90 m.

Wave farm effects on the wave field and shoreline position were assessed by means of several ad hoc indicators, comparing significant wave height, LST rates, shoreline advance and dry beach surface between scenarios with wave farm and the natural (no-wave farm) baseline scenario. These indicators act as a benchmark of the performance of each wave farm scenario with respect the natural situation, allowing to study the impact of the wave farm on each parameter involved in the shoreline evolution. Finally, the dry beach surface difference is obtained as a representation of the overall impact on the whole stretch of beach. More precisely, the effects of the alongshore location, the layout and the inter-device spacing of a wave farm were studied.

Regarding the alongshore position of the wave farm, the results indicate that the wave farm location is a key parameter in terms of coastal protection; indeed, it was found that only three of the eight locations studied generated a weighted increase in dry beach surface with respect to the baseline. The rest of wave farm locations generated loss in dry beach area at the studied stretch of beach with respect to the baseline, thus producing

negative effects in terms of coastal protection. The most advisable location for the wave farm increased the dry beach area in 25.58 m^2 per storm whereas in the worst location 13.17 m^2 are lost. These results show that the alongshore position of a wave farm needs to be carefully selected, as this parameter is able to turn the behaviour of a coast from accretionary to erosionary. In addition, different layouts consisting of a variation in the number of rows of wave energy converters composing the wave farm keeping constant their number are investigated. Results indicate that the best layout is that composed of two rows of WECs. In this case, the increase in dry beach surface with respect to the baseline scenario is 25.94 m^2, whereas the farms with 3 and 4 rows yield a lower increase in beach surface. This shows that the extent of coast covered by the wave farm prevails over the number of rows as the impact of the shadow produced by the wave farm reaches a longer stretch of coast. Finally, four inter-device spacings were modelled. In this case, a lower spacing between devices increases local accretion in the lee of the wave farm but rises erosion elsewhere, whereas a greater spacing counter this erosion but accretion is also reduced. The best results were obtained for a spacing of 2D, where D = 90 m is the space between the two bows of the WaveCat.

As main findings of this thesis, the research carried out in this work shows that the most important parameter in order to achieve the expected results in terms of coastal protection performance of a dual wave farm is the alongshore position. The analysis of the alongshore position effects shows that the location of the wave farm is a key parameter, not only in terms of energy production but also in order to use the wave farm as a coastal management element. Once the alongshore position is fixed, layout and inter-device spacing may help to improve the obtained results. A wave farm with a greater number of rows does not perform better in terms of coastal protection, as the extension of the stretch of coast covered is more relevant. A similar conclusion can be drawn from the inter-device spacing impact study. Wave farms with a lower inter-device spacing produce higher local peaks of accretion in their lee. On the contrary, wave farms with greater spacing reduce this erosion but accretion is also weaker, affecting the dry beach area difference with respect to the baseline. In this case, the wave farms with an intermediate spacing achieve a balance between these two extremes and stand as the best alternatives.

The methodology followed in this work constitutes a useful decision-aid tool which can be applied to other gravel-dominated coasts worldwide. It considers the repercussions for nearshore hydrodynamics and shoreline morphology. The results obtained open up the possibility of using wave farms not only to produce carbon-free energy but also to mitigate coastal erosion problems on coasts across the globe.

Table of contents

List of figures **xix**

List of tables **xxv**

1 Introduction **1**

1.1 Context and motivation 1

1.2 Aims and objectives 4

1.3 Thesis outline 5

2 Literature review **7**

2.1 Wave energy 7

2.1.1 History of wave energy development 7

2.1.2 Description of wave energy converter technologies 9

2.1.3 Wave energy resource 16

2.2 Wave energy transmission of WECs 19

2.3 Wave farm impacts on the wave field 21

2.4 Wave farm impacts on coastal erosion 29

2.5 Longshore sediment transport 30

2.5.1 CERC equation 31

2.5.2 D.L. Inman and R. Bagnold (1963) 31

2.5.3 Kamphuis (1991) 32

2.5.4 Van Rijn (2014) 32

2.5.5 Application of longshore sediment transport formulas to the study site 33

2.6 Novelty of the present thesis with respect the state of the art 34

3 Methodology **37**

3.1 Methodological framework 37

3.2 Wave propagation model 39

3.2.1 Input data 43

3.2.2 Bathymetry 44

3.2.3 Wavecon file 45

3.2.4 Model parameters 45

3.3 Wave farm modelling 47

3.4 Modelled sea-states 49

3.5 LST formulation and one-line modelling 50

3.6 Shoreline state indicators 53

4 Study Site **55**

4.1 Metocean data 56

4.1.1 Wind climate 56

4.1.2 Wave climate 57

4.1.3 Water level 60

4.2 Sediment transport 61

4.3 Site description 61

5 Results **65**

5.1 Introduction 65

5.2 Setting up the modelling tools: baseline results 65

5.2.1 Wave propagation 66

5.2.2 Longshore sediment transport 67

5.2.3 Shoreline evolution 67

5.3 Wave farm position impact study 70

5.3.1 Wave propagation patterns 71

5.3.2 Grid sensitivity 71

5.3.3 Breaking line 74

5.3.4 Wave height at breaking 75

5.3.5 Longshore sediment transport rates 77
5.3.6 Shoreline evolution 78
5.3.7 Dry beach surface 84
5.4 Wave farm layout and coastal defence 86
5.4.1 Wave propagation patterns 88
5.4.2 Breaking line 89
5.4.3 Wave height at breaking 90
5.4.4 Longshore sediment transport 91
5.4.5 Shoreline evolution 94
5.4.6 Dry beach surface 97
5.4.7 Overall performance of the wave farm scenarios 98
5.5 Inter-device spacing interaction with the wave field 100
5.5.1 Wave propagation patterns 100
5.5.2 Longshore sediment transport 104
5.5.3 Shoreline position 106
5.5.4 Dry beach surface 108
5.5.5 Overall performance of the wave farm 110
5.6 Discussion 112

6 Summary and future work **119**
6.1 Conclusions and main findings 119
6.2 Future research lines 123

References **125**

List of figures

2.1 WEC technologies classification (de O. Falcão, 2010). Permission to reproduce this figure has been granted by Elsevier. 10

2.2 OWC chamber and governing parameters (de O. Falcão, 1999).$p_a + p$ is the pressure of the air inside the chamber, m the mass of air contained inside the chamber, w the mass flow rate through the turbine, w_v the mass flow rate through the by-pass valve and ρ and V are respectively the density and the volume of the air inside the chamber. Permission to reproduce this figure has been granted by Elsevier. 11

2.3 Oscillating body WEC scheme (de O. Falcão, 2007). Permission to reproduce this figure has been granted by Elsevier. 13

2.4 Schematic of the WaveCat (Fernandez et al., 2012). Permission to reproduce this figure has been granted by Elsevier. 15

2.5 Variations of transmission coefficient C_t versus B/L for the (a) 10-cm draught, (b) 15-cm draught and (c) 20-cm draught (He and Huang, 2014). Permission to reproduce this figure has been granted by Elsevier. 20

2.6 (a) ΔH_s for the reference sea state ($H_s = 3.3$ m, $T_m = 11$ s, $D = 1$ °), and varying wave energy transmission percentages at the Wave Hub site, (b) $\Delta H_s/H_s$ along the coastline for reference sea state, and varying wave energy transmission percentages at the Wave Hub site (Millar et al., 2007). Results at 10 m contour. Permission to reproduce this figure has been granted by Elsevier 22

2.7 Results along the grid transect at 100 m intervals using the modified SWAN transmission for a narrow and wide PTF (Smith et al., 2012). Lines represents different distances to the wave farm location (1000m, 5000m and 10000m). Permission to reproduce this figure has been granted by Elsevier 24

2.8 Absolute significant wave height difference along the 10 m water depth contour without and with wave farm for the monthly median significant wave height in: a) January, b) July and c) October (Palha et al., 2010). Permission to reproduce this figure has been granted by Elsevier 25

2.9 Wave power pattern in the wave farm region for the winter case studies (H_s = 3.3 m, T_p = 12 s and mean wave direction θ = 307°). Distance to the coast: 6 km (left), 4 km (middle) and 2 km (right) (Iglesias and Carballo, 2014). Permission to reproduce this figure has been granted by Elsevier . 26

2.10 Enlargement of Fig 2.9 showing Wave power detail around the wave farm (Iglesias and Carballo, 2014). Permission to reproduce this figure has been granted by Elsevier 27

2.11 Significant wave height percentage decrease using SNL-SWAN for model runs specifying 50 B-OF type WECs with 6 m spacing on the 40 m depth contour (Chang et al., 2016). Permission to reproduce this figure has been granted by Elsevier 28

3.1 General methodology and workflow 38

3.2 Location and layout of the eight wave farm scenarios. Black dots indicate the centre of the wave farm. The top panel shows the layout of each farm. Rodriguez-Delgado et al. (2018b). 38

3.3 Selected location for the wave farm and definition of the four scenarios of wave farm shape. Rodriguez-Delgado et al. (2018a). 39

3.4 Definition of the four case studies. Rodriguez-Delgado et al. (2019). . . . 40

3.5 Upper left panel: Location of the study site (Guadalfeo delta, southern Spain).Central panel: bathymetric contours, grids used in the wave propagation model, position of the Salobreña Rock, Guadalfeo River mouth, Playa Granada,Punta del Santo, Poniente Beach and Motril Port. Rodriguez-Delgado et al. (2019). 44
3.6 Sketch of wave farm model produced in CAD Software 48
3.7 Reduction of significant wave height due to the presence of WECs 49
3.8 Diagram of one-line model for shoreline evolution. Rodriguez-Delgado et al. (2018b). 52

4.1 (a) Location of the study site (Guadalfeo delta, southern Spain). (b) Plan view of the coast, including bathymetric contours (in meters) and the locations of Salobreña Rock, Guadalfeo River mouth, Punta del Santo and Motril Port. Rodriguez-Delgado et al. (2018b). 55
4.2 Histogram of wind velocity. 56
4.3 Prevailing wind directions at Playa Granada. WindV (m/s), radial axis shows the percentage of wind states coming from each direction. 57
4.4 Histograms of significant wave height (left) and peak period (right). Hourly data from 1958 to 2015. 57
4.5 Prevailing wave directions at Playa Granada. H_s (m), radial axis shows the percentage of sea states coming from each direction. 58
4.6 Monthly boxplot of significant wave height at Playa Granada 59
4.7 Extreme wave climate at Playa Granada: measured data (points), fitted distribution (blue line), confidence intervals (dashed line). 60
4.8 Aerial photographs of the Guadalfeo River Delta before (left) and after (right) river damming. Rodriguez-Delgado et al. (2018a). 62
4.9 Flow discharge downstream of Rules' dam (Bergillos et al., 2016d). Permission to reproduce this figure has been granted by AGU publications. . 62
4.10 Shoreline evolution since the Guadalfeo River damming in 2004. Rodriguez-Delgado et al. (2018b). 63

4.11 Terminal erosion (a) and renourishment works (b) in Playa Granada. Rodriguez-Delgado et al. (2019). 64

5.1 Spectral significant wave height at the study site. Baseline scenario. . . . 66

5.2 (a) Aerial photograph of Playa Granada. (b) Sediment volume transported after 48 h. Baseline scenario. 68

5.3 Vertical coordinate difference between the initial position of the shoreline and the final position after 48 h. Positive (Negative) values mean advance (retreat). 69

5.4 Position sensitivity study workflow. Rodriguez-Delgado et al. (2018b). . . 71

5.5 Variation in significant wave height induced by the presence of the wave farm under westerly (1) and easterly (2) storm waves: (a) scenario 2, (b) scenario 4, (c) scenario 6, (d) scenario 8. The shoreline position is indicated with a white line. Rodriguez-Delgado et al. (2018b). 72

5.6 Grid size comparison. 73

5.7 Significant wave height differences between the greater and smaller grids. Scenario 5. 74

5.8 Water depth at breaking for scenarios 2, 4, 6 and 8 under westerly (a) and easterly (b) storms (1) and low energy (2) conditions. 75

5.9 Non-dimensional wave height reduction under westerly (a) and easterly (b) storm conditions: scenarios 1-4 (2), scenarios 5-8 (3). Rodriguez-Delgado et al. (2018b). 76

5.10 Non-dimensional wave height reduction under westerly (a) and easterly (b) low energy conditions: scenarios 1-4 (2), scenarios 5-8 (3). Rodriguez-Delgado et al. (2018b). 77

5.11 Non-dimensional LST rate reduction under westerly (a) and easterly (b) storm conditions: (2) scenarios 1-4, (3) scenarios 5-8. Rodriguez-Delgado et al. (2018b). 79

5.12 Non-dimensional LST rate reduction under westerly (a) and easterly (b) low energy conditions: (2) scenarios 1-4, (3) scenarios 5-8. Rodriguez-Delgado et al. (2018b). 80

5.13 Non-dimensional shoreline advance under westerly storm conditions. Rodriguez-Delgado et al. (2018b). 81
5.14 Non-dimensional shoreline advance under easterly storm conditions. Rodriguez-Delgado et al. (2018b). 82
5.15 Non-dimensional shoreline advance under westerly low energy conditions. 83
5.16 Non-dimensional shoreline advance under easterly low energy conditions. 83
5.17 Temporal evolution of the dry beach area for westerly (a) and easterly (b) waves under storm (1) and low energy conditions (2). ΔA = difference in beach surface between each scenario and scenario 0 (no-wave farm). Rodriguez-Delgado et al. (2018b). 84
5.18 (a) Weighted values of the non-dimensional wave height reduction (η_w), (b) LST rate reduction (τ_w) and (c) shoreline advance (υ_w). Rodriguez-Delgado et al. (2018b). 87
5.19 Wave farm layout sensitivity study workflow. Rodriguez-Delgado et al. (2018a). 88
5.20 Changes in wave propagation patterns induced by the presence of the wave farm under westerly (a) and easterly (b) storm conditions for scenarios 1, 2, 3 and 4. Rodriguez-Delgado et al. (2018a). 89
5.21 Water depth at breaking under westerly (a) and easterly (b) storms (1) and low energy (2) conditions. 90
5.22 (a1) (b1) Aerial photograph of study site. Non-dimensional wave height reduction (η) for westerly low-energy (a2), easterly low-energy (b2), westerly storm (a3) and eaterly storm (b3) conditions. Rodriguez-Delgado et al. (2018a). 92
5.23 Non-dimensional LST rate reduction (τ). Rodriguez-Delgado et al. (2018a). 93
5.24 Non-dimensional shoreline advance (υ) under low-energy conditions. Rodriguez-Delgado et al. (2018a). 95
5.25 Non-dimensional shoreline advance (υ) under storm conditions. Rodriguez-Delgado et al. (2018a). 96

5.26 Changes in dry beach area between each scenario and the baseline scenario under westerly (a) and easterly (b) low energy (1) and storm (2) conditions. Rodriguez-Delgado et al. (2018a). 97

5.27 Weighted values of the non-dimensional wave height reduction (c), LST rate reduction (d), shoreline advance (e) and dry beach area (f). Rodriguez-Delgado et al. (2018a). 99

5.28 Workflow applied in the inter-device spacing impact study. Rodriguez-Delgado et al. (2019). 101

5.29 Ratio of the significant wave height in each of the wave farm cases (H_s) to the baseline (H_{s0}); from top to bottom, scenarios 1 - 4; westerly (a, left) and easterly (b, right) storm conditions. Rodriguez-Delgado et al. (2019). 102

5.30 Aerial photograph of Playa Granada (a1-b1). Alongshore variation of the non-dimensional significant wave height reduction under westerly (a) and easterly (b), low energy (2) and storm (3) conditions. Rodriguez-Delgado et al. (2019). 103

5.31 Aerial photograph of Playa Granada (a1-b1). Alongshore variation of the non-dimensional LST rate reduction (τ) under westerly (a) and easterly (b), low energy (2) and storm (3) conditions. Rodriguez-Delgado et al. (2019). 105

5.32 Alongshore variation of the non-dimensional shoreline advance, westerly (a) and easterly (b) low energy conditions. Rodriguez-Delgado et al. (2019). 107

5.33 Alongshore variation of the non-dimensional shoreline advance, westerly (a) and easterly (b) storm conditions. Rodriguez-Delgado et al. (2019). . . 108

5.34 Temporal evolution of the dry beach surface difference between each scenario and the baseline for low energy (1), storm (2), westerly (a) and easterly (b) conditions. Rodriguez-Delgado et al. (2019). 109

5.35 (a,b) Aerial photograph of the beach; (c) η_w (weighted value of η); (d) τ_w (weighted value of τ); (e) υ_w (weighted value of υ); and (f) ΔA_w (weighted value of ΔA) in the four scenarios. Rodriguez-Delgado et al. (2019). . . . 111

List of tables

2.1 Reflection (K_r) and transmission (K_t) coefficients of WaveCat device (Fernandez et al., 2012). Permission to reproduce this table has been granted by Elsevier. 20

2.2 $C = V_{mod}/V_{obs}$ Coefficient (Rodriguez-Delgado, 2016) 33

3.1 Values of the modelled deep-water variables [H_{s0} = significant wave height; T_p = peak period; θ = mean wave direction]. Rodriguez-Delgado et al. (2018a). 50

4.1 Significant wave height - peak period bivariate table. 58

4.2 Significant wave height - mean wave direction bivariate table. 59

4.3 Extreme waves at the study site with 90% confidence intervals. 60

4.4 Tide levels at the Motril Port. 61

5.1 Weighted average difference (considering the number of both westerly/easterly and low energy/storm sea states) in dry beach surface for each scenario [m^2]. Rodriguez-Delgado et al. (2018b). 86

5.2 Non-dimensional alongshore-averaged wave height reduction ($\overline{\eta}$) [%]. Rodriguez-Delgado et al. (2018a). 92

5.3 Non-dimensional alongshore-averaged LST rate reduction ($\overline{\tau}$) [%]. Rodriguez-Delgado et al. (2018a). 94

5.4 Non-dimensional alongshore-averaged shoreline advance ($\overline{\upsilon}$ [%].). Rodriguez-Delgado et al. (2018a). 96

5.5 Longshore average of the non-dimensional significant wave height reduction ($\overline{\eta}$) [%]. Rodriguez-Delgado et al. (2019). 104

5.6 Longshore average of the non-dimensional LST rate reduction ($\overline{\tau}$) [%]. Rodriguez-Delgado et al. (2019). 106

5.7 Longshore average of the non-dimensional shoreline advance ($\overline{\upsilon}$) [%]. Rodriguez-Delgado et al. (2019). 108

Chapter 1

Introduction

1.1 Context and motivation

The repercussions of the use of fossil fuels, not least climate change and the subsequent sea level rise, have drawn attention to the development of new renewable, carbon-free energies. Indeed, the undesirable effects of climate change have even forced the European Commission to adopt the replacement of carbon fuels by carbon-free alternatives as one of the main targets for the XXI century (European Commission, 2007). Because of this, in the last decade, the exploitation of renewable energy resources as sustainable alternatives to fossil fuels has received increasing research interest. However, the high cost of carbon-free energy is the main barrier to the development of this kind of technology. This problem is especially remarkable in developing countries, whose CO_2 emissions are an important part of the global pollution (Huenteler et al., 2016; Kung et al., 2017).

Among the different renewable energy sources, marine renewable energy and, more importantly, wave energy are becoming more important thanks to the extensive worldwide resource and high power density, especially in the South Hemisphere where mean wave power above 120 kW/m is achieved (Astariz and Iglesias, 2015; Cornett, 2008). In the North Hemisphere, the greatest values of wave energy resource are located in the North Atlantic and Pacific, where mean wave power values above 80 kW/m can occur. In addition, its comparatively low environmental impacts for both nearshore and offshore areas poise wave energy as one of the most important carbon-free energies in the near future (Clément et al., 2002).

Wave farms, composed of arrays of wave energy converter (WEC) devices, absorb and dissipate a proportion of the incident energy when waves propagate through them, altering the wave patterns and, therefore, the spatial distribution of wave heights (Abanades et al., 2015a; Millar et al., 2007; Veigas et al., 2014). This reduction in wave energy and, consequently, in wave height may lead to a decrease in the coastal erosion in the lee of the wave farm (Abanades et al., 2014a,b; Bergillos et al., 2018a), allowing the use of this technology not only for carbon-free energy production purposes but also as coastal defence elements on eroding beaches. In fact, *Dual wave farms*, i.e., wave farms with the dual purpose of renewable energy production and coastal protection, have been recently proposed (Abanades et al., 2018).

Dual wave farms are a good tool to reduce erosion on coastal systems in which erosion is going to increase due to human intervention and climate change in years to come. One of the areas where dual wave farms may be useful are deltaic coasts, which have been particularly affected by erosion in recent decades. Human interventions in their catchment areas such as reforestation, river damming, discharge regulation and dredging have resulted in a reduction of the sediment flux and, consequently, in shoreline retreat (Anthony et al., 2014; Aragonés et al., 2016; Bergillos et al., 2018b; Brown and Nicholls, 2015; Pagán et al., 2017). Indeed, 85% of the world's deltas have experienced severe flooding in the XXI century, resulting in more than 260,000 km^2 of land temporary submerged (Syvitski et al., 2009). This situation will be exacerbated by future sea-level rise, increasing the area vulnerable to flooding (Payo et al., 2016; Sánchez-Arcilla et al., 2016; Spencer et al., 2016).

Strategies to counter this retreat of the shoreline have traditionally included the so-called "hard engineering" approaches. Coastal structures such as seawalls, jetties or groins have been constructed to reduce erosion in coasts worldwide. The main disadvantage of this approach is that it produces an armoured, artificial seafront which is hardly capable of adapting to changes in the maritime climate and sea-level. Indeed, there are several examples of hard-engineering coastal structures which have failed due to the effects of climate change in recent years. During the storms of winter 2013-2014, the seawall protecting the railway line at Dawlish (SW England) failed which caused the disruption of

the train traffic. Recent research has related this fail with sea-level rise occurred during XX century (Dawson et al., 2016; Kendon, 2015; Sibley et al., 2015). In addition, the recent increase in storminess has also boosted coastal erosion and levels of coastal retreat have reached maximum values in recent years (Castelle et al., 2015; Senechal et al., 2015). Because of this, beach nourishment is also very common nowadays, altering the natural sediment size of beaches and affecting their morphodynamic response and increasing the need of new tools to counter erosion as dual wave farms.

Coastal protection performance of wave farms in sandy beaches has been studied recently. Research performed by Abanades et al. (2014a,b) has shown that wave farms produce a positive effect in beach profile reducing erosion. The results have depicted that wave farms can achieve a similar performance than traditional approaches, reducing erosion up to 50%. They are even capable of changing the modal state of the beach (Abanades et al., 2015b). In this sense, wave farms work similarly to detached breakwaters. Although in these research works the effects produced by the wave farms have been presented as totally positive, the impact on longshore sediment transport should be also taken into account due to the possibility of producing negative effects on adjacent beaches, the same as happens in the case of other traditional approaches.

The high density of the resource, which has been claimed to be the highest among renewable energies (Clément et al., 2002) and availability, with waves generating power 90% of the time (Pelc and Fujita, 2002), along with the high efficiency ratios presented by wave energy converters (between 54% and 85%, (Fernandez-Diez, 2004)) make Wave farms one of the most promising renewable energies. Besides, wave farms present several advantages to counter erosion as they are capable not only of reducing shoreline retreat but also of producing carbon-free energy whereas this synergy cannot be achieved by traditional approaches. Moreover, the floating nature of WECs allows them to adapt naturally to sea-level rise, keeping their coastal protection performance whereas traditional coastal structures effectiveness is reduced with the increment of the water level (Bergillos et al., 2019).

However, the effects of wave farms on sediment transport have been comparatively less studied on gravel-dominated beaches, common in high-latitude coastal regions and on

coasts with steep hinterlands across the world (Bergillos et al., 2017a), and with different morphodynamic behaviour from that of sandy beaches. Gravel dominated beaches present steeper slopes than sandy beaches due to the bigger sediment size that forms the coast (Jennings and Shulmeister, 2002). These steeper slopes produce higher wave reflection and energy dissipation, producing important changes in wave run-up and wave overtopping (McCall et al., 2014). In addition, the wider range of sediment size makes gravel dominated beaches difficult to classify (Kirk, 1980) and present a complex environment where erosion is dominated more by wave run-up than by wave height (Bergillos et al., 2016c). These elements combined result in sediment transport and morphological evolution being more complex than in sandy beaches (Foti and Blondeaux, 1995).

Finally, if wave farms are poised to fulfil this dual function and perform as coastal defence elements, the design process of this kind of project needs to be reformulated. In this sense, the wave farm needs to be designed to achieve a balance between the carbon-free energy production and the control of the erosion on the coast in their lee. More precisely, there is a gap in the literature regarding the influence of key parameters in the design of a wave farm such as the alongshore position and the different aspects of the layout (number of rows and inter-device spacing). An integrated methodology based on existing formulations and numerical models would be a useful tool for designers and stakeholders in order to optimise the performance of wave farms for coastal protection. This thesis contributes to these gaps in the literature, increasing the knowledge on the positive impacts of wave farms on eroded beaches. This may be a key factor in the development of wave energy, increasing its economic competitiveness incorporating these externalities and enhancing the presence of wave energy in the global energy mix.

1.2 Aims and objectives

The global objective of this research is to study the impacts of wave farms on the shoreline evolution and dry beach area of gravel dominated beaches and explore the potential benefits for combined energy production and coastal protection. To this end, combination of different numerical models, including a third-generation spectral wave propagation model and a shoreline evolution (one-line) model, and longitudinal sediment transport (LST)

formulations are applied to diverse scenarios in a case study: Playa Granada (Southern Iberian Peninsula).

The following specific objectives were developed in the research process of this thesis:

I. To study the influence of the alongshore position of the wave farm on the shoreline evolution during storms.

II. To explore the impact of the layout and, specifically, the number of rows composing the wave farm on the control of the erosion in beaches situated in its lee.

III. To characterise the effects of the inter-device spacing in the changes produced on the dry beach area.

1.3 Thesis outline

The structure of this thesis is as follows. Chapter 2 details the current development of wave energy and the main research on wave farm impacts. Chapter 3 explains the methodology applied to achieve the objectives of this thesis. A detailed description of the case study selected (Playa Granada, Southern Iberian Peninsula), including morphology and wave climate is presented in Chapter 4. Chapter 5 presents the main results obtained in this thesis including: (i) a position sensitivity study of the role of the longshore position of the wave farm on the nearshore wave propagation patterns under both storm and low-energy conditions, the resulting changes in the longshore sediment transport (LST) trends and the consequences for the shoreline evolution and therefore, the dry beach area, (ii) the characterisation of the role of the wave farm layout on coastal protection, and (iii) the influence of the inter-device spacing. To this end, 16 scenarios corresponding to wave farms with different alongshore position (8 scenarios), layouts (4 scenarios) and inter-device spacing (4 scenarios) were defined and the changes produced in the dry beach area with respect to the baseline (natural) scenario were obtained. Finally, the main conclusions drawn and the description of future lines of research are presented in Chapter 6.

Chapter 2

Literature review

2.1 Wave energy

The global objective of this thesis is focused on exploring the potential benefits and synergies for combined energy production and coastal protection. In this section, as an introduction to this topic, the basic concepts of wave energy are presented. To do so, first, a brief history of WEC development is presented. Second, a description of the currently developed technologies along with the research conducted so far will be depicted. And finally, the global energy resource is characterised, in order to illustrate the potential of wave energy to increase renewable energy in the global energy mix.

2.1.1 History of wave energy development

The energy shown by the sea has always raised fascination and research interest. Especially after storms, the power of waves has been observed by the damage produced on coastal structures and also by the changes experienced by the geometry of the coast (shoreline and beach profile). The first patent of a wave energy converter (WEC) is dated from 1799, by Messrs Girard (Ross, 1995). Since then, thousands of WECs have been patented even when the technology is in an early stage of development due to the fact that the energy extracted from the motion of the waves can be harnessed in a number of ways, which will be explained in the next section. Although the first patent appeared in the 18th century,

the first oscillating water column buoys were commercialised in Japan during the 1960s (Clément et al., 2002).

Modern research on wave energy exploitation began in the 1970s (Salter, 1974), when the first concepts of WECs appeared (Clare et al., 1982; Moody, 1979; Platts, 1979). During this decade, the British government developed a research and development (R&D) programme focused on wave energy. This programme consisted in the funding of a number of projects for WEC development with the objective to develop a wave energy plant which was able to produce 2000 MW of power. As the objective of the program was too ambitious, the majority of these projects failed. Despite this fact, during the early 1980s the British government systematically funded R&D projects related to wave energy, but finally it was concluded that wave energy was too expensive even with the improvements in the technology (Davies et al., 1985; Thorpe, 1992) and British program came to an end (Cruz, 2008). Among others, the reasons which led to the failure of these WECs were (Kerr, 2007): (a) the low energetic performance of the devices, (b) the great electrical losses and (c) the lack of studies about the wave energy resource, which led to install WECs in areas with high waves but far from the main distribution grid.

Due to the oil crisis the interest in developing renewable energy sources to avoid dependency on carbon energy sources emerged. However, when the crisis had passed, this research interest decreased (Miller, 2004). After that, public funding decreased and the activities around wave energy just remained at academic level. During the 1980s, smaller devices were developed trying to decrease the economic cost of WECs (Whittaker et al., 1995) and this was particularly the case in Norway, where a number of devices where designed and tested (Malmo and Reitan, 1986). This changed drastically in 1991 when the European Commission included wave energy in its R&D programme on renewable energy (de O. Falcão, 2010). From 1992 until now, a number of projects have been funded by the European Union leading to the establishment of a number of research teams focused on wave energy across Europe. Recently, the challenges derived from climate change have highlighted the need to avoid dependency on fossil fuels and to promote an energetic future based on renewable sources. Then, in this context, R&D in wave energy has reached currently its maximum level.

Therefore, in 2000 the LIMPET was deployed in Islay, Scotland and it became in the first wave farm to be commissioned and connected to the UK electrical grid. During 2000s, the Pelamis device were extensively developed using modern tool such as numerical modelling and laboratory tests. From 2004 to 2007, prototype testing at the European Marine Energy Centre (EMEC) in Scotland was carried out. After this testing, the first operating wave farm in Portugal (Aguçadoura) was installed, although it was decommissioned two months after the opening due to technical problems. After that, different wave farms have been installed across Europe in Spain (Mutriku Breakwater Wave Plant), Israel (SDE Sea Waves Power Plant) and UK (Orkney Wave Power Station and Siadar Wave Power Station). However, these developments have not come without failures (Charlier et al., 2010; Torre-Enciso et al., 2010). For that reason, (Weber, 2012) defined technology readiness according to a performance matrix in order to improve the reliability of wave energy development.

2.1.2 Description of wave energy converter technologies

The main aim of this thesis is to study the impact of wave farms on the shoreline evolution and dry beach area of gravel dominated beaches. A classification of the different WEC technologies developed so far is depicted in Figure 2.1. In this section, these devices are described including their principle of operation and main findings in their research, in order to justify the selection of a WEC to study the impact on the longshore sediment transport and shoreline position.

Oscillating Water Column

Oscillating water columns (OWC) are one of the most successful wave energy technologies so far, in fact some OWC devices have successfully reached full scale phase (Boake et al., 2002; Pecher et al., 2011). This WEC consists of a chamber, partially filled by air, open to the wave action (Fig. 2.2). When the waves reach the chamber, the water inside oscillates and the air is forced to pass through a bi-directional air turbine which turns the energy transmitted to the air into electrical energy (Greaves and Iglesias, 2018).

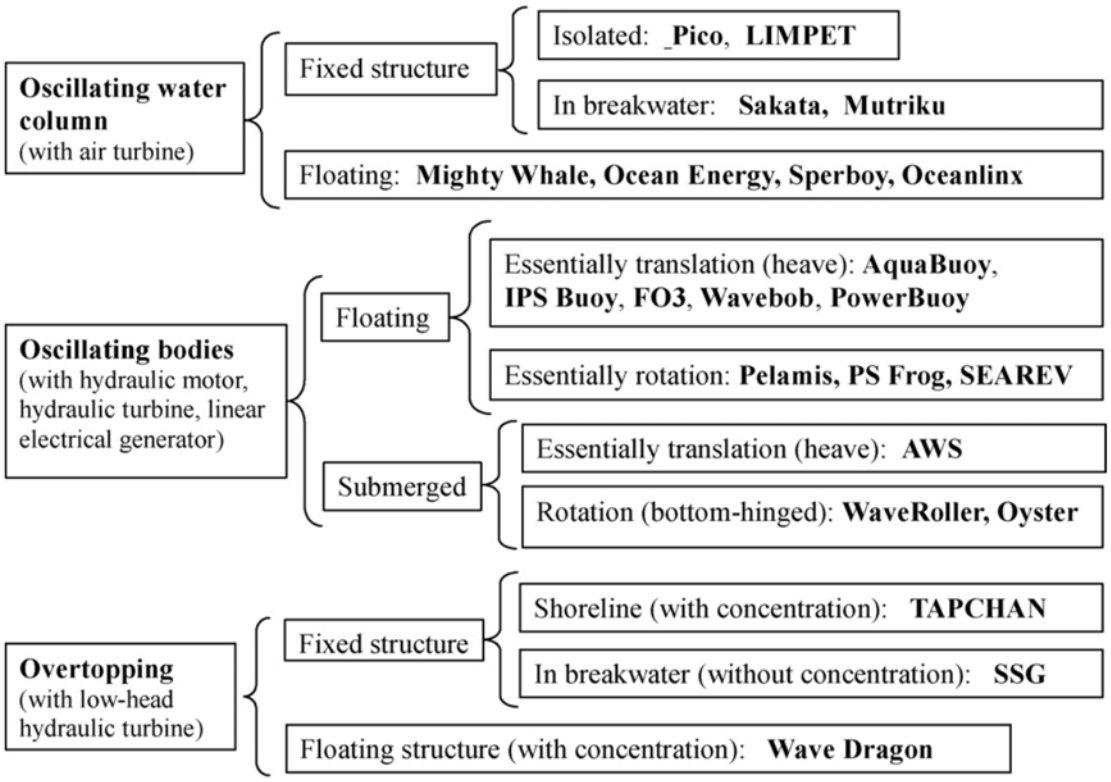

Fig. 2.1 WEC technologies classification (de O. Falcão, 2010). Permission to reproduce this figure has been granted by Elsevier.

OWC technology has attracted extensive research interest in recent years, most of it focused on the characteristics of the chamber (Viviano et al., 2016) or the turbine (Medina-López et al., 2017; Moñino et al., 2017), where Wells is the most popular type (Raghunathan, 1995). However, one of the most important aspects in the design of an OWC is the turbine-chamber interaction. López et al. (2018, 2015a,b) studied the influence of turbine damping and tidal variability through experimental campaigns, numerical models (López et al., 2014) and artificial intelligence (López and Iglesias, 2014).

One of the advantages of OWCs is that they can be integrated into breakwater structures (Boccotti, 2003; Torre-Enciso et al., 2010). There is also OWC WECs developed to be installed offshore. This kind of devices are normally floating freely so the movements of pitch and heave have to be taken into account in order to assess the performance. The first floating OWC devices were developed by Masuda and commercialised in Japan in 1965 (Mas, 1990). During the period 1985-1990 bottom standing OWCs were built (Graw, 1996). The first theoretical model of a floating OWC device was developed by McCormick (1974). Recently, a 1:4 scale model of a buoy converter (Ocean Energy) was deployed in Galway (Rourke et al., 2009). Another recent developed device is the Sparbuoy (de O. Falcão

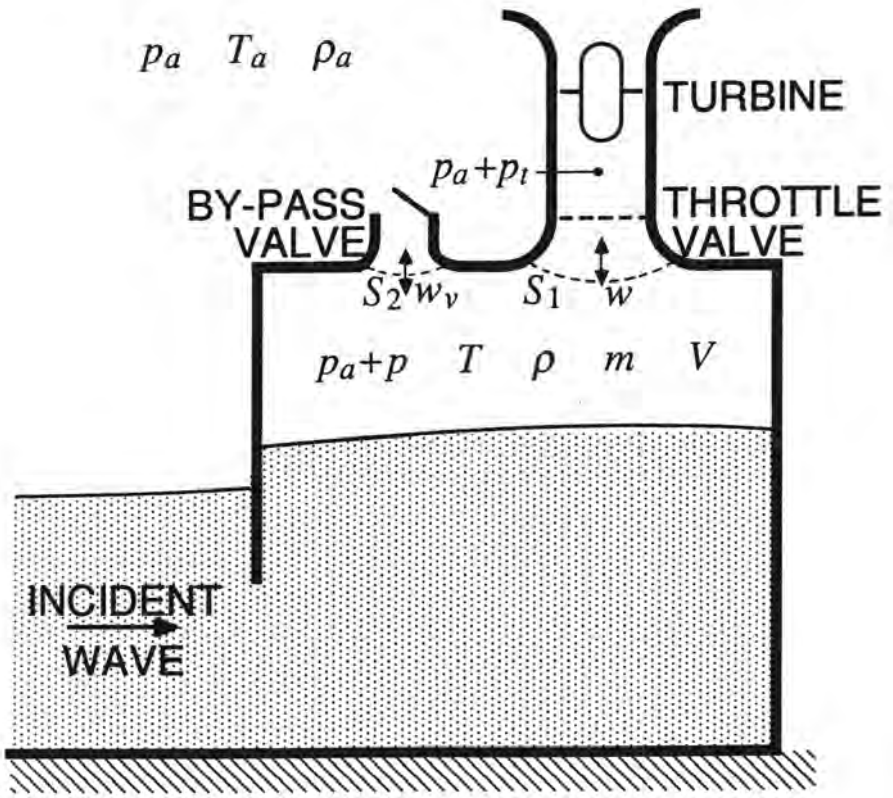

Fig. 2.2 OWC chamber and governing parameters (de O. Falcão, 1999).$p_a + p$ is the pressure of the air inside the chamber, m the mass of air contained inside the chamber, w the mass flow rate through the turbine, w_v the mass flow rate through the by-pass valve and ρ and V are respectively the density and the volume of the air inside the chamber. Permission to reproduce this figure has been granted by Elsevier.

et al., 2012). This floating OWC consists of a submerged vertical tail-tube-fixed to an axisymmetric floater that oscillates with waves. Oceanlinx, is a device consisting of a floating platform with eight air chambers (Gareev, 2011). "Mighty Whaale" is a floating OWC device recently developed in Japan (Osawa et al., 2002; Washio et al., 2000).

Full scale onshore OWCs have been constructed in Scotland (Heath et al., 2001), Portugal (Falcão, 2000) and Spain (Torre-Enciso et al., 2009). An alternative to traditional OWC devices is the U-OWC (Boccotti, 2003). As mentioned above, one advantage of onshore devices is they can be embedded in traditional coastal defence structures such as breakwaters, providing the structure a dual function (Hammons, 2008). However, the main disadvantage of onshore devices is the loss energy due to friction with the sea-bottom (Stagonas et al., 2010).

Although this technology is currently one of the most important in wave energy, OWCs are mostly installed onshore and consequently, this kind of devices cannot be used for coastal protection. For this reason, OWC will not be considered in the development of this thesis.

Oscillating Bodies

Oscillating bodies have received increasing research interest in recent years. In this type of technology, the action of the waves drives an oscillator whose motion is transformed into electrical power by a generator (Greaves and Iglesias, 2018). The simplest case is when an oscillating reacts to the wave motion against the seabed which is connected to a PTO. Examples of WECs in this group are Seabased, a seabed-referencing WEC with a linear electric-generator (Boström et al., 2009), and BOLT, a device attached to the seabed through a winch (Bjerke et al., 2011). Oscillating bodies can be also installed submerged, as with the Archimedes Wave Swing (AWS). This WEC is composed of a silo and a floater that heaves with waves (Valério et al., 2007).

Two body oscillating WECs are self-referencing. Among the different WEC devices in this category, Wavebob has reached an advanced stage of development, including sea trials with a model at $1/4^{th}$ scale (Weber et al., 2009). PowerBuoy is another device in this category, which has a high-pressure-oil hydarulic circuit which lies between the float and a

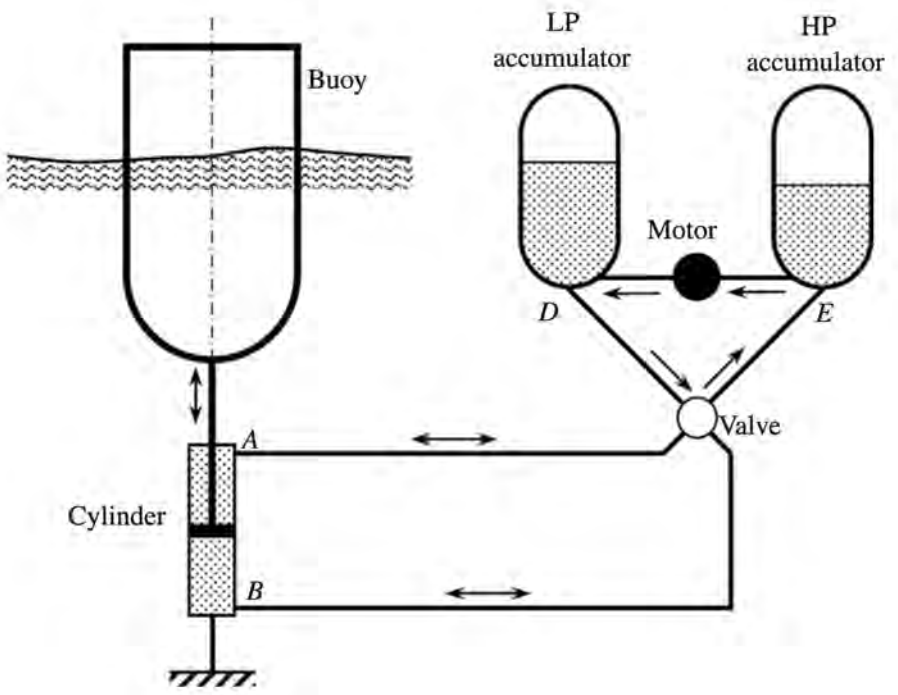

Fig. 2.3 Oscillating body WEC scheme (de O. Falcão, 2007). Permission to reproduce this figure has been granted by Elsevier.

reaction plate (Chozas and Soerensen, 2009). AquaBuOY, for its part, includes a high-head hydraulic turbine situated between the surface buoy and submerged masses (Weinstein et al., 2004).

Among the floating multibody, heaving devices we find FO3, which has been tested in Norway at 1:3 scale (Taghipour et al., 2008) and Wave Star, developed in Denmark and tested in the North Sea in 2009 (Hansen et al., 2013). Alternatively we have floating oscillating body pitching like Salter's Duck (Salter, 1974), developed in 1979 including a gyroscope PTO, and McCabe Wave Pump, deployed during 9 years from 1996 in the Shanon Estuary, Ireland (Kraemer et al., 2001). In other devices, the floater reacts against an internal body. In this group we find: Searev (Clément et al., 2005), developed in France, and Penguin WEC (Boren et al., 2014), developed in Finland.

The Pelamis is a WEC that works by rotation (Henderson, 2006). Consisting of a set of semi-submerged cylinders, the wave motion of the ocean produces a motion in the different cylindrical sections that if transmitted to the PTO system (Yemm, 1999). M4, for its part, is a three body heave, pitch and surge device (Stansby et al., 2015). And last but not least, we find flap type devices in which the body is submerged and attached to the seabottom, acting by pitching. These devices are often deployed nearshore, like the Oyster (Whittaker

et al., 2007), which includes a high-pressure seawater PTO, and Waveroller (Mäki et al., 2014), similar to the latter but with a high-pressure oil PTO.

Although they are mainly installed offshore and can be deployed in wave farms, their principle of operation leads to smaller reductions of the wave height at their lee than other offshore WECs. For this reason, they are not going to be studied in this thesis, as their impact on the coast is limited.

Overtopping devices

In this type of WECs sea water coming from overtopping waves is collected in a reservoir above the sea level. The water in the reservoir is then released back to the sea passing through a turbine which turns the potential energy of the water into useful energy (Greaves and Iglesias, 2018). Overtopping devices have been developed both fixed onshore and floating offshore.

Among the most important fixed onshore prototypes, the Sea-wave Slot-cone Generator (SSG) is found, described by Margheritini et al. (2009); Vicinanza et al. (2012, 2013b). This device is composed of a number of reservoirs placed on top of each other, including a low-head turbine in each reservoir (Vicinanza and Frigaard, 2008). Waves are forced to flow over a narrow channel, concentrating the energy and increasing the wave height. The Overtopping BReakwater for Energy Conversion (OBREC) (Contestabile et al., 2017), is a similar device but this time embedded into the structure of a traditional rubble mound breakwater. Other prototypes of this technology include smaller devices, more suitable for microtidal coasts such as the Mediterranean Sea (Buccino et al., 2015). TAPCHAN (Tjugen, 1994) is an example of an overtopping shoreline device but, in this case, without concentration. Similar to onshore OWC devices, this kind of technology cannot be used for coastal protection as they are deployed onshore.

Floating offshore overtopping devices work under the same principle, with the main difference of being moored offshore and fixed to the bottom by buoys. These are the most interesting devices in terms of coastal protection as they are situated offshore and, as they do not rely on resonance with waves, they can be constructed very large, decreasing their wave transmission coefficient and, consequently, decreasing significant wave height at their

lee. Wave Dragon (Kofoed, 2002; Kofoed et al., 2006) uses two reflectors to concentrate waves in a ramp which leads to a reservoir where the water is collected.

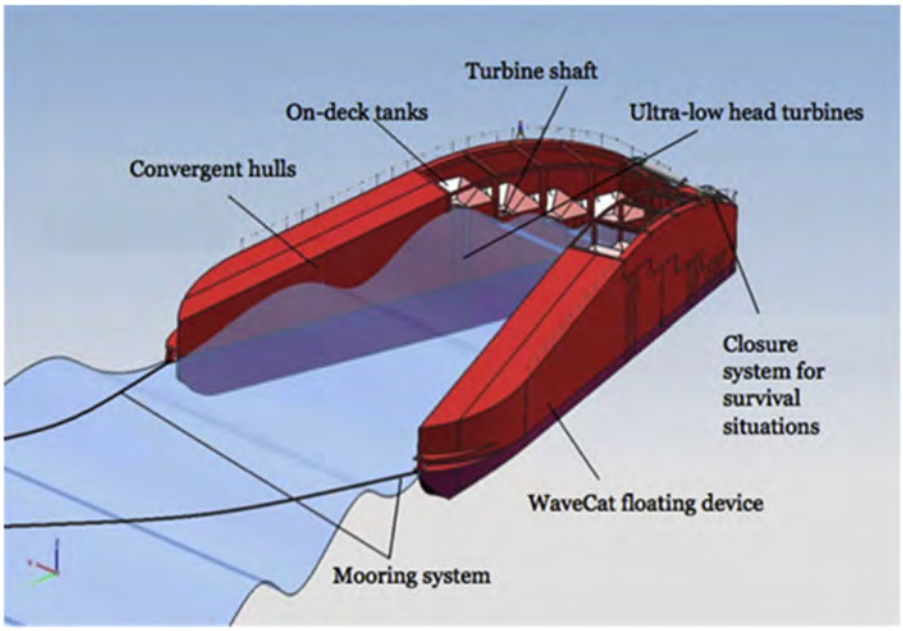

Fig. 2.4 Schematic of the WaveCat (Fernandez et al., 2012). Permission to reproduce this figure has been granted by Elsevier.

WaveCat (Fernandez et al., 2012) is an overtopping-type floating offshore device which consists of two hulls, similar to those found in a catamaran (hence its name) (Figure 2.4). Unlike a catamaran, the two hulls are not parallel but converging. Incoming waves propagate through the space between the two hulls and, eventually, the wave crests overtop the inner hull sides, collecting sea water into reservoirs over the sea level. It uses a single-point mooring to a CALM buoy. One of the main characteristics of WaveCat is that both the freeboard and the angle between hulls may be varied. The latter is an important advantage for the device. In the case of extreme sea states, the angle between hulls can be closed completely, converting it into a conventional monohull ship. This increase the survivability of the device which is one of the main issues for offshore floating devices. This advantage, along with its high wave energy absorption, depicted by the transmission coefficients obtained by Fernandez et al. (2012) during experimental campaigns, makes WaveCat suitable for coastal protection in eroded beaches. For this reason, WaveCat will be used in this thesis to study the impact of wave energy converters on gravel dominated coasts.

2.1.3 Wave energy resource

Wave energy resource has been extensively characterised worldwide in the existing literature. In this heading, the main studies regarding the wave energy resource in coasts across the globe will be presented. These studies are focused on the investigation of the wave energy availability (the maximum potential wave energy available on site) more than on the wave energy extraction (the actual conversion of wave energy into electrical energy, which depends on different aspects such as the performance of the device). The aim of this section is to identify case studies in which wave farms could be used for both carbon-free energy production and coastal protection. In this sense, two factors will be analysed: (i) the wave energy resource should be large enough to justify the deployment of a wave farm, (ii) the existence of eroded gravel dominated beaches in which the wave farm could have a positive impact countering shoreline retreat.

Atlantic coast

The Atlantic coast of Europe and America are two of the coastal areas with a higher wave energy resource. According to Cornett (2008), an annual mean wave power over 70 kW/m can be found in these regions. Because of this, many studies investigating the wave energy resource and selecting potential locations for wave farms in the Atlantic Ocean may be found in the literature.

For instance, Silva et al. (2015) studied the wave energy resource in the Iberian North and West coast. Coupling two numerical models, WAVEWATCHIII for wave generation and SWAN for wave propagation the wave energy resource of the Portuguese west coast and Spanish northwestern coast was assessed. Iglesias and Carballo (2011) presented a methodology to select the location for the deployment of a wave farm. Based on a case study in the South West of Galicia (Iberian Peninsula), they studied the sensitivity of the computed wave power to the number of sea states considered to determine *nearshore hotspots* i.e. areas of wave energy concentration due to refraction and shoaling over the bathymetry. Carballo et al. (2014) analysed the wave energy resource of the Death Coast (NW Spain), the coast with the biggest resource in the Iberian Peninsula. Using high resolution spectral numerical models, a geospatial database with the wave energy resource

was produced. Carballo et al. (2015), studied intra-annual power performance of different kind of WECs based on a case study in the same region: Galicia (NW Spain). Their methodology enabled the calculation of monthly high-resolution characterisation matrices, characterising the monthly performance of any WEC-site combination studied. Research on the wave energy resource in the Iberian Peninsula started in the Atlantic Ocean, due to the higher wave heights present on this part of the coast. Higher resolution, third generation numerical models enabled modeling of the wave propagation from offshore to nearshore and therefore, the wave energy resource characterisation including the identification of nearshore hotspots which reached 40 kW/m in this region.

On the American Atlantic coast, Defne et al. (2009) investigated the wave power potential along the southeast Atlantic coast of the United States. Mean wave power in the nearshore region was determined to be 9 kW/m, whereas in some offshore areas the mean power can reach 15 kW/m.

Wave energy may reduce the carbon footprint in developing countries. Contestabile et al. (2015), characterised the wave energy resource in Santa Catarina, Brazil, which is one of the largest electrical markets in South America. Analysing hindcast data from the European Centre for Medium-Range Weather Forecasts (ECMWF), they found that the annual offshore wave power was 15.25 kW/m. Although it is situated on the Pacific coast, Peru is an emerging country with an increasing electrical power demand and highly dependent on fossil fuels. López et al. (2015c) concluded that the wave energy resource in Peru exceeds more than seven times the total electric demand of the country.

Finally, wave energy resource on the Atlantic coasts may be a way for islands to achieve energy self-sufficiency. Veigas and Iglesias (2014), studied the case of Fuerteventura, an island in the Canary archipelago which is a UNESCO Biosphere Reserve, and concluded that the energy produced by a wave farm constitutes an excellent approach to satisfying the energy needs of the island.

Mediterranean Sea

Although the majority of the research interest has been focused on the coasts of the Atlantic and Pacific Oceans due to their higher wave energy resource, in recent years, the finite

nature of fossil fuels along with their undesirable effects, i.e. climate change and sea level rise, have forced researchers to study the implementation of wave energy in less energetic coasts such as the Black and the Baltic seas (Rusu, 2009; Soomere and Eelsalu, 2014). The Mediterranean Sea presents an intermediate wave energy resource between the open oceanic coasts and these enclosed basins.

The wave climate for the Mediterranean Sea have been extensively studied (Arena et al., 2015; Liberti et al., 2013). Besio et al. (2016) characterised the wave energy resource using a state-of-the-art wave hindcast with a spatial and temporal resolution of about 10 km and one hour, respectively. They identified some areas where the mean wave power reaches the order of 10 kW/m, similar to some Atlantic Ocean coasts. Zodiatis et al. (2014) focused their study on the Eastern Mediterranean Levantine Basin and identified some regions with increased values of wave energy potential: the western and southern coastlines of Cyprus island, the sea area of Lebanon and Israel, as well as the coastline of Egypt especially around Alexandria.

Vicinanza et al. (2013a) studied the wave energy resource on the coast of Sardinia (Italy) the second largest island in the Mediterranean Sea and found the annual offshore wave power ranged between 8.91 kW/m and 10.29 kW/m, with two nearshore “hot spots” where the average wave power is respectively 9.95 and 10.91 kW/m. Iuppa et al. (2015a,b) studied the wave energy resource around Sicily (Italy) identifying "hot spots" where the mean wave power is within the range of 5.33–7.52 kW/m.

In recent years, the Alboran Sea situated in the Mediterranean part of the south of the Iberian Peninsula has received increased research interest. Bozzi et al. (2018) investigated the possibility of adapting downscaled prototypes of existing offshore WEC technologies to the Mediterranean Sea. He found that the Alboran Sea is one of the most promising Mediterranean areas for wave energy with mean wave power of 5-7 kW/m. Playa Granada is a gravel dominated beach facing the Alboran Sea (South West Iberian Peninsula). López-Ruiz et al. (2016) studied the performance of a wave farm composed by WaveCats in 24 locations off this coast. Based on a 25 years-length forecasting of the wave climate on this coast, and assessing the uncertainty by means of Monte Carlo simulation, the wave energy resource in some of the 24 location studied produced an average mean wave power

of 5.5 kW/m. In addition, this stretch of coast has suffered important erosion problems in recent years due to river damming (Bergillos et al., 2016d). The characteristics of the sediment of the beach, dominated by the gravel fraction, its erosion problems along with the promising wave energy resource make Playa Granada an ideal option to locate a wave farm with a dual purpose, wave energy generation and coastal protection. For this reason, Playa Granada has been selected as study site for this thesis, in order to characterise the impacts of wave farms on the shoreline evolution of a gravel dominated beach.

2.2 Wave energy transmission of WECs

In order to study the impact of wave farms on the coast, the most important performance parameter of a WEC is the transmission coefficient (K_t). This coefficient is defined as the ratio of the wave height in the lee to that in front of the structure ($K_t = H_{st}/H_{si}$). There is limited information about transmission coefficients of WECs in the literature because in this stage of development of the technology, research works are focused on other aspects such as the development of new devices, wave energy resource, optimisation of the performance or economic viability. In this section, some research works presenting transmission coefficients of some WECs will be reviewed.

As a notion of the wave energy transmission of OWC devices the results obtained by He and Huang (2014) can be taken. The main objective of this research works was to address the hydrodynamic performance of pile-supported OWC-type structures as part of a breakwater. In the experimental campaign the characteristics of the chamber are varied changing size and shape of an opening in the top cover. The effects of three parameters: (i) relative breadth, (ii) draught, and (iii) shape and size of the opening on wave transmission, wave reflection, wave dissipation and pressure fluctuation inside the chamber are investigated.

Offshore overtopping-type devices are also suitable for providing coastal protection as, because of their size, they produce a shadow effect that reduces wave height in their lee. Fernandez et al. (2012) studied the WaveCat device though laboratory experiments carried out in the wave tank of the Faculty of Engineering of the University of Porto. Fernandez et al. (2012) tested the performance of WaveCat under different angles between hulls. Two

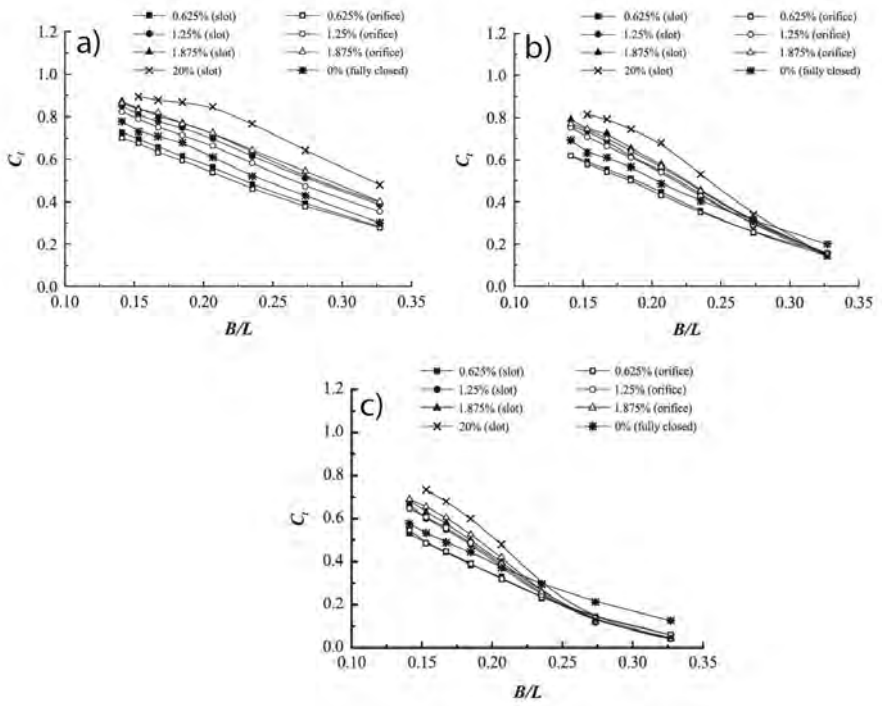

Fig. 2.5 Variations of transmission coefficient C_t versus B/L for the (a) 10-cm draught, (b) 15-cm draught and (c) 20-cm draught (He and Huang, 2014). Permission to reproduce this figure has been granted by Elsevier.

sea states were used during the experimental campaign (H_s = 2.5 m, T_p = 11.0 s and H_s = 3.0 m, T_p = 12.0 s). The results obtained are depicted in Table 2.1. As can be observed, the transmission coefficient did not vary significantly, with K_t about 0.8 in all tests except one, where it was lower.

Table 2.1 Reflection (K_r) and transmission (K_t) coefficients of WaveCat device (Fernandez et al., 2012). Permission to reproduce this table has been granted by Elsevier.

H_s	T_p	α	K_r	K_t
2.50	11.0	30	0.425	0.806
3.00	12.0	30	0.438	0.777
2.50	11.0	45	0.441	0.777
3.00	12.0	45	0.428	0.756
2.50	11.0	60	0.421	0.507
3.00	12.0	60	0.431	0.760
2.50	11.0	90	0.470	0.749
3.00	12.0	90	0.470	0.772

The results obtained by Fernandez et al. (2012) show that transmission coefficients of WaveCat are similar to other WECs devices. WaveCat is an overtopping type device in development, whereas the results obtained by He and Huang (2014) have been obtained using notional parameters or devices. The use of a real WEC in the development of this

thesis has the advantage that results are related to an specific device and a better proof of the effects we can expect in real life situation. In addition, WaveCat presents the following advantages: (i) WaveCat is intended to operate offshore, in water depths between 50 m and 100 m where the wave energy resource is larger and (ii) WaveCat has a lower environmental and visual impact because of its floating nature and absence of a superstructure. Because of these features, the Wave cat device is worthy of further investigation and this will be the focus of this dissertation.

2.3 Wave farm impacts on the wave field

Since the development of wave energy has advanced enough to install the first wave farms in a prototype scale, the interest on the impacts of wave energy extraction on the wave field has increased. In this section, the main research work with regard to the impact produced by a wave farm on the wave climate in its lee will be highlighted.

The Wave Hub is a submerged grid point connection for the deployment of wave energy converter prototypes situated in the north coast of Cornwall (South West UK). The extraction of wave energy at this offshore site will produce an impact, most likely the reduction in wave height and power, in the wave climate in its lee. This impact raised concerns within the surfing community of this area. Millar et al. (2007) studied the changes produced in the wave climate by devices installed at Wave Hub. With this aim, SWAN – a third generation numerical wave model – was applied. It is able to reproduce wave propagation, including wave refraction, shoaling and reflection or transmission due to obstacles. Two computational grids were employed: a coarse computational grid with 5000 m and a nested fine grid with 200 m resolution. A set of 529 different wave states, obtained from twelve hourly WAVEWATCHIII estimates of significant wave height, mean wave period and wave direction were propagated.

The arrays of WEC devices installed on the Wave Hub site were simulated by means of 4 km long partially transmitting obstacles, deployed approximately parallel to the incoming waves at the study site. Four different transmission coefficients were employed: i) 0%, representing complete absorption of the wave energy incoming at the obstacle, ii) 70% representing an array of densely distributed WEC devices with high efficiency, iii) 90%

representing a wave farm with more separated WECs and lower efficiency, and IV) 40% included in the study in order to establish trends. Two sets of results were extracted from the model: significant wave height, mean period, wave direction and energy transport at 500m intervals across the whole domain of the fine grid, and these same parameters but distributed along the 10 m bathymetry, at approximately 500 m spacing.

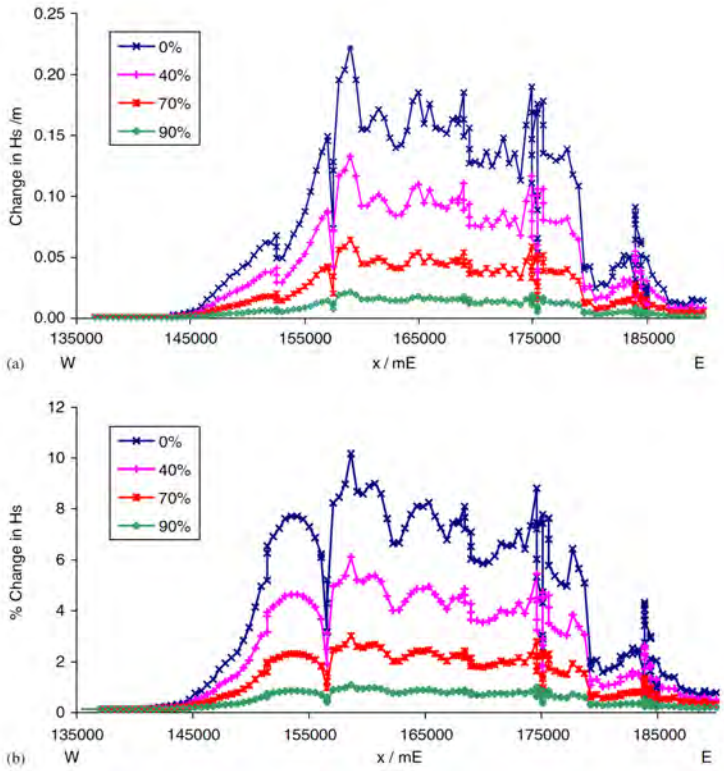

Fig. 2.6 (a) ΔH_s for the reference sea state ($H_s = 3.3$ m, $T_m = 11$ s, $D = 1$ °), and varying wave energy transmission percentages at the Wave Hub site, (b) $\Delta H_s/H_s$ along the coastline for reference sea state, and varying wave energy transmission percentages at the Wave Hub site (Millar et al., 2007). Results at 10 m contour. Permission to reproduce this figure has been granted by Elsevier

The main results obtained are depicted in Figure 2.6. As can be observed, both the change in H_s (ΔH_s) and the ratio $\Delta H_s/H_s$ are reduced as the wave energy transmission coefficient increases.

This paper was one of the firsts research works produced on impact of wave farms on the wave climate in its lee. However, from the methodology applied a number of questions arise. First, the 200 m resolution of the fine grid was not able to reproduce individually the WECs installed in the wave farms. Because of this reason, the wave farms were modelled as a whole and the changes produced in the wave field by the interaction

between devices was not modelled. In addition, the authors took notional wave energy transmission coefficients due to the lack of laboratory data.

Smith et al. (2012) also researched the Wave Hub site studying the influence of multi-modal sea states. Again, the SWAN model was applied, but this time, a modification was made to implement a frequency-dependent wave energy transmission coefficient. After that, the results were compared with those obtained by Millar et al. (2007) and differences were analysed. The response function of the devices was described as a power transfer function (PTF). As the developers do not usually share this function for specific devices, this study considered two theoretical responses: (i) a wide bandwidth PTF, which energy captured across the spectrum but with a lower maximum absorption, and (ii) a narrow bandwidth PTF, which is able to capture energy only in a narrow section of the spectrum. The calibration of the model was not considered necessary by the authors and SWAN was run with its default parameters. Three sea states representative of the wave climate at Wave Hub were propagated including bi-modal, wind-sea and swell waves.

Results show that, for the narrow PTF the largest reduction is observed for wind-sea sea state (maximum 10.4%), whereas the reduction in the bi-modal and swell sea states are lower (5.01% and 2.72%, respectively). This is because the centre of the narrow PTF does not exactly match the peak frequency of any of the sea states modelled. However, this impact changes entirely for the wide PTF with reductions of 16.3%, 15.1% and 10.92% for the swell, wind-sea and bi-modal sea states, respectively (Fig. 2.7). The main conclusion drawn was that a narrower PTF produces a lower impact but also with a lower energy production efficiency. However, the methodology applied did not resolve the questions produced by the previous paper. Again, the transmission coefficients of the WECs were theoretical and the resolution of grid was still too coarse to reproduce the interaction between devices.

Palha et al. (2010) studied the impact of wave energy extraction on the wave climate of the Maritime Pilot Zone, an area of about 320 km^2 off the Portuguese coast for wave energy development created by the Portuguese government in 2008. This research work is focus on the estimation of the changes on the wave conditions nearshore produced by the installation of an offshore wave farm of Pelamis WECs – a semi submerged, articulate structure which

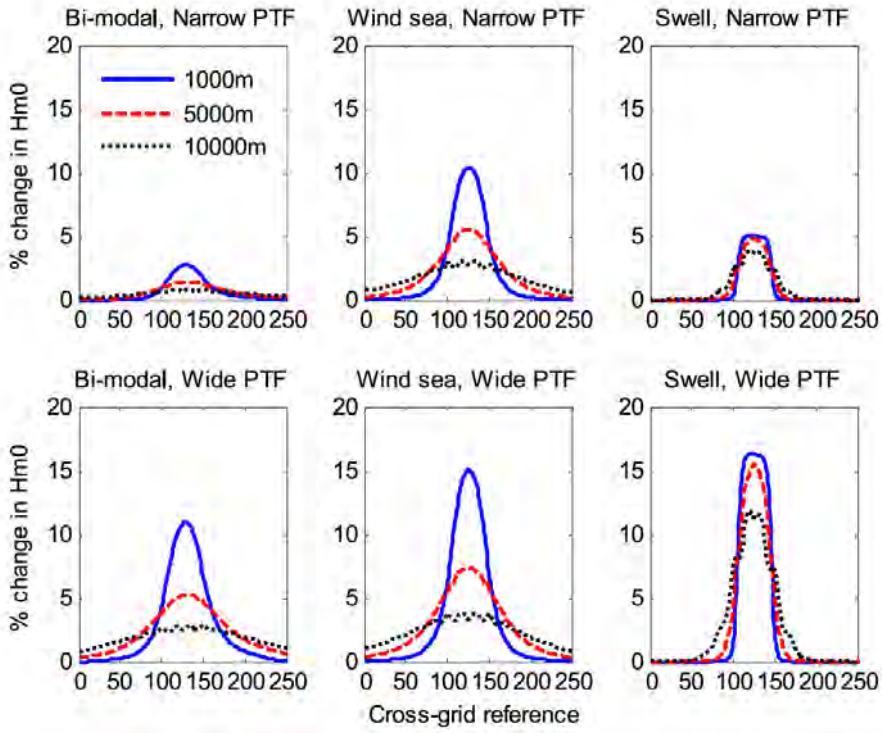

Fig. 2.7 Results along the grid transect at 100 m intervals using the modified SWAN transmission for a narrow and wide PTF (Smith et al., 2012). Lines represents different distances to the wave farm location (1000m, 5000m and 10000m). Permission to reproduce this figure has been granted by Elsevier

is made of cylindrical sections linked by hinged joints. The main advance with respect Millar et al. (2007) and Smith et al. (2012) works was that in this case the transmission coefficient was not notional but the estimated percentages provided by Pelamis developer.

Five different configurations of the wave farm were tested, all sharing the same installed power (202.5 MW) and alignment 'parallel to the incoming waves at the Pilot Zone'. Three different sea states were modelled, corresponding to the monthly median, minimum and maximum along the year. The wave transmission coefficient were adjusted for each one based on Pelamis technical specifications. Wave propagation was calculated using REFDIF, a numerical model based on the parabolic approximation of the mild slope equation, which is able to simulate propagation of regular waves over the bathymetry. This model has two main limitations: (i) It can only be applied to monochromatic waves and (ii) mild slope bottoms (1:3 or less). The bathymetry of the Pilot Zone was based on the hydrographic charter n.3 of the Instituto Hidrográfico at a scale of 1:150000.

The main findings were that the length of coast affected by the wave energy extraction is related to the length of the wave farm parallel to the incident wave crest (Fig. 2.8). In

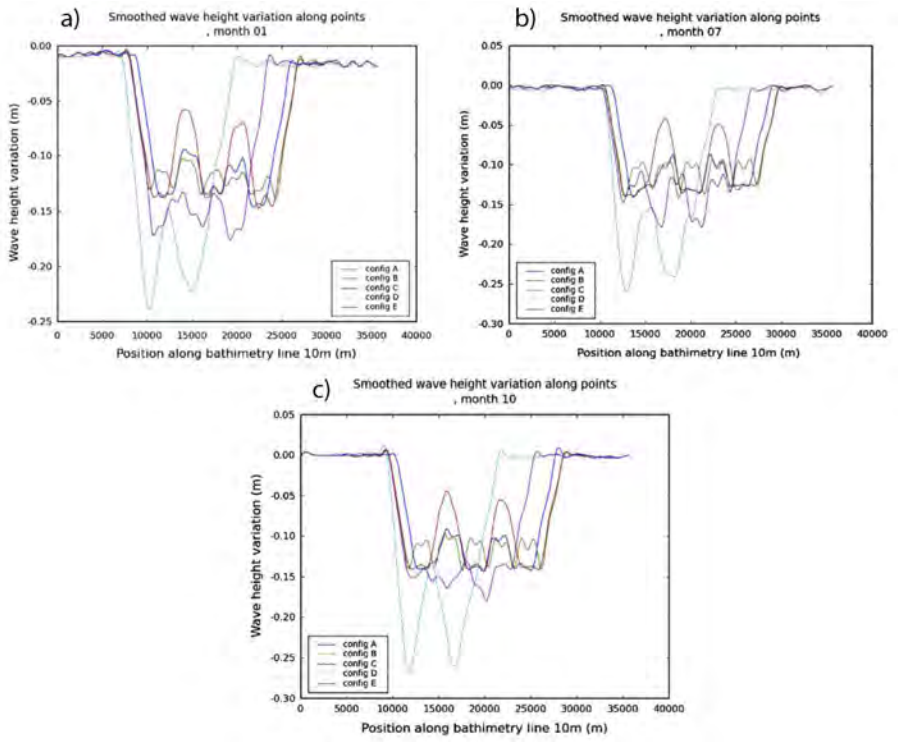

Fig. 2.8 Absolute significant wave height difference along the 10 m water depth contour without and with wave farm for the monthly median significant wave height in: a) January, b) July and c) October (Palha et al., 2010). Permission to reproduce this figure has been granted by Elsevier

addition, two or more rows of WECs produced a higher maximum value of the wave height variation nearshore. And finally, the width of the navigation channels around the wave farm is related also to the impact produced on the wave conditions nearshore. Narrower channels increase overlapping of the cone shaped area of affect of each wave farm, enhancing the wave height reduction.

This works supposed an advance in the research as, for the first time, real values were used for the transmission coefficient, allowing the assessment of the real impacts produced by wave farms of Pelamis devices. However, some limitation can be observed in this work. First, the monochromatic nature of the wave propagation model does not allow to assess the impact on the full spectrum. Second, the limitations of the mild slope equation does not permit to apply this methodology to complex bathymetries with slopes steeper than 1:3. And finally, the resolution of the bathymetry (1:150000), although sufficient to reproduce offshore areas, is not detailed enough to reproduce the nearshore features of the coast.

Iglesias and Carballo (2014) studied how the impact of a wave farm on the nearshore wave climate changes with the distance between the farm and the shoreline. With this

objective, eight case studies were studied on the Death Coast (Costa da Morte), situated in Galicia (NW Spain). This region have one of the greatest wave energy resource in Europe (50 kW/m). These case studies were made combining different coast-to-farm distances (2 km, 4 km and 6 km) plus a baseline (no-wave farm scenario) with two sea states representing winter and summer conditions. The main novelty of this work is that the interaction between waves and the WEC devices were modelled based on ad-hoc laboratory tests. Through these physical model experiments the wave transmission coefficient were assessed. The WEC device studied in this research work was WaveCat, described in Section 2.1.2. The wave farm layout was made of 20 devices divided in two rows.

Again, SWAN was the numerical model chosen for wave propagation in this work, but this time the model was calibrated based on offshore and coastal wave buoy data. Two computational grids were used: (i) a coarser grid of varying grid size from 270 m to 470 m, and (ii) a nested grid with a grid size of 18 - 31 m. The smallest grid size was applied to the wave farm region in order to properly model the wave-WEC interaction.

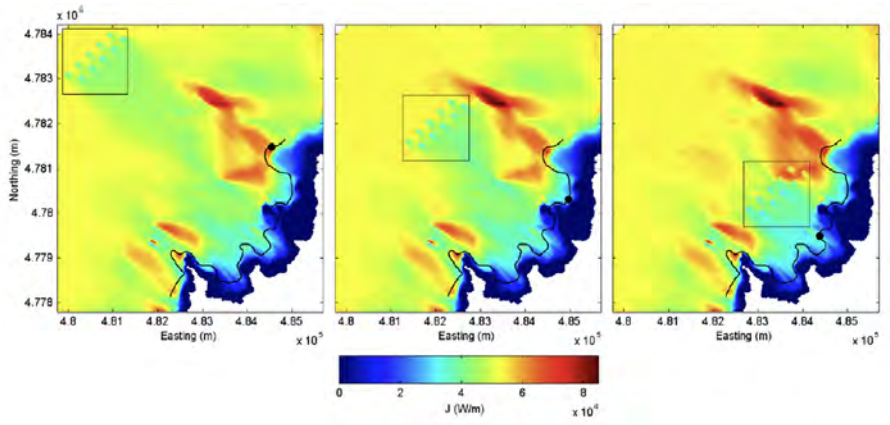

Fig. 2.9 Wave power pattern in the wave farm region for the winter case studies (H_s = 3.3 m, T_p = 12 s and mean wave direction θ = 307°). Distance to the coast: 6 km (left), 4 km (middle) and 2 km (right) (Iglesias and Carballo, 2014). Permission to reproduce this figure has been granted by Elsevier

The results obtained (Figures 2.9 and 2.10) show that overall power values decrease when the wave farm is situated closer to the coast, as a result of the bottom friction, that reduce wave height when waves propagate through intermediate and shallow waters. In addition, it is clear that the closer the wave farm to the shoreline, the larger the direct impact on the shoreline, with the larger increase between 6 km and 4 km case studies. However, although the direct shadow of the wave farm over the coast is reduced when the

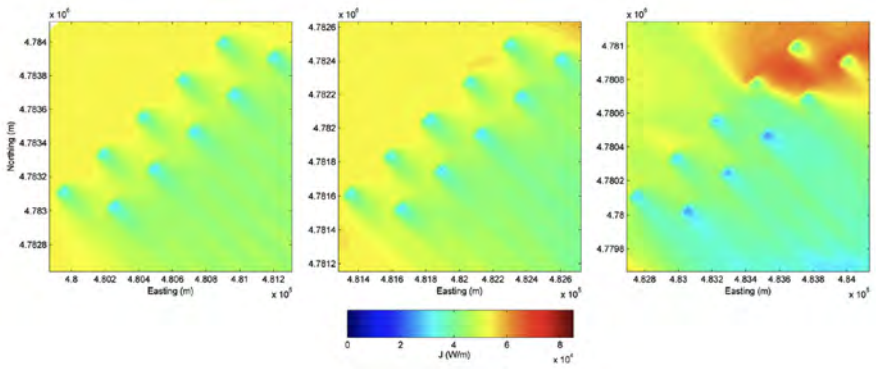

Fig. 2.10 Enlargement of Fig 2.9 showing Wave power detail around the wave farm (Iglesias and Carballo, 2014). Permission to reproduce this figure has been granted by Elsevier

farm to coast distance is increased, that does not guarantee a reduction in the maximum absolute nearshore impact as the impact on the coast can be felt a long way away from the direct shadow in the shoreline. For this reason, the main conclusion is that to increase the wave farm to coast distance does not solve all the impacts produced on the shoreline and a detailed impact assessment is mandatory to assess the impact produced on the coast.

Chang et al. (2016) developed a modified version of SWAN (SNL-SWAN) based on the work performed by Smith et al. (2012), in order to allow the direct input of relative capture width (RCV) or power matrices to simulate the WEC performance. They applied this new version of the code to investigate the effects of a wave farm on the wave climate in the nearshore in its lee. SNL-SWAN incorporates a WEC module that accounts for device specific wave absorption and transmission.

The impact produced on the nearshore wave climate was investigated by means of numerical model simulations of eight different WEC devices. Although these devices were based on real WECs under development important differences may exist between these models and their real prototypes, so the performance applied is notional. The devices were arranged in different diamond-shapes layouts varying the number of WECs (10, 50, 100) and inter-device spacing (4, 6 and 8 diameters). The wave conditions along the boundaries were extracted from wave-buoy data of Monterrey Bay, CA which median values are H_s = 1.7 m and T_p = 12.5 s.

The model set-up was variable depending on the size of the device. All case studies share the coarser grid (0.001°, both in latitude and longitude). The devices with a diameter greater than 15 m were modelled with a nested grid of cell size equal to the diameter, in

order to model each WEC by a single cell. Those models whose diameter was smaller than 15 m were modelled using three grids.

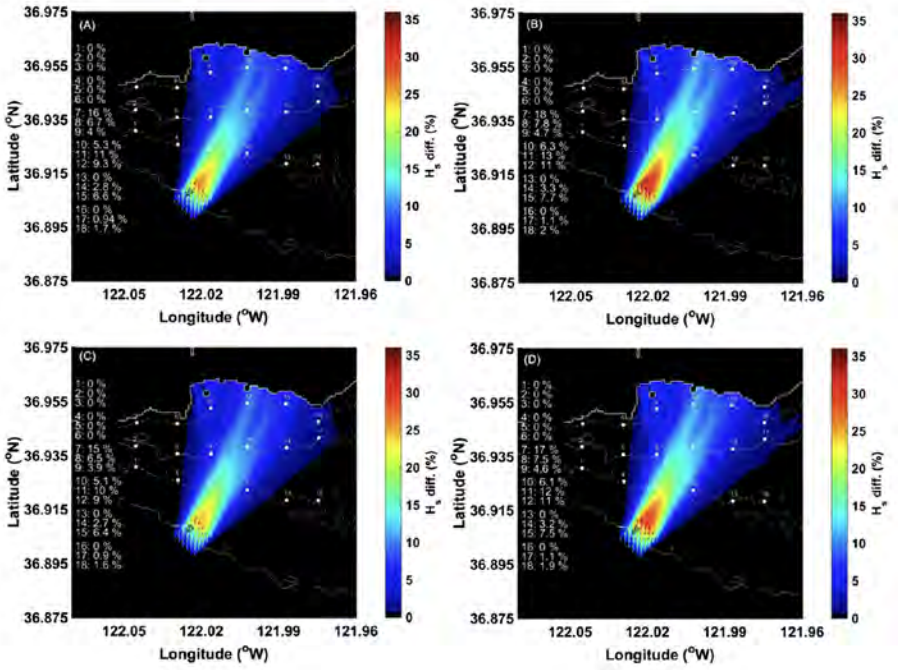

Fig. 2.11 Significant wave height percentage decrease using SNL-SWAN for model runs specifying 50 B-OF type WECs with 6 m spacing on the 40 m depth contour (Chang et al., 2016). Permission to reproduce this figure has been granted by Elsevier

The results depict that significant wave heights decrease up to 30% with respect to the baseline scenario in the case of the buoy type device (Fig. 2.11). Different buoy type devices decreased significant wave heights up to 15%, however WEC devices with a diameter lower than 10 m yield lowers reductions of the wave height. Although buoy type device yielded the larger absolute reduction, the impact produced by OWC type device extended over a larger extension of the coast and therefore, it has a greater potential impact. Although this work was an advance in the comparison of the performance of different type of WECs, the transmission coefficients applied were notional and therefore, the results obtained could differ from the real performance of the devices.

In conclusion, the main recommendations that can be extracted from these research works are: (i) the importance of the use of a phase resolving wave propagation model and (ii) the use of computational grids fine enough to properly reproduce wave-WEC interaction and therefore, a detailed bathymetry.

2.4 Wave farm impacts on coastal erosion

In this section, current research on the impacts produced by wave farms will be presented. Due to the wave energy absorption capabilities of the floating offshore WEC technologies, especially the overtopping-type devices, some authors started to investigate the possibility to use wave farms as coastal protection elements.

Vidal et al. (2007) studied the impact of a wave farm formed by buoys (oscillating bodies) located at Santoña. They coupled two different numerical models, OLUCA-SP for the wave propagation and EROS-SP for the sediment transport. Ruol et al. (2011) analysed the impacts of a wave farm composed by DEXA, a WEC of the wave activated body type, situated in front of Marina di Ravenna beach, in the Adriatic coast (Italy). Based on the CERC formula, longshore sediment transport was evaluated. This study shown that the DEXA could be designed so that the effect on sediment transport becomes quite significant reducing and even changing the net direction. Rusu and Onea (2016) also studied numerically generic wave farms in the central part of Portugal, based on wave data from the European Centre for Medium-Range Weather Forecasts (ECMWF). The results of this study shown that the nearshore impact of a wave farm can be significant and it could assure an effective coastal protection.

Lately, different authors started to base their research in a combination of laboratory experiments and numerical models, rather than use only generic transmission coefficients. Zanuttigh and Angelelli (2013), studied the impacts of another wave activated body WEC based on 3D laboratory experiments carried out in Aalborg University. Wave Dragon impacts on the coast were investigated by Nørgaard et al. (2013). The transmission coefficients obtained in laboratory experiments involving different wave conditions, stiffness of the mooring system and reflector joints were used in a numerical case study: Santander Bay (Northern Spain). Carballo and Iglesias (2013) studied the wave-WEC interaction of WaveCat through laboratory experiments. Based on a case study, a wave farm of WaveCats on the Death Coast (NW Spain), ad hoc laboratory tests based on the wave climate of the study site were carried out. Using wave transmission coefficients obtained in the laboratory tests, the impacts of the wave farm on the nearshore wave climate were computed using a high-resolution spectral wave model: SWAN.

The latter laboratory experiments were the basis for a series of journal papers related to the impact of WaveCat on the coast. Abanades et al. (2014a) studied the impacts of a wave farm composed by WaveCats on the coast during storms. Based on a case study, Perranporth Beach (UK), two numerical models were joined: a high-resolution wave propagation model (SWAN) and a coastal processes and sediment transport model (XBeach). A number of ad hoc indicators were defined to compare two scenarios: with and without wave farm. A similar methodology was followed by Abanades et al. (2014b) to study the impact on the beach profile. Results showed that a positive impact was produced by the wave farm, reducing erosion on the beach face. Abanades et al. (2015a) analysed the role of the distance from the coast to the wave farm, concluding that the closer the wave farm is situated to the coast the bigger the reduction of the erosion. The long-term impact of wave farms on the modal state of the beach profile was analysed by Abanades et al. (2015b). Finally, the impact produced in a dune system (Xago beach, Asturias, N Spain) were assessed by Abanades et al. (2018).

As can be seen from the number of research works presented in this chapter, wave farm impacts on the coast is a growing research topic. The majority of the studies presented in this section were carried out on sandy beaches. However, gravel dominated beaches are very common in high latitudes and steeper hinterlands and their number is growing in recent years due to artificial nourishment projects using gravel sediments on sandy beaches. For wave farms to become potential coastal defence elements, impacts produced on gravel dominated beaches, which morphodynamics differ from sandy beaches, need to be fully understood. In addition, the knowledge that can be found in the literature about the impacts on the longshore sediment transport (LST) is limited due to the fact that the majority of the existent literature is focused on the beach profile. LST drives the shoreline position in the long term and, therefore, the dry beach area available at the coast.

2.5 Longshore sediment transport

The application of LST formulations and a one-line model to assess changes in the shoreline is a must in order to develop wave farms for coastal protection purposes as LST drives the longterm evolution of a coastal system. In this sense, the main objectives of this thesis are

to study the impacts of wave farms on the shoreline position and dry beach area of gravel dominated beaches. The methodology applied to carry out this research, coupling different numerical models and formulations will be described in the next chapter.

A wide range of LST formulations can be found in the literature. All of them compute the LST rate based on the breaking conditions. In this section, a number of LST formulations will be described.

2.5.1 CERC equation

The most widely used formula in coastal engineering practice for the total LST rate is the CERC equation (USACE, 1984). It is based on the principle that the LST volume is proportional to the longshore wave power per unit length of the beach, and it can be expressed as follows:

$$Q = \frac{K\rho\sqrt{g}}{16\sqrt{\gamma}(\rho_s - \rho)(1-p)} H_{s,br}^{2.5} \sin(2\theta_{br}) \tag{2.1}$$

where Q is the LST rate in volume per unit of time, K is an empirical coefficient, ρ_s and ρ are the sediment and water density, respectively, p is the porosity index, $H_{s,br}$ is the significant wave height at breaking, γ is the breaker index and θ_{br} is the wave angle from shore-normal at breaking.

2.5.2 D.L. Inman and R. Bagnold (1963)

D.L. Inman and R. Bagnold (1963) proposed a theory whereby wave energy is expected to suspend and support sediment above the bottom, and where any unidirectional current superimposed on the orbital wave motion can, in turn, produce net transport in the current direction. The LST formula derived based on this theory may be expressed as follows:

$$Q = \frac{\sqrt{2}}{8} \frac{K\rho\sqrt{g}}{(\rho_s - \rho)(1-p)} H_{s,br}^{2.5} \sin(2\theta_{br}) \tag{2.2}$$

As may be observed, this formula is equivalent to the CERC equation (USACE, 1984) for a breaker index of 0.125.

2.5.3 Kamphuis (1991)

Another formulation was developed by Kamphuis (1991) for estimating LST rates. It is expressed as follows:

$$Q_m = 2.27 H_{s,br}^2 T_p^{1.5} \tan(\beta)^{0.75} D_{50}^{-0.25} \sin(2\theta_{br})^{0.6} \tag{2.3}$$

where Q_m is the LST rate of immersed mass per unit of time and $\tan\beta$ is the beach slope. The immersed weight can be related to the volumetric rate as $Q_m = (\rho_s - \rho)(1-p)Q$. This formulation is based on laboratory experiments but is applicable for both field and laboratory measurements (Kamphuis, 2002). The main advantage of this formulation against the previous equations described is that it accounts for the beach slope and the grain size. These are important variables to calculate sediment transport in gravel dominated beaches, with complex morphologies and sediment heterogeneity.

2.5.4 Van Rijn (2014)

Finally, in recent years Van Rijn (2014) proposed the following formulation:

$$Q_m = 0.00018 K_{vr} \rho_s g^{0.5} \tan(\beta)^{0.4} D_{50}^{-0.6} H_{s,br}^{3.1} \sin(2\theta_{br}) \tag{2.4}$$

where K_{vr} is a wave correction factor that accounts for the effect of swell waves on LST, since these waves have been demonstrated to yield much larger LST rates than wind waves of the same wave height.

This formula, as Kamphuis (1991) equation, accounts for the sediment size and the beach slope. The main advantage of this formulation against the rest of the equations presented in this section is that it was derived for sand, gravel and shingle beaches, based on laboratory and numerical experiments. On the contrary, the rest of the formulations were focused on sandy beaches. These characteristics make Van Rijn (2014) formulation suitable to accomplish the objectives proposed in this thesis.

2.5.5 Application of longshore sediment transport formulas to the study site

Rodriguez-Delgado (2016) applied the formulae presented in the previous section to Playa Granada (Southern Spain) in order to compare the performance of this methodology to predict the evolution of artificial beach nourishment on gravel beaches. Numerical modelling and a topographical and bathymetrical measurement campaign were combined to assess the ability of the different LST formulae to model the behaviour of the system. With this purpose, two profiles were measured using a Differential GPS taking five periodic topographic measures. Different sediment sizes were tested in order to check the dominant sediment fraction in the study site. Results are shown in Table 2.2.

Table 2.2 $C = V_{mod}/V_{obs}$ Coefficient (Rodriguez-Delgado, 2016)

		Profile 1		Profile 2	
		C1-C3	C3-C5	C1-C3	C3-C5
CERC	D_{50} = 2 mm	0.73	5.47	1.59	0.65
	D_{50} = 0.35 mm	15.09	89.48	32.97	10.7
	D_{50} = 5 mm	0.73	5.47	1.59	0.65
	D_{50} = 20 mm	0.73	5.47	1.59	0.65
Inman	D_{50} = 2 mm	1.84	10.93	4.03	1.31
	D_{50} = 0.35 mm	38.18	226.36	83.4	27.06
	D_{50} = 5 mm	1.84	10.93	4.03	1.31
	D_{50} = 20 mm	1.84	10.93	4.03	1.31
Kamphuis	D_{50} = 2 mm	2.29	32.06	9.2	7.56
	D_{50} = 0.35 mm	3.6	14.49	50.5	11.91
	D_{50} = 5 mm	1.82	25.5	7.32	6.01
	D_{50} = 20 mm	1.29	8.03	5.17	4.25
Van Rijn	D_{50} = 2 mm	2.37	10.77	3.89	1.15
	D_{50} = 0.35 mm	7.06	69.4	11.57	3.39
	D_{50} = 5 mm	1.37	6.12	2.24	0.66
	D_{50} = 20 mm	1.01	2.66	0.98	0.39.

Results show that the most accurate formula was Van Rijn (2014), with the largest sediment size (2 mm). The average *C* coefficient (taken as the ratio between the modelled and observed transport volume) for this formula was 1.26. CERC formula (USACE, 1984) obtained the most similar results to those obtained by Van Rijn (2014) (average *C* of 2.11), whereas D.L. Inman and R. Bagnold (1963) and Kamphuis (1991) tend to overestimate LST with an average *C* of 4.53 and 4.69, respectively. Based on these results, Van Rijn (2014) formula will be used to model LST volume in the development of this thesis.

2.6 Novelty of the present thesis with respect the state of the art

With respect to research works concerning wave farms and their interaction with the wave field, as it has been described in this chapter, previous works have dealt with the impact produced by wave farms on the wave field and the implications in the coastal areas situated at their lee (Carballo and Iglesias, 2013; Palha et al., 2010; Ruol et al., 2011; Rusu and Soares, 2013; Zanuttigh and Angelelli, 2013). These works have also focused on the wave farm effects on the beach profile of sandy beaches (Abanades et al., 2015b) and the morphological response (Millar et al., 2007), but the wave farm implications on gravel dominated beaches had not been investigated so far.

Relating to research works carried out in the study site, it is important to know that gravel dominated beaches have received limited attention in recent years and they are comparatively less studied than sandy beaches (Bergillos et al., 2016a). Rodriguez-Delgado (2016) combined numerical wave propagation and the one-line model to study the shoreline evolution in Playa Granada after an artificial nourishment project. Other works have also focused on the characterisation of the potential resource over a 25-years period time (López-Ruiz et al., 2016, 2018). But in these cases, numerical models have not been applied so far to reproduce the wave farm effects and the particularities of the wave field interaction with these structures on gravel dominated coasts.

However, to my best knowledge, the effects of wave farms in the shoreline evolution of gravel dominated beaches have not been studied yet. More precisely: (1) the implications of the alongshore position of the wave farm have not been assessed so far; (2) the influence of the layout, specifically the number of rows, has not been studied; and (3) the role of the inter-device spacing has not been investigated.

This thesis investigates, for the first time, the impact produced by wave farms on the shoreline evolution of gravel dominated coasts. For that, numerical models previously calibrated at the study site are modified to be able to reproduce the wave-WEC interaction, the alterations in LST transport and the shoreline evolution. The individual WECs forming a wave farm are designed using CAD tools and incorporated to a third-generation spectral

wave propagation model. The measurements of an experimental campaign (Fernandez et al., 2012) are used as input by the wave propagation model to reproduce the response of the WECs to the incoming waves. Then, different scenarios are studied and compared to the natural situation in order to assess the effects produced by the wave farm. These scenarios serve to investigate three parameters involved in the design of wave farm, which had not been analysed so far, mentioned in the previous paragraph. The individual effect of each parameter on the shoreline evolution of gravel dominated coasts are discussed. To this end, new methods are described in this thesis in order to compare the shoreline evolution after the construction of the wave farm to the natural (no-wave farm) scenario. Finally, a number of ad-hoc indicators, specifically designed with this objective, are proposed and applied. The results and conclusions of this thesis constitute an advance in the knowledge of the design of wave farms, allowing to predict their impact and using it in their own benefit to protect eroded coasts.

Chapter 3

Methodology

3.1 Methodological framework

In this chapter the methodology applied to fulfil the objectives of this research is presented. The general workflow of this work is depicted in Figure 3.1. In order to assess the impact of the wave farm on the shoreline evolution and dry beach area of the gravel dominated beach, a suite of numerical models was applied. Wave-WEC interaction and breaking parameters was modelled by means of SWAN (Holthuijsen et al., 1993), a third generation spectral wave propagation model. The output produced by SWAN was used as the input for LST formulation, obtaining LST rates derived from the modelled sea states. Based on this output, a one-line model is used to model the shoreline evolution of the beach and the resulting dry beach area was assessed.

This general methodology was applied to different wave farms in order to achieve each specific objective. The overtopping WEC *WaveCat* (Iglesias et al., 2009) was selected because its performance for coastal defence has been widely modelled in recent years (Abanades et al., 2014a,b, 2015a,b). The wave farm that yielded the best performance in terms of coastal protection was used as the input to test the next parameter. At the end of this workflow the optimum location and layout for the study site is selected.

In order to study the influence of the alongshore position on wave propagation patterns, longshore sediment transport and shoreline evolution in the study zone, a position sensitivity study including eight longshore locations of the wave farm (henceforth referred to as scenarios) was carried out. The layout proposed by Carballo and Iglesias (2013) was

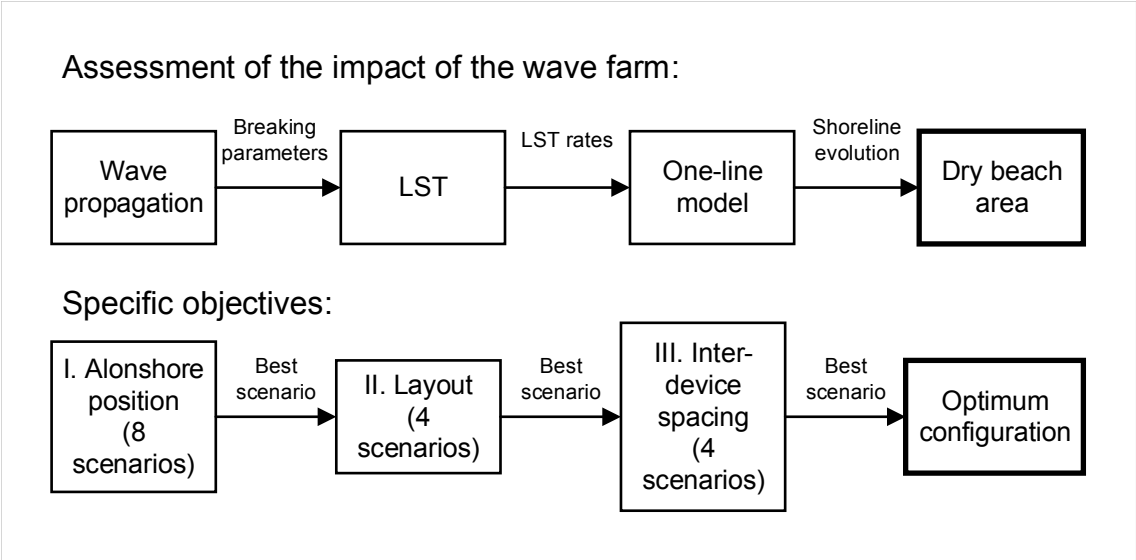

Fig. 3.1 General methodology and workflow

used, with the wave farm consisting of 11 WECs distributed on two rows (Fig. 3.2). The distance between adjacent WECs was $2D$, where $D = 90$ m is the space between the two bows of the *WaveCat*. The wave farms were located at a 30 m water depth, as these are the best positions in terms of power and availability of the wave energy resource, according to López-Ruiz et al. (2016).

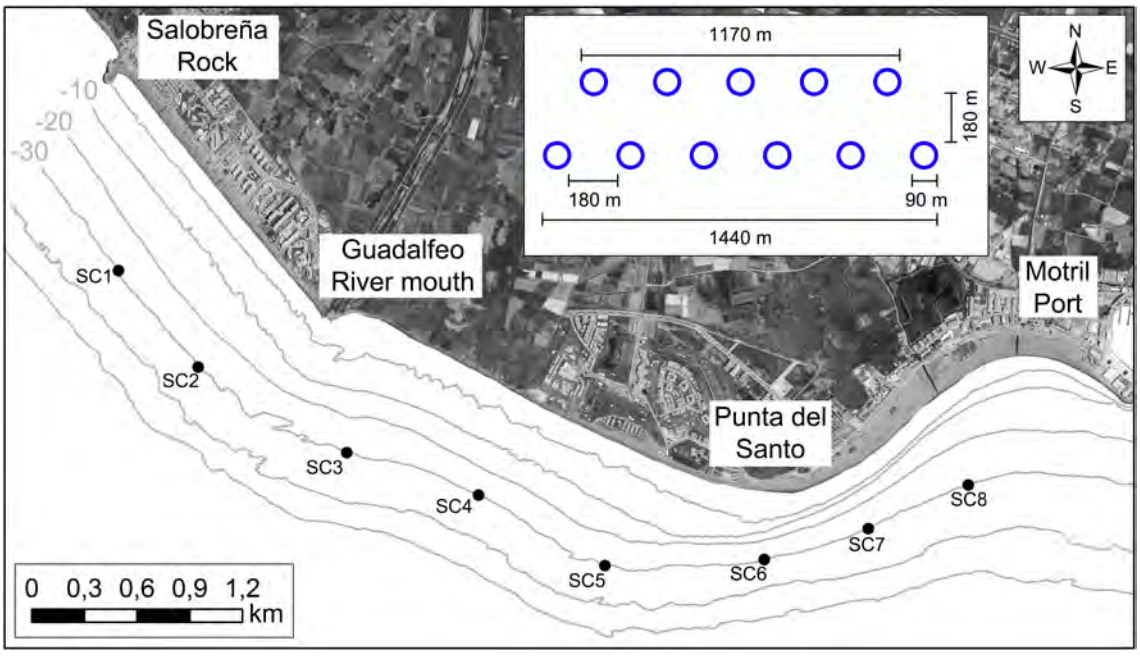

Fig. 3.2 Location and layout of the eight wave farm scenarios. Black dots indicate the centre of the wave farm. The top panel shows the layout of each farm. Rodriguez-Delgado et al. (2018b).

Next, four scenarios corresponding to different layouts were modelled in the optimum alongshore location obtained. The four layouts were defined varying the number of rows

from 1 to 4 (Fig. 3.3) but keeping constant the number of WECs (11) and their separation ($2D$, where $D = 90$ m). These values were selected based on the layout proposed by Carballo and Iglesias (2013) and Abanades et al. (2015a), among others. The geometrical centres of the four scenarios are located at the same position over the -30 m bathymetric line, as shown in Fig. 3.3.

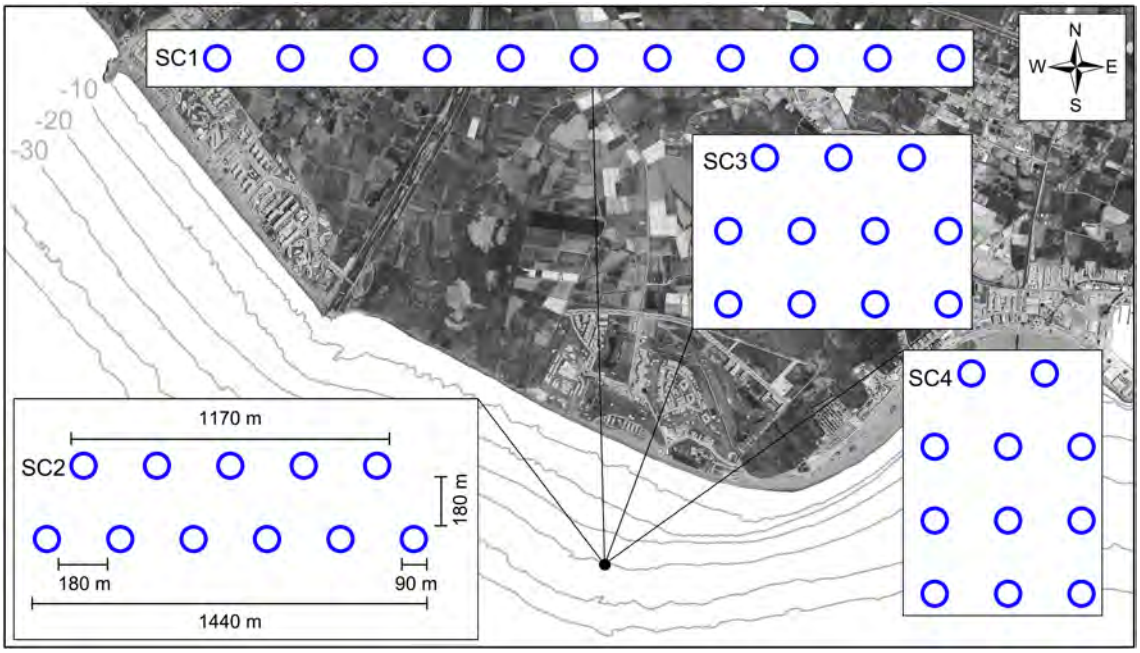

Fig. 3.3 Selected location for the wave farm and definition of the four scenarios of wave farm shape. Rodriguez-Delgado et al. (2018a).

Finally, to analyse the effects of inter-WEC spacing (S) on wave transmission, LST and the evolution of the coastline, four scenarios were defined based on the optimum layout and alongshore position. The selected wave farm case studies have the same number of WECs and rows, but different spacings between WECs: D, $2D$, $3D$, and $4D$ (Figure 3.4), with $D = 90$ m (Carballo and Iglesias, 2013). The geometrical centres of the defined case studies are all located at the same position, which was found to be optimum in terms of coastal protection.

3.2 Wave propagation model

Wave-WEC interaction has been studied in recent research works by means of laboratory experiments and numerical models, jointly. Among them, two different types can be found: phase-resolving and phase-averaged models. Phase-resolving numerical models include

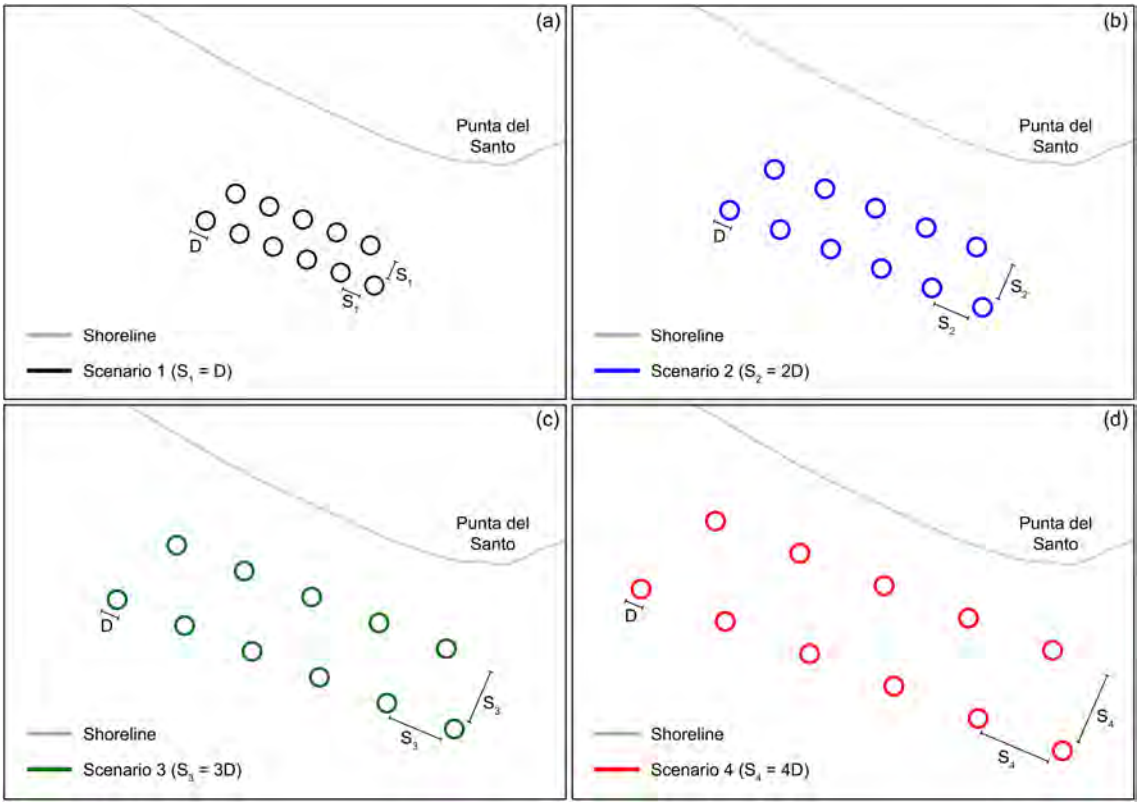

Fig. 3.4 Definition of the four case studies. Rodriguez-Delgado et al. (2019).

actual wave equations as Boussinesq and mild-slope. This kind of models computes every phase in the wave train individually. In this way, they are able to obtain the actual water level at a given time. CFD models are numerical models which resolve Navier-Stokes equations. These are more complex numerical models. They are able to deal with processes like two-phase flows, turbulence or viscous effects. These characteristics have important advantages as these models are able, for instance, to compute breaking parameters. However, the high resolution required both spatially and in time by these models make them very demanding computationally. Navier-Stokes models are very useful to study the interaction between a single WEC and a wave train, for example, to assess the performance of an OWC. Other kinds of phase-resolving models like Boussinesq and mild slope decrease the computational demand but, in exchange, they consider the flow is irrotational.

Phase-averaged models, on the contrary, are spectral models which obtain the wave spectrum in any given point resolving the wave action balance equation. They are able to propagate waves over a given bathymetry by means of the energy conservation equation. Among them, SWAN (Simulating WAves Nearshore) (Holthuijsen et al., 1993) is one of

the most popular in the existing literature about wave farm impacts (Abanades et al., 2014b; Carballo and Iglesias, 2013; Millar et al., 2007). It is able to compute the most important wave parameters (significant wave height, wave period, mean wave direction and fraction breaking) from offshore to shallow waters. In addition, it represents accurately complex wave transformation processes including shoaling, depth-induced refraction, wind forcing, whitecapping, bottom friction dissipation and depth-induced breaking. SWAN can be used with ease to study impacts of wave farms as the WECs composing the wave farm can be incorporated to the model as obstacles by means of their reflection and transmission coefficients, which can be obtained by means of laboratory experiments.

All these advantages make SWAN the best candidate to achieve the objectives of this work. Moreover, SWAN has been calibrated and validated in the study site in previous works (Bergillos et al., 2017b; Rodriguez-Delgado, 2016). Because of this, SWAN will be used in the rest of this thesis to assess the impact of wave farms on the wave field nearshore.

SWAN uses the two-dimensional wave action density spectrum, $N(\sigma,\theta)$ with σ the angular wave frequency and θ the wave direction, instead of the wave energy density spectrum, $E(\sigma,\theta)$, to describe the wave field. Wave action density is equal to wave energy density divided by the frequency: $N(\sigma,\theta)=\frac{E(\sigma,\theta)}{\sigma}$. Therefore, the evolution of wave energy is described by the spectral wave action balance equation from arbitrary conditions of wind, currents and bathymetry.

This equation, in its general form, can be expressed as follows:

$$\frac{\partial N}{\partial t}+\frac{\partial\left(c_z N\right)}{\partial x}+\frac{\partial\left(c_y N\right)}{\partial y}+\frac{\partial\left(c_\sigma N\right)}{\partial \sigma}+\frac{\partial\left(c_\theta N\right)}{\partial \theta}=\frac{S}{\sigma}. \tag{3.1}$$

The first term on the left-hand side of the equation accounts for the evolution in time of the wave action density, the second and third terms, by their part, represent the wave action density propagation in the geographic space, with c_x and c_y the propagation velocities. The final terms stand for the shifting of the relative frequency, with propagation velocity c_σ, and the depth- and current-induced refraction, with propagation velocity c_θ, respectively. The right-hand side of the equation stands for the source term which generates, dissipate

or redistribute energy:

$$S = S_{in} + S_{nl} + S_{ds,w} + S_{ds,br} + S_{ds,b}, \tag{3.2}$$

where S_{in} stands for the energy transfer due to the wind, S_{nl}, the non-linear triad redistribution of wave energy, $S_{ds,w}$, the energy dissipation due to whitecapping, $S_{ds,br}$ the energy dissipation due to depth-induced breaking and $S_{ds,b}$, the energy dissipation due to bottom friction. For a more detailed description of the different equations and the model itself, the reader is referred to Booij et al. (2008).

For the model set-up of this thesis, a consistent test condition is needed to ensure the reliability of the conclusions obtained in the comparison between the baseline and the wave farm scenarios. In this sense, the shoreline position and the bathymetry are kept constant for the shake of comparison. The initial shoreline position is a key parameter as it is the basis for the conclusions extracted about the evolution of the dry beach area in the different scenarios. To ensure consistency, bathymetric line 0 has fixed as the initial position of the shoreline. This position has been verified using aerial photographs. The grids used in the wave propagation are also important to ensure the accuracy of the results. A two-grid-model (coarse and nested) has been used to reduce computational cost. The coarse grid has been designed to reach the wave data point (SIMAR 2041080, Section 3.4), and to cover the whole deltaic region, including boundary conditions for LST. The nested grid has been designed to cover the nearshore region, where the wave farm is situated in the different scenarios, and the more complex coastal processes appear (e.g. wave breaking). Finally, the model parameters are also part of the test conditions as they have been kept constant. These parameters were calibrated and validated one-by-one to provide the best fit to data obtained in experimental campaigns.

The wave conditions have been also kept constant along the whole scenarios tested in this thesis. As explained in previous sections, in order to assess the full behaviour of the system, both high- and low-energy conditions have been tested.

The variation in the test conditions that form the different scenarios are the configurations of the wave farm. First, a baseline, no-wave-farm scenario has been tested. In this case, the test conditions are run with no wave farm implemented in the wave propagation

model. These results have been used to evaluate the positive/negative effects produced by the farms. The configurations of the wave farms are explained in Section 3.1. The objective was to evaluate three different parameters involved in the design of the wave farm: alongshore position, layout (number of rows) and inter-device spacing. In order to assure a proper modelling of the individual WECs forming the wave farm, the nested (finer) grid has been designed to encompass all the wave farm scenarios.

3.2.1 Input data

In this section, the different input data needed in order to obtain the appropriate results are described.

Shoreline

Shoreline position is needed by SWAN in order to properly limit the boundary between the water and land zones of the grid. For this work, the shoreline was generated from the bathymetric data combined with information of aerial photographs of the study site. The shoreline was created by means of CAD tools and the xyz coordinates were exported using a LISP script.

Grid

A proper grid system needs to be generated in order to model the physical domain of the study site. The criteria for a proper generation of the grid was to ensure a proper nesting of the different grids, to avoid concentration of energy and to choose a proper orientation for the grid in order to correctly propagate the dominant mean wave direction.

Finally, two grids were defined: a coarse grid and a nested grid in order to increase the resolution in the wave farm and nearshore area. In this way, the precision required to model the wave-WEC interaction and wave breaking is ensured. Figure 3.5 depicts the final configuration of grids along with the modelled shoreline. In the wave propagation model, the results of the coarse grid along the boundary of the nested grid are used as input for the latter. Because of this, to ensure proper integration between the two grids, it is

recommended that the size of the cells in the nested grid was no less than 5 times smaller than the cells in the coarse grid.

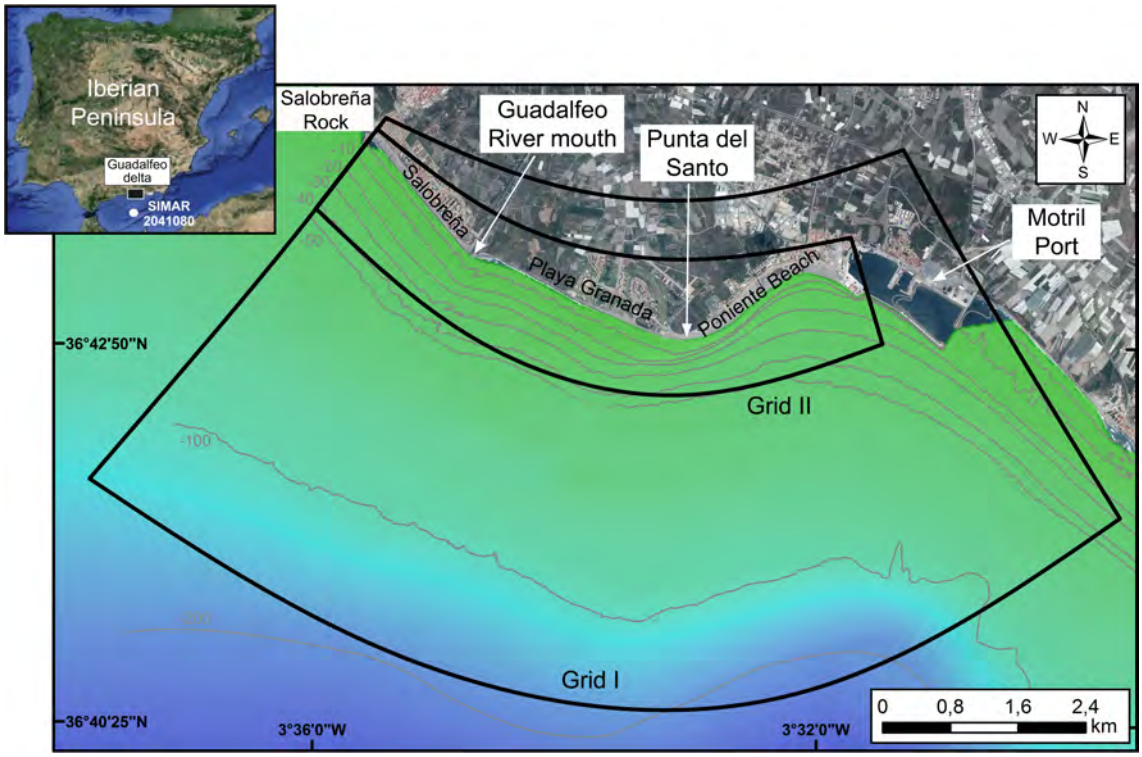

Fig. 3.5 Upper left panel: Location of the study site (Guadalfeo delta, southern Spain).Central panel: bathymetric contours, grids used in the wave propagation model, position of the Salobreña Rock, Guadalfeo River mouth, Playa Granada,Punta del Santo, Poniente Beach and Motril Port. Rodriguez-Delgado et al. (2019).

Coarse grid

This grid covers the entire deltaic region from offshore to nearshore. It is formed by four contours, one coincident to the land area whereas the other three are open to the sea, covering the two prevailing directions in the study site (West and East). The grid is formed by 82x82 cells of varying sizes that decrease with depth from 170x65 to 80x80 m.

Nested grid

The second is a nested grid covering the beach area with 244 and 82 cells in the alongshore and cross-shore directions, respectively, and with cell sizes of approximately 25x15 m.

3.2.2 Bathymetry

The bathymetric data was provided by the Spanish *Ministerio de Medio Ambiente y Medio Rural y Marino*. This bathymetry covers the area from nearshore to the -50 m contour and

contains 30-40 data points by square meter reaching 80-100 in the nearshore area. This data was combined with information from charts obtained from the *Instituto Hidrográfico de la Marina* in the deeper area.

The combination was carried out using CAD tools and the XYZ coordinates exported using a LISP script. SWAN was used to interpolate the bathymetric data and assign a depth value to each cell.

3.2.3 Wavecon file

The sea states to propagate are introduced in SWAN using a plain text file called wavecon. This file contains eight columns including: time reference, significant wave height, peak period, mean wave direction, dispersion, water level, wind velocity and mean wind velocity. The following is an example of the input needed in the wavecon file:

```
* Itdate Hs Tp Dir ms wl windspeed wind dir.
E
2 8 * number of rows number of columns
0.000000 3.1 8.400000 107.000000 4 0 0 0
60.000000 3.1 8.400000 107.000000 4 0 0 0
```

The JONSWAP spectral shape was used to generate the input spectrum, as it supposes an improvement against the Pierson-Moskowitz spectrum which is the other option available in SWAN. These sea states where used as boundary conditions in the wave propagation model. The model tests were divided in two depending on the mean direction of the sea states. In the first group of tests, westerly sea states were run with waves coming from the west and south boundaries of the coarse grid and no waves coming into the model from the east boundary. In the second group, easterly sea states were run with the opposite configuration, waves coming from the east and south boundaries and no input from the west.

3.2.4 Model parameters

The model was calibrated and validated for the study site in previous works (Rodriguez-Delgado, 2016). To this end, model results were compared with field data collected from

December 23rd, 2014 to January 30th, 2015 by means of two ADCPs. For the spectral resolution of the frequency space, 37 logarithmically distributed frequencies ranging from 0.03 to 1 Hz were used, whereas for the directional space, 72 directions covering 360° in increments of 5° were defined.

In the model depth-induced breaking was introduced. Non-linear triad interactions was modelled, increasing the accuracy in shallow waters where triad wave-wave interactions transfer energy from lower frequencies to higher frequencies often resulting in higher harmonics. Bottom friction was modelled using Collins (1972) drag law model. Dissipation of waves due to whitecapping was also modelled following the expression of van der Westhuysen et al. (2007). Finally, diffraction and refraction were also modelled.

The final parameters adopted were:

- Depth-induced breaking:
  - Alpha: 1
  - Gamma: 0.73
- Non-linear triad interactions:
  - Alpha: 0.1
  - Gamma: 2.2
- Bottom friction:
  - Model: Collins
  - Gamma: 0.02
- Diffraction:
  - Smoothing coefficient: 0.6
  - Smoothing steps: 900
- Whitecapping: Van der Westhuysen
- Refraction: activated

- Constants:
  - Gravity: 9.81 m/s^2
  - Water density: 1025 kg/m^3

The high resolution of the nested grid allows to properly define the WEC position, which is a prerequisite to simulate the wake of the devices accurately (Carballo and Iglesias, 2013). The interaction between the wave field and the WEC devices – WaveCat as stated in Section 2.1.2 – was simulated through the transmission (K_t) and reflection (K_r) coefficients. Based on the laboratory experiments carried out by Fernandez et al. (2012), $K_t = 0.76$ and $K_r = 0.43$ were selected. These values have been used widely and successfully to model the effects of WaveCat farms (Abanades et al., 2014a,b, 2015a,b). The modelling of the shape and position of the different WECs has been detailed in Section 3.3. When an obstacle is defined in a cell, SWAN reduces the energy obtained by the model by the factor corresponding to the transmission coefficient, decreasing the energy of the spectrum. These coefficients have been tested in the conditions modelled in this thesis and therefore, they can be applied. However, the research carried out in this thesis is a "best case" scenario where the version of WaveCat deployed in the study site could be engineered to operate during Mediterranean storms conditions.

3.3 Wave farm modelling

SWAN is able to estimate wave transmission through obstacles based on their reflection and transmission coefficients. In this section, the methodology to model the wave farm inside SWAN is described. For this work, the individual WECs forming the wave farm have been modelled. To do so, the WECs have been modelled in their actual size, location and orientation in AutoCAD® software (Fig. 3.6). Once the design of the wave farm has been model in the CAD, the vertices coordinates of each WEC are exported using a specifically designed LISP script.

In order to include the obstacles in SWAN model, two files need to be added. First, an *.*obt* file which includes transmission and reflection coefficients, as well as the modelling type for the obstacle. The following is an example of a WEC definition inside an *.*obt* file:

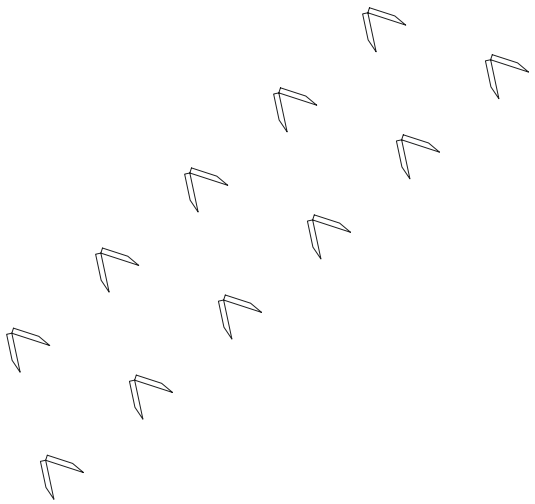

Fig. 3.6 Sketch of wave farm model produced in CAD Software

```
[ObstacleFileInformation]
   FileVersion  = 02.00
   PolylineFile = obstacle.pol
[Obstacle]
   Name         = C1_1
   Type         = sheet
   TransmCoef   =  7.5999999e-001
   Reflections  = specular
   ReflecCoef   =  4.3099999e-001
```

The shape and position of the obstacles inside the SWAN grid are defined in a **.pol* file. Each obstacle defined in the **.obt* file needs to be included in the **.pol* file, specifying its name, number of vertices and coordinates of each vertex. The following is an example of a WEC definition inside an **.obt* file, in order to summarise only 5 of the 282 rows have been depicted:

```
C1_1
282 2
 447205.224     4063633.740     0
 447205.196     4063632.740     0
 447205.146     4063631.742     0
 447205.074     4063630.744     0
```

```
447204.980      4063629.749      0
...
```

With this information, the shape of the WECs is implemented in the model. This produces a reduction of the wave height in the cells occupied by the device, driven by the transmission coefficient. Therefore, the final implementation can be observed in the model if we look at the wave height in the vicinity of the wave farm. In the next Figure, the effect of the WEC in wave propagation, which is a representation of the shape of the device inside the model is depicted. We have to take into account that, since we can only see WECs inside SWAN by their effect on significant wave height, the blue zones in the Figure represents not only the device itself but also the wake effect produced in wave propagation.

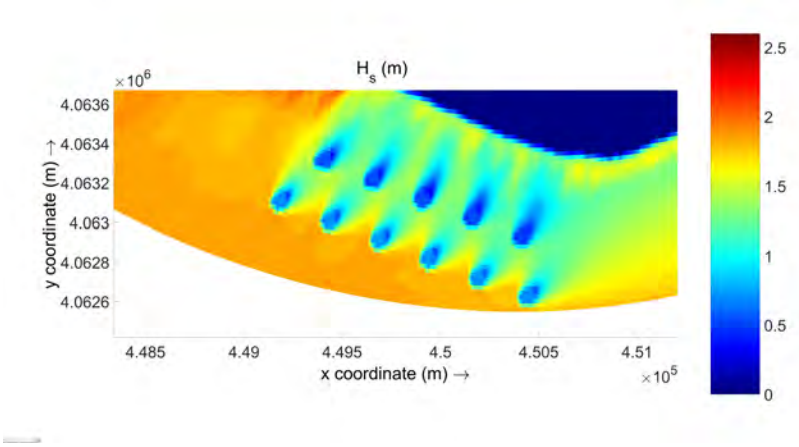

Fig. 3.7 Reduction of significant wave height due to the presence of WECs

3.4 Modelled sea-states

The wave data series used in this thesis came from SIMAR data point 2041080 provided by *Puertos del Estado*. This data set includes hourly data from 1958 to present. SIMAR data are formed by hindcast wave and wind time series. The wind time series are generated by dynamic downscaling using atmospheric model RCA3.5 forced by reanalysis data obtained from ERA-Interim and ERA40 data sets. Hourly averaged 10 m high wind data are provided. Wave data have been generated combining two numerical models: WaveWatch III and WAM. Hourly data of significant wave height, spectral peak period, spectral mean period (momentum 0 and 2) and mean wave direction are provided.

The modelled sea states was kept constant along the development of this thesis in order to properly compare the results obtained. The selected deep-water wave heights corresponded to the 50th percentile for low-energy conditions ($H_{s0} = 0.5$ m) and the 99.9th percentile for storm conditions ($H_{s0} = 3.1$ m). The selected wave heights allow to model the individual WECs based on the laboratory experiments carried out by Fernandez et al. (2012) as they are included in the range of sea states analysed in the experimental campaign. For these H_{s0} values, the most frequent associated values of spectral peak period and wave direction were considered. Details of the wave climate of the study site can be found in Section 4.1.2. These sea states, which are summarised in Table 3.1, were modelled for four different durations (12h, 24h, 36h and 48 h) to further explore the effects of the sea state persistence on shoreline evolution. As will be shown in the next chapter, Playa Granada has a bi-directional wave climate, with storms coming from both east and west. Storm magnitude is similar for both directions and therefore, for simplicity H_s has kept equal regardless the direction. This also allows comparison between the effects of storms with both mean directions.

Table 3.1 Values of the modelled deep-water variables [H_{s0} = significant wave height; T_p = peak period; θ = mean wave direction]. Rodriguez-Delgado et al. (2018a).

	Low energy		Storm	
	East	West	East	West
H_{s0} (m)	0.5	0.5	3.1	3.1
T_p (s)	4.5	4.5	8.4	8.4
θ (°)	107	238	107	238

3.5 LST formulation and one-line modelling

LST rates were computed through the equation proposed by Van Rijn (2014), as it was explained in Section 2.5.5. This formulation can be expressed as follows:

$$Q_{t,mass} = 0.00018 K_{swell} \rho_s g^{0.5} (\tan\beta)^{0.4} (d_{50})^{-0.6} \left(H_{s,br}\right)^{3.1} \sin(2\theta_{br}), \qquad (3.3)$$

where $Q_{t,mass}$ is the total longshore sediment transport rate (in kg/s), ρ_s the sediment density (in kg/m^3), g the acceleration of gravity (in m/s^2), $\tan\beta$ the slope of the surf zone, d_{50} the grain size (in m), $H_{s,br}$ the significant wave height at breaking (in m), and θ_{br} the

wave angle from shore-normal at breaking. K_{swell} is a factor that accounts for the effects of swell waves on LST. The sediment size used was 2 mm, as has been proved to yield the best results in the study site (see Section 2.5.5).

Breaking parameters were computed using the results of the propagation model. They were calculated for 341 shore-normal profiles, equally distributed (1 every 20 m) along the deltaic shoreline between Salobreña Rock and the Port of Motril. To this end, a Matlab script was developed. Based on the results of the wave propagation model, the cells where 5% of the waves break were located. Once the breaking cells were found, the breaking line was defined joining the centre of these cells. Finally, the Matlab script interpolates breaking parameters ($H_{s,br}$ and θ_{br}) in the location where each shore-normal profile intercepts the breaking line.

Shoreline plane shape models are developed from the work conducted by Pelnard-Considère (1956) and they are known as *one-line* models. These models are based on two general hypothesis. The first one states that beach profiles keep their general shape in the long-term. In this sense, a single contour line is sufficient to describe changes in the beach plan shape. The second hypothesis is that the sediment displacement occurs in a limited space of the beach profile, between the active berm and the depth of closure. The efficiency of this kind of models is higher when breaking waves form an angle with the line tangent to the shoreline, as it is the case of Playa Granada.

Pelnard-Considère (1956) based his work on the continuity equation of sediment over the beach longitudinal axis (x). Therefore, the shoreline position in the transverse axis (y_s) may be expressed as a function of x, $y_s = y_s(x)$. Considering D as the vertical distance between the berm and the depth of closure and taking into account the second hypothesis, the volume gradient can be expressed as:

$$\Delta V = \Delta x \Delta y D. \tag{3.4}$$

This volume gradient is the result of sediment balance along the longitudinal axis (Fig. 3.8). With Q the sediment flux, obtained in this thesis using the LST formulation described in the previous section, volume gradients in a stretch of coast is produced if the balance

between the input and output of sediments is different from 0 ($\Delta Q \neq 0$):

$$\Delta Q \Delta t = \frac{\partial Q}{\partial x} \Delta x \Delta t. \tag{3.5}$$

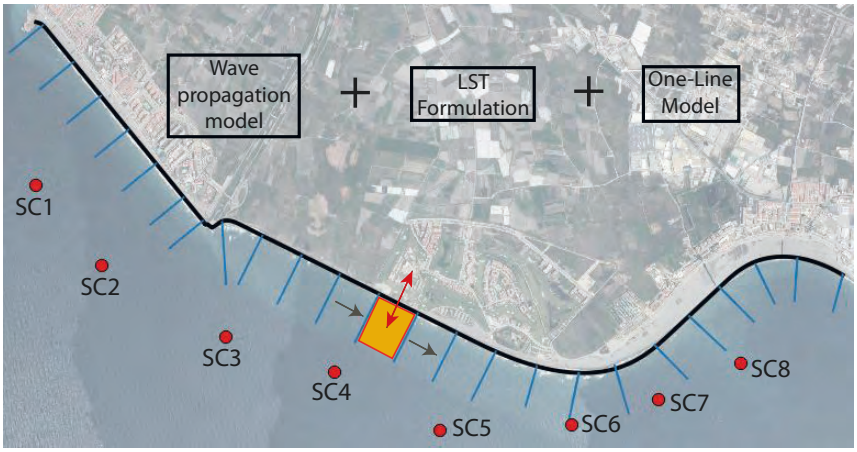

Fig. 3.8 Diagram of one-line model for shoreline evolution. Rodriguez-Delgado et al. (2018b).

Combining Eq. 3.4 and Eq. 3.5, this expression is obtained:

$$\Delta x \Delta y D = \frac{\partial Q}{\partial x} \Delta x \Delta t, \tag{3.6}$$

and finally, grouping terms and taking the limit as $\Delta t \to 0$, it is found that:

$$\frac{\partial y_s}{\partial t} = \frac{1}{D} \left(-\frac{\partial Q}{\partial x} \right). \tag{3.7}$$

This numerical scheme (LST formulation and one line model) was programmed in a Matlab script. To this end, the shoreline was divided in 340 cell points, one between each shore-normal profile. Therefore, the coordinates of the control points of the shoreline may be expressed as: $(x_n, y_{m,n})$ with $n = 1, 2, ..., 340$ indicating the control point and m the time point. The one line model was solved numerically using the following expression:

$$y_{s,m+1n} = y_{s,mn} + \frac{\Delta t}{D} \left(-\frac{Q_{mn+1} - Q_{mn}}{\Delta x} \right) \tag{3.8}$$

where $\Delta t = t_{m+1} - t_m$ is the time step and $\Delta x = x_{n+1} - x_n$ is the horizontal distance between two consecutive control points. The sediment fluxes are calculated using the aforemen-

tioned LST formulation in each time step. The stretch of coast is limited by Salobreña Rock and the Port of Motril (Chapter 4). Therefore, the no-flux condition ($Q_1 = Q_{340} = 0$) has been adopted as boundary condition. The initial position of the shoreline has been taken as the actual measured position. The depth of closure was taken from field measures comparing beach profiles from different campaigns. No movement in the beach profile was observed from 10 m water depth.

3.6 Shoreline state indicators

In order to quantify the impact produced by the wave farm on the coast in its lee, the significant wave height at breaking, LST rates and shoreline position of each scenario were compared to those obtained by the baseline (no-wave farm) scenario. This comparison was illustrated using different *ad-hoc* indicators.

To investigate the effects of these changes in the wave propagation patterns on the nearshore, the non-dimensional wave height reduction is defined as

$$\eta = 1 - \left(\frac{H_{s,br}}{H_{s,br0}} \right), \tag{3.9}$$

where $H_{s,br}$ and $H_{s,br0}$ are the significant wave height at breaking in the scenario considered and in the baseline scenario, respectively.

Changes in LST rates produced by the wave farm with respect the baseline case study were assessed by means of the non-dimensional LST rate reduction (τ), defined as,

$$\tau = 1 - \left(\frac{Q}{Q_0} \right), \tag{3.10}$$

where Q_0 and Q are, respectively, the LST rates in the baseline case and the case with wave farm under consideration.

For a proper comparison between the beach displacement under the different wave conditions, the non-dimensional shoreline advance is expressed as

$$\upsilon = \frac{\Delta y - \Delta y_0}{\max\left(|\Delta y_0|\right)}, \tag{3.11}$$

where Δy and Δy_0 are the total displacement of a generic shoreline point relative to its initial position in the scenario considered and the baseline scenario, respectively.

Chapter 4

Study Site

Playa Granada is a 3-km-long beach situated on the Mediterranean coast of southern Spain, facing the Alboran Sea (Fig. 4.1). Limited to the west by the Guadalfeo river mouth and to the east by Punta del Santo (a shoreline horn located at the former location of the river mouth), this beach belongs to the Guadalfeo deltaic coast, extending between Salobreña Rock and the Port of Motril. The morphodynamic response of the beach is dominated by the coarse gravel fraction (Bergillos et al., 2016c, 2017b).

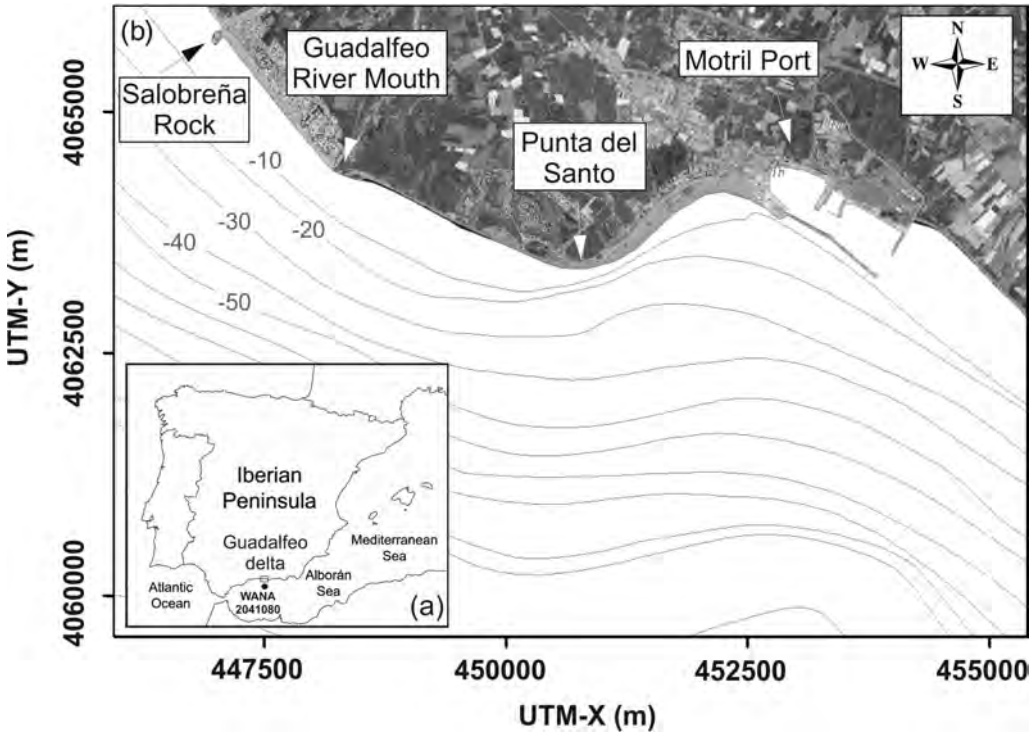

Fig. 4.1 (a) Location of the study site (Guadalfeo delta, southern Spain). (b) Plan view of the coast, including bathymetric contours (in meters) and the locations of Salobreña Rock, Guadalfeo River mouth, Punta del Santo and Motril Port. Rodriguez-Delgado et al. (2018b).

4.1 Metocean data

In this section, the available metocean data of Playa Granada is analysed in order to highlight the characteristics of the climate at the study site. The data series used was SIMAR 2041080 point provided by *Puertos del Estado* which is formed by more than 50 years of hourly data. The wave and wind climate, along with the astronomical tide and storm surge will be studied in the following subsections.

4.1.1 Wind climate

The region is subjected to the passage of Mediterranean storms and extra-tropical Atlantic cyclones, with average wind speeds of 18–22 m/s (Ortega-Sánchez et al., 2017), which generate wind waves under fetch-limited conditions (approximately 300 km). The most common observed wind velocity was between 1 m/s and 2 m/s (Figure 4.2). The maximum registered wind velocity was 20.6 m/s.

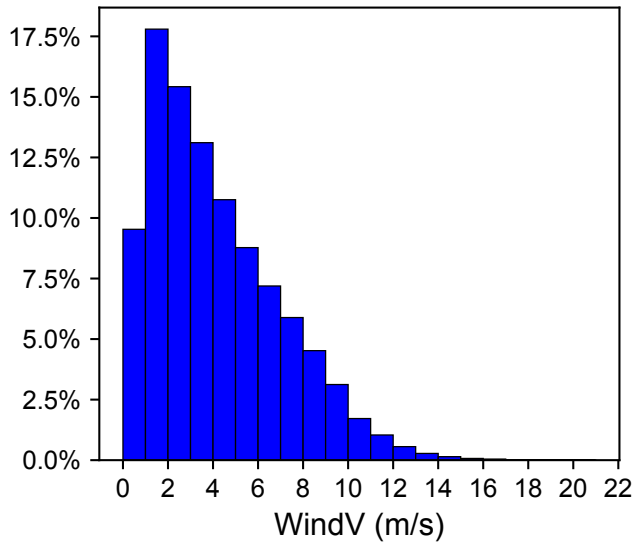

Fig. 4.2 Histogram of wind velocity.

As in the case of the wave climate, the wind climate is bidirectional. The prevailing wind directions are E (16.6%) and W (15.9%) followed by WSW (11%), ESE (10.4%) and WNW (10%). The distribution of wind directions at the study site is depicted in Figure 4.3.

Although wind data are not used in the modelling carried out in this research, the characteristics of the wind climate in Playa Granada is presented in this chapter in order

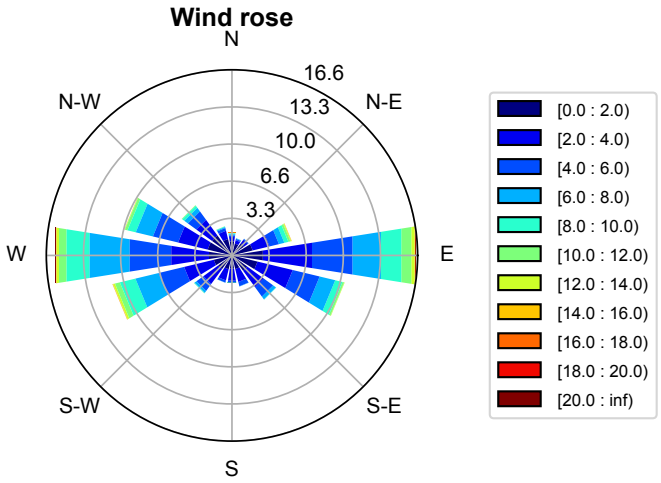

Fig. 4.3 Prevailing wind directions at Playa Granada. WindV (m/s), radial axis shows the percentage of wind states coming from each direction.

to show the origin of the bi-directional wave climate prevailing in the Southern Iberian Peninsula. This bi-directional wave climate, which will be studied in the next section, explains the behaviour of the LST in Guadalfeo Delta coast.

4.1.2 Wave climate

The most frequent significant wave height at the study site is between 0.4 m and 0.6 m (Figure 4.4). The significant wave heights in deep water with non-exceedance probabilities of 0.5, 0.99 and 0.999 are 0.5 m, 2.1 m and 3.1 m, respectively. The highest observed significant wave height was 5.1 m. The most frequent peak period is between 4.5 s and 5 s and the maximum observed period was 19.4 s.

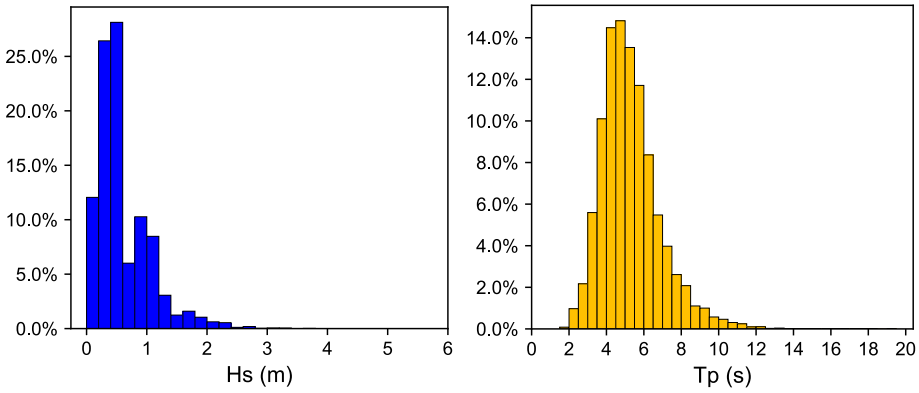

Fig. 4.4 Histograms of significant wave height (left) and peak period (right). Hourly data from 1958 to 2015.

The wave climate is bidirectional with prevailing east-southeast (Mediterranean storms) and west-southwest (extra-tropical cyclones) directions (Bergillos et al., 2016c). The prevailing wave directions are ESE (27%) and SW (26.7%) followed by E (20.6%) and WSW (17.3%). The distribution of wave directions at the study site is depicted in Figure 4.5. Wave-peak period and wave-mean direction bivariate tables are shown in Tables 4.1 and 4.2, respectively.

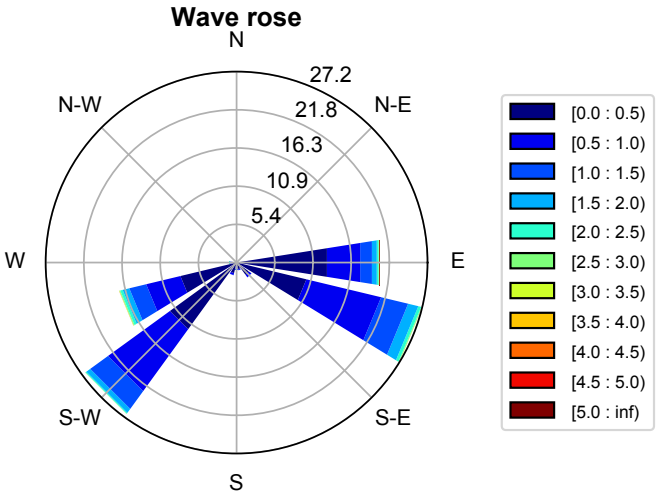

Fig. 4.5 Prevailing wave directions at Playa Granada. H_s (m), radial axis shows the percentage of sea states coming from each direction.

Table 4.1 Significant wave height - peak period bivariate table.

Hs (m)	Tp (s)										Total
	0.0-2.0	2.0-4.0	4.0-6.0	6.0-8.0	8.0-10.0	10.0-12.0	12.0-14.0	14.0-16.0	16.0-18.0	>18.0	
0.0-0.5	0.084	16.097	23.334	6.735	2.289	0.572	0.102	0.022	0.009	0.005	49.251
0.5-1.0	0.000	2.710	24.056	5.621	0.837	0.368	0.043	0.007	0.000	0.000	33.642
1.0-1.5	0.000	0.030	6.404	4.198	0.783	0.095	0.026	0.001	0.002	0.000	11.538
1.5-2.0	0.000	0.000	0.725	2.659	0.449	0.046	0.007	0.000	0.000	0.000	3.887
2.0-2.5	0.000	0.000	0.016	0.948	0.185	0.018	0.003	0.000	0.000	0.000	1.170
2.5-3.0	0.000	0.000	0.000	0.230	0.091	0.012	0.004	0.000	0.000	0.000	0.336
3.0-3.5	0.000	0.000	0.000	0.042	0.071	0.004	0.001	0.000	0.000	0.000	0.117
3.5-4.0	0.000	0.000	0.000	0.003	0.030	0.002	0.001	0.000	0.000	0.000	0.035
4.0-4.5	0.000	0.000	0.000	0.000	0.016	0.001	0.000	0.000	0.000	0.000	0.017
4.5-5.0	0.000	0.000	0.000	0.000	0.007	0.000	0.000	0.000	0.000	0.000	0.007
>5.0	0.000	0.000	0.000	0.000	0.001	0.000	0.000	0.000	0.000	0.000	0.001
Total	0.084	18.837	54.536	20.435	4.758	1.117	0.186	0.030	0.011	0.005	100.000

Climatic patterns at the study sites exhibit a significant contrast between summer and winter as showed in Figure 4.6. Higher significant wave heights are found between October and April, whereas wave heights between May and September are lower. The highest significant wave height of the data series was observed in January.

Extreme waves at the study site have been obtained by the annual maxima method. The highest significant wave height of each year of the data series have been extracted.

Table 4.2 Significant wave height - mean wave direction bivariate table.

Hs (m)	Direction																Total
	N	NNE	NE	ENE	E	ESE	SE	SSE	S	SSW	SW	WSW	W	WNW	NW	NNW	
0.0-0.5	0.012	0.032	0.015	0.022	13.045	10.240	2.145	0.957	0.886	1.552	11.754	8.243	0.227	0.059	0.036	0.026	49.251
0.5-1.0	0.010	0.037	0.009	0.009	4.800	10.965	0.469	0.179	0.163	0.295	10.909	5.018	0.567	0.109	0.059	0.043	33.642
1.0-1.5	0.000	0.001	0.000	0.001	1.697	3.960	0.021	0.012	0.015	0.029	3.143	2.480	0.159	0.009	0.004	0.008	11.538
1.5-2.0	0.000	0.000	0.000	0.000	0.700	1.497	0.002	0.001	0.000	0.001	0.695	0.974	0.017	0.000	0.000	0.000	3.887
2.0-2.5	0.000	0.000	0.000	0.000	0.242	0.425	0.000	0.000	0.000	0.000	0.152	0.351	0.000	0.000	0.000	0.000	1.170
2.5-3.0	0.000	0.000	0.000	0.000	0.082	0.109	0.000	0.000	0.000	0.000	0.025	0.119	0.001	0.000	0.000	0.000	0.336
3.0-3.5	0.000	0.000	0.000	0.000	0.027	0.036	0.000	0.000	0.000	0.000	0.013	0.041	0.000	0.000	0.000	0.000	0.117
3.5-4.0	0.000	0.000	0.000	0.000	0.010	0.005	0.000	0.000	0.000	0.000	0.002	0.017	0.000	0.000	0.000	0.000	0.035
4.0-4.5	0.000	0.000	0.000	0.000	0.004	0.002	0.000	0.000	0.000	0.000	0.002	0.009	0.000	0.000	0.000	0.000	0.017
4.5-5.0	0.000	0.000	0.000	0.000	0.002	0.001	0.000	0.000	0.000	0.000	0.001	0.004	0.000	0.000	0.000	0.000	0.007
>5.0	0.000	0.000	0.000	0.000	0.000	0.000	0.000	0.000	0.000	0.000	0.001	0.000	0.000	0.000	0.000	0.000	0.001
Total	0.022	0.070	0.024	0.033	20.609	27.240	2.637	1.149	1.064	1.878	26.696	17.256	0.970	0.177	0.099	0.078	100.000

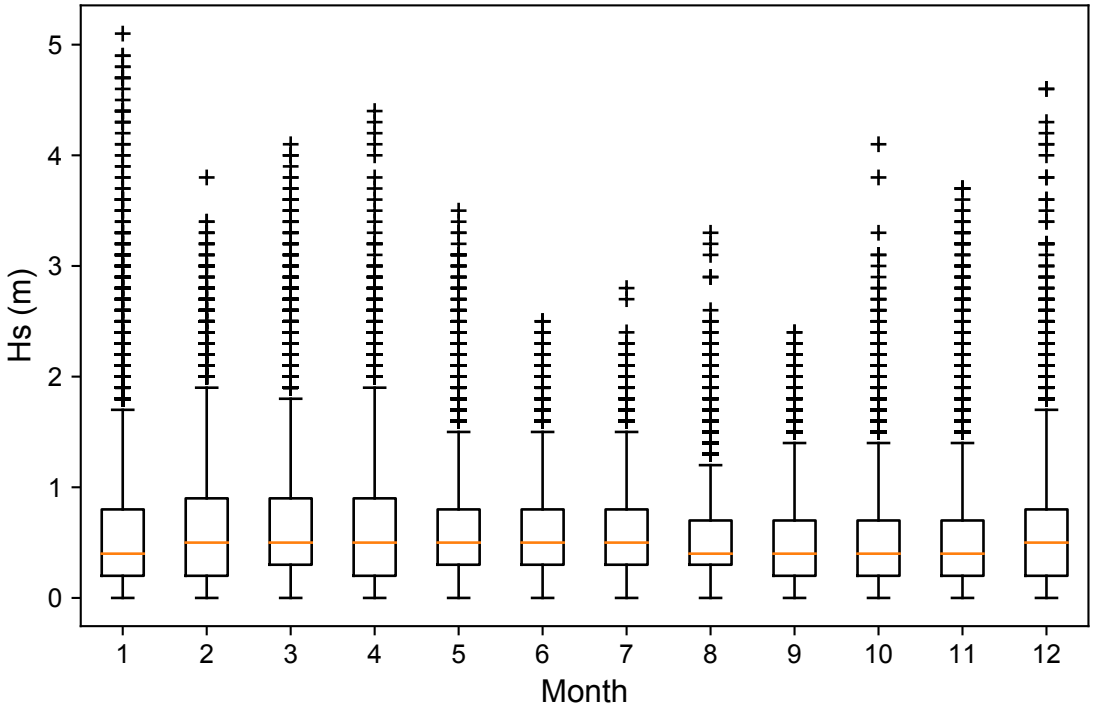

Fig. 4.6 Monthly boxplot of significant wave height at Playa Granada

The Gumbel distribution was then fitted to the annual maxima, obtaining a correlation coefficient $R^2 = 0.989$. The results are shown in Figure 4.7. Significant wave heights values for relevant return periods are depicted in Table 4.3.

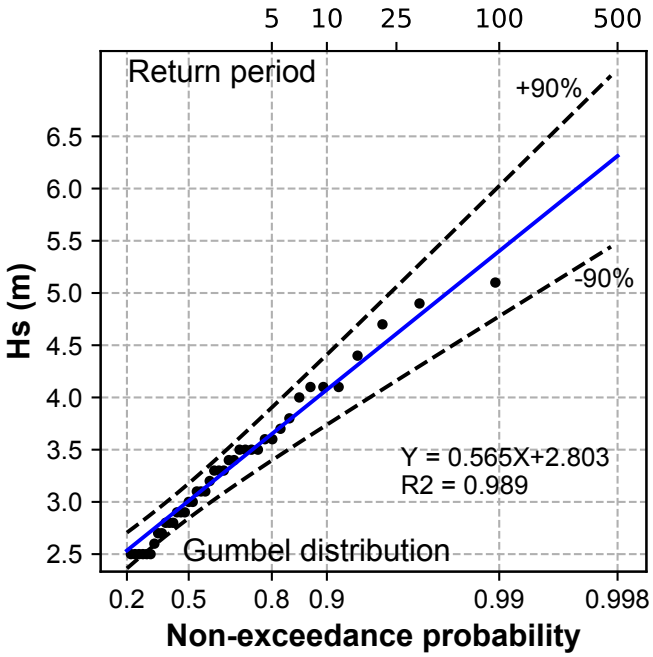

Fig. 4.7 Extreme wave climate at Playa Granada: measured data (points), fitted distribution (blue line), confidence intervals (dashed line).

Table 4.3 Extreme waves at the study site with 90% confidence intervals.

Return period (years)	H_s (m)	C.I. = 90%
5	3.65	3.90
10	4.07	4.41
25	4.61	5.06
50	5.01	5.54
100	5.40	6.03
200	5.79	6.51
500	6.31	7.14

4.1.3 Water level

Water level data from the tide gauge of the Motril Port has been analysed. It is a micro-tidal coast, with an astronomical maximum tidal range of ~ 0.8 m (Table 4.4), with the difference between mean high water spring (MHWS) and mean low water spring (MLWS) of ~ 0.6 m. Due to the lower astronomical tidal-range, tidal currents and circulation are

weak at this site (Jabaloy-Sánchez et al., 2014; Lobo et al., 2005). Storm surge may exceed 0.5 m.

Table 4.4 Tide levels at the Motril Port.

Tide level	Water level (cm)
HAT	40.88
MHWS	27.37
MLWS	-28.23
LAT	-42.12

4.2 Sediment transport

The particle size distribution on the beach is complex, including both sand and gravel sediment sizes. Although three fractions are predominant –sand (0.35 mm), fine gravel (5 mm) and coarse gravel (20 mm)– (Bergillos et al., 2015a), the morphodynamic response of the beach is dominated by the coarse gravel fraction due to the selective removal of the finer material (Bergillos et al., 2016c) and the reflective shape of the profile is similar to those found on gravel beaches (Masselink et al., 2010; Poate et al., 2013). Previous numerical works also demonstrated that the best fits to the measured profiles (Bergillos et al., 2016b, 2017a) and shorelines (Bergillos et al., 2017b) are obtained by assuming that the beach is made up of coarse gravel.

4.3 Site description

The Andalusian littoral of the Mediterranean Sea is characterised by the presence of high mountainous relief and short fluvial streams, and the main contributor of sediments to the beach is the Guadalfeo River (Bergillos et al., 2016d). Its basin covers an area of 1252 km^2, including the highest peaks in the Iberian Peninsula ($\sim 3,400$ m.a.s.l.), and the river is associated with one of the most high-energy drainage systems along the Spanish Mediterranean coast (Millares et al., 2014). The river was dammed 19 km upstream from its mouth in 2004 (Fig. 4.8), regulating 85% of the basin run-off (Losada et al., 2011). The total capacity of the Rules' Reservoir (117 hm^3) was planned to be used for the following purposes: irrigation (40%), supplies for residential developments along the coast (19%),

energy generation (9%), flood control (30%) and environmental flow (2%). However, the river damming modified the natural flow regime and altered the behaviour of the system downstream. According to Bergillos et al. (2016d), after the construction of the reservoir the coast has lost 0.3 hm^3 of sediments. The maximum impact has been produced around the Guadalfeo river mouth generating a maximum retreat of 87 m. The sediment volume in the beach profile decreased by up to 820 m^3, with maximum impact around the mouth (214 m^3). In absence of the reservoir, more than 2 hm^3 of sediments would have reached the coast. Figure 4.9 depicts the flown downstream Rules' dam from 1999 to 2014. As can be seen, since the construction of the reservoir the discharge to the river has been limited, being zero most of the time. Water is only discharged to the flow during storm events and the flow during the period observed has never exceed 50 m^3/s. Because of this limited impact, river discharge has not been taken into account in this research.

Fig. 4.8 Aerial photographs of the Guadalfeo River Delta before (left) and after (right) river damming. Rodriguez-Delgado et al. (2018a).

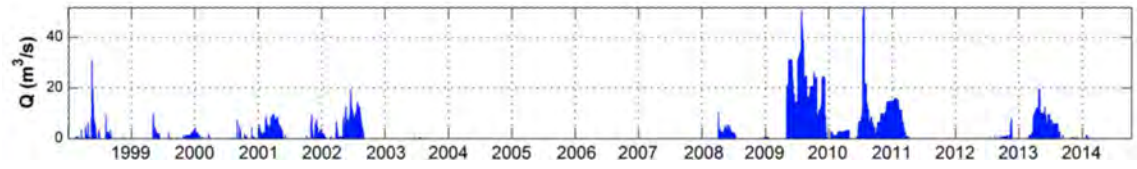

Fig. 4.9 Flow discharge downstream of Rules' dam (Bergillos et al., 2016d). Permission to reproduce this figure has been granted by AGU publications.

As a consequence, the deltaic coast, whose dynamics have been historically governed by the sediment supply of the river during intense events (Hoffmann, 1987; Jabaloy-Sánchez et al., 2014), currently presents coastline retreat and severe erosion problems (Figure 4.10). The stretch of Playa Granada has been particularly affected, with more severe coastline retreat in recent years than both the western (between Salobreña Rock and

Guadalfeo River Mouth) and eastern (between Punta del Santo and Motril Port) stretches (Bergillos et al., 2018a, 2016c).

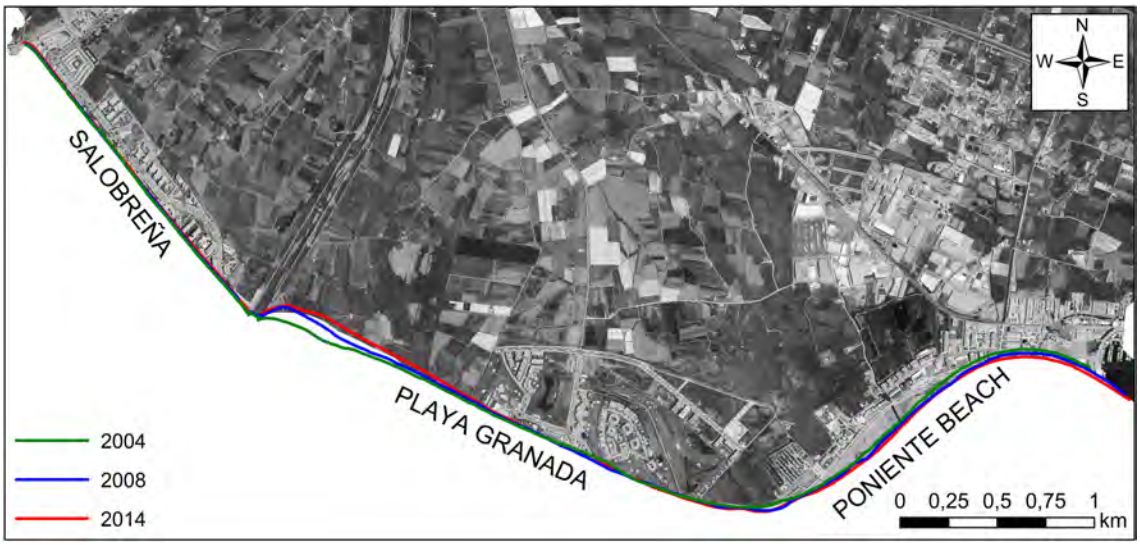

Fig. 4.10 Shoreline evolution since the Guadalfeo River damming in 2004. Rodriguez-Delgado et al. (2018b).

Playa Granada is occupied by farms, an exclusive resort, residential properties that are primarily summer homes, golf fields and restaurants. Hence, this stretch of beach has high environmental and tourism value, and its exploitation requires a large area of dry beach (Félix et al., 2012). For this reason, artificial nourishment projects have been frequent since the river damming (Bergillos et al., 2015b). However, the success of these interventions has been very limited (Fig. 4.11) since the loan material remained in place on average less than three months (Bergillos et al., 2017b; Ortega-Sánchez et al., 2017). The combination of erosion and gravel sediment along with this limited success of traditional, hard-engineering solutions make Playa Granada a suitable candidate to act as study site in this research.

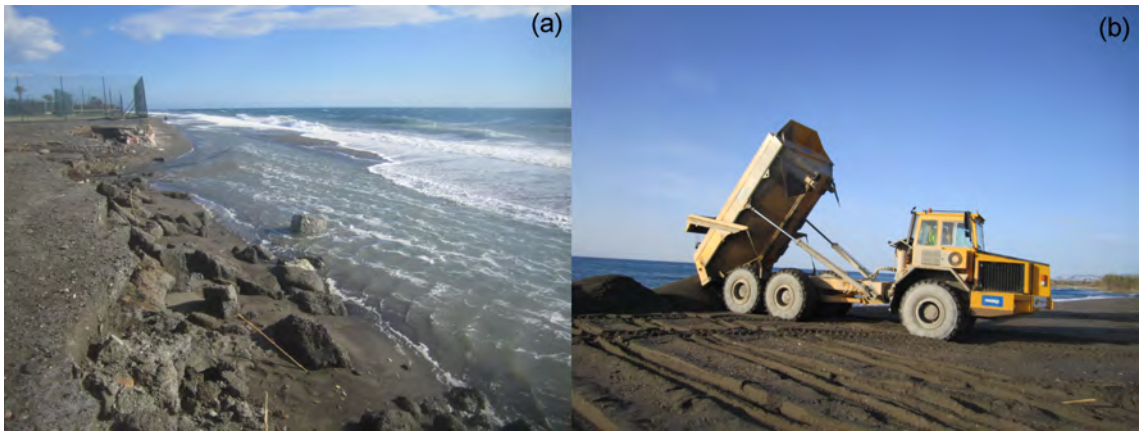

Fig. 4.11 Terminal erosion (a) and renourishment works (b) in Playa Granada. Rodriguez-Delgado et al. (2019).

Chapter 5

Results

5.1 Introduction

In this chapter, the results obtained after the application of the methodology described in Chapter 3 will be shown. In order to fulfil the specific objectives of this thesis, three aspects involved in the design of a wave farm project were taken into consideration: (i) the alongshore location of the farm, (ii) the wave farm layout and, (iii) the inter-device spacing. In order to study the effects of these parameters on the shoreline evolution, a wave propagation model (SWAN) was applied. This was the basis to study LST transport by means of a specific formulae and the shoreline displacement was assessed by means of a one-line model. In order to measure the impact produced by the wave farm on the coast, the results of each modelled wave farm were compared with the baseline scenario (without wave farm) using ad-hoc indicators. The study site selected was Playa Granada (Southern Iberian Peninsula) a gravel dominated beach suffering important erosion problems. Details about the study site were included in Chapter 4.

5.2 Setting up the modelling tools: baseline results

The focus of this thesis is to assess the impacts produced by a wave farm, measuring the variations with respect a baseline case study, the natural scenario in absence of wave farm. In the following sections, four variables will be analysed: wave propagation patterns, longshore sediment transport, shoreline evolution and dry beach surface. These variables

will be study by means of the ad-hoc indicators outlined in Chapter 3, which compare the results obtained by the different wave farm scenarios to the baseline. In this section, the results of the baseline scenario will be shown in order to illustrate the base benchmark for the modelled wave farms.

5.2.1 Wave propagation

Wave propagation patterns are dominated by the bidirectional wave climate which prevails in the study site. As can be observed in Figure 5.1, significant wave heights at the study site are bigger under westerly waves than under easterly sea states. The geography of the study site, which is divided by Punta del Santo into two stretches of coast of different alignment, shelters most of the study site from easterly waves. This phenomenon can be observed clearly in the particular case of Playa Granada (X-UTM = 4.485×10^5 to X-UTM = 4.507×10^5). In this beach, significant wave height reaches values of 3 m under westerly storms whereas in the case of easterly waves the significant wave height is about 1.5 m. A similar result is observed under low energy conditions, significant wave height under westerly waves is higher (about 0.4 m) than under easterly sea states (0.2 m). However, easterly sea states stills reach the easternmost area of the study site, to the east of Punta del Santo, where are situated between Poniente Beach and the Motril Port.

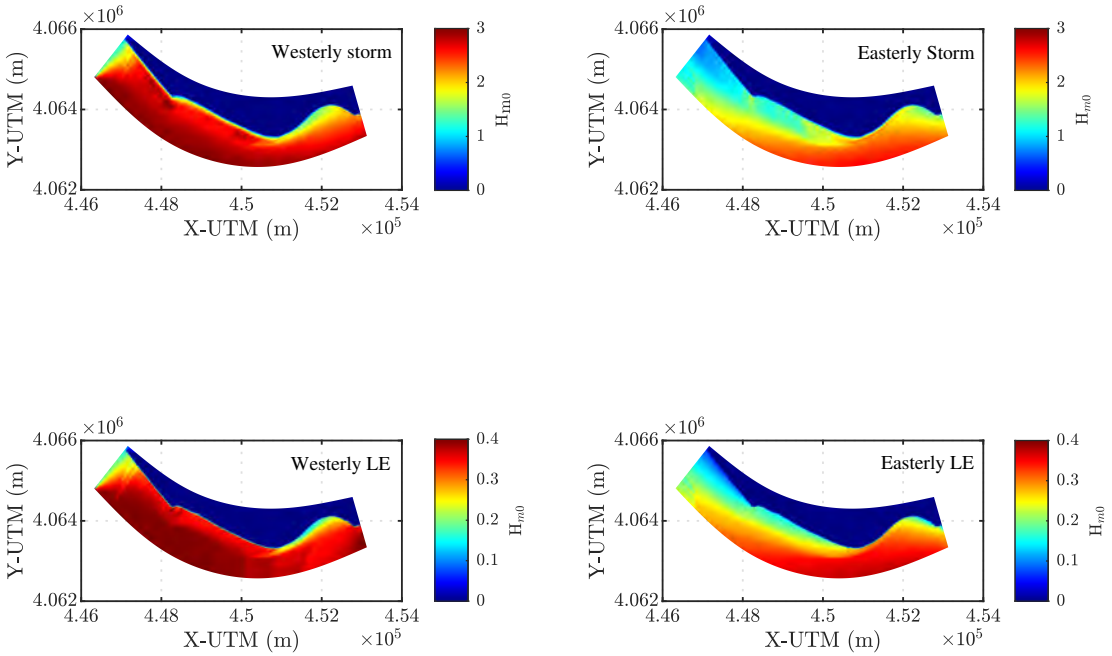

Fig. 5.1 Spectral significant wave height at the study site. Baseline scenario.

5.2.2 Longshore sediment transport

Based on the results of the wave propagation, LST rates have been obtained by means of Van Rijn (2014) formulation. The sea states studied have been modelled for a duration of 48 h in order to illustrate the dynamics present at the system. The system behaviour is different for storms coming from west and east directions (Fig. 5.2. For the westerly storm, the minimum volume transported is about 100 m^3 whereas this volume is increased in the central stretch of the beach (X-UTM about 4.497×10^5) reaching more than 200 m^3. The positive values mean that the sediment transport comes from the west towards the east. In the case of the easterly storm, the minimum sediment volume is obtained in the west end of the beach (X-UTM = 4.485×10^5) with -100 m^3. The sediment volume transported increase to the east reaching a maximum of almost -300 m^3. The negative values indicate transport from east to west. Sediment transport volume for low energy sea states are lower, as might be expected.

The results show that the area where the maximum transport is found is just the zone where the resorts and recreative areas are found (from X-UTM = 4.493×10^5 to X-UTM = 4.505×10^5). This is especially important for the westerly storm as the LST rates shows that erosion exist in this area (sediment transport increasing from X-UTM = 4.495×10^5 to X-UTM = 4.497×10^5). This material is deposited eastwards in the east end of the beach (Punta del Santo). In the case of the easterly storm the LST rates show transport from east to west, with material deposition in the west end (sediment transport decreasing in absolute value from X-UTM = 4.49×10^5 to X-UTM = 4.485×10^5).

5.2.3 Shoreline evolution

The one-line model has been applied to obtain the evolution of the shoreline along the 48 h modelled. Under the westerly storm the results confirm the observations made in the previous section (Fig. 5.3). The greatest change of position happens from X-UTM = 4.495×10^5 to X-UTM = 4.5×10^5. In the easternmost part of the beach, the shoreline suffers accretion reaching a maximum advance of about 0.2 m in X-UTM = 4.5×10^5. This accretion is turned into erosion in the western part of the beach, with a maximum retreat of the shoreline of up to 0.18 m. These results suggest that for westerly storms, the sediments

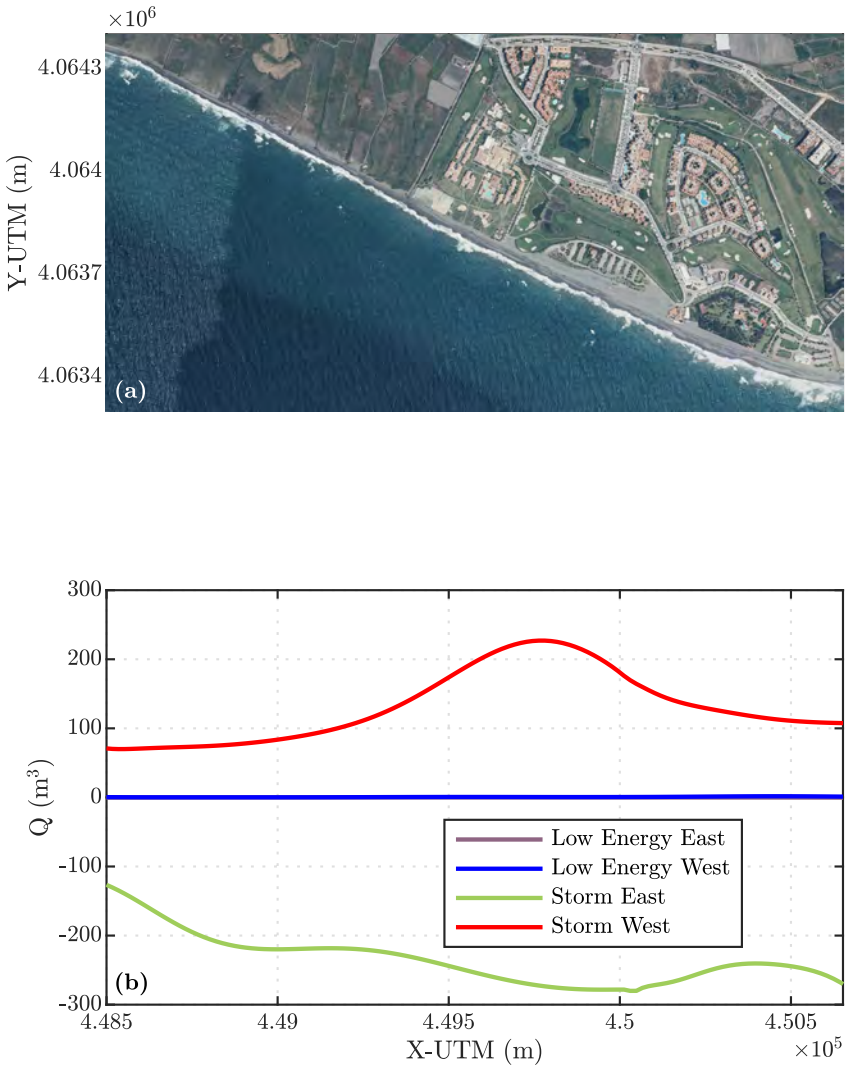

Fig. 5.2 (a) Aerial photograph of Playa Granada. (b) Sediment volume transported after 48 h. Baseline scenario.

present at Playa Granada are transported to the east from the west part of the Beach, as expected.

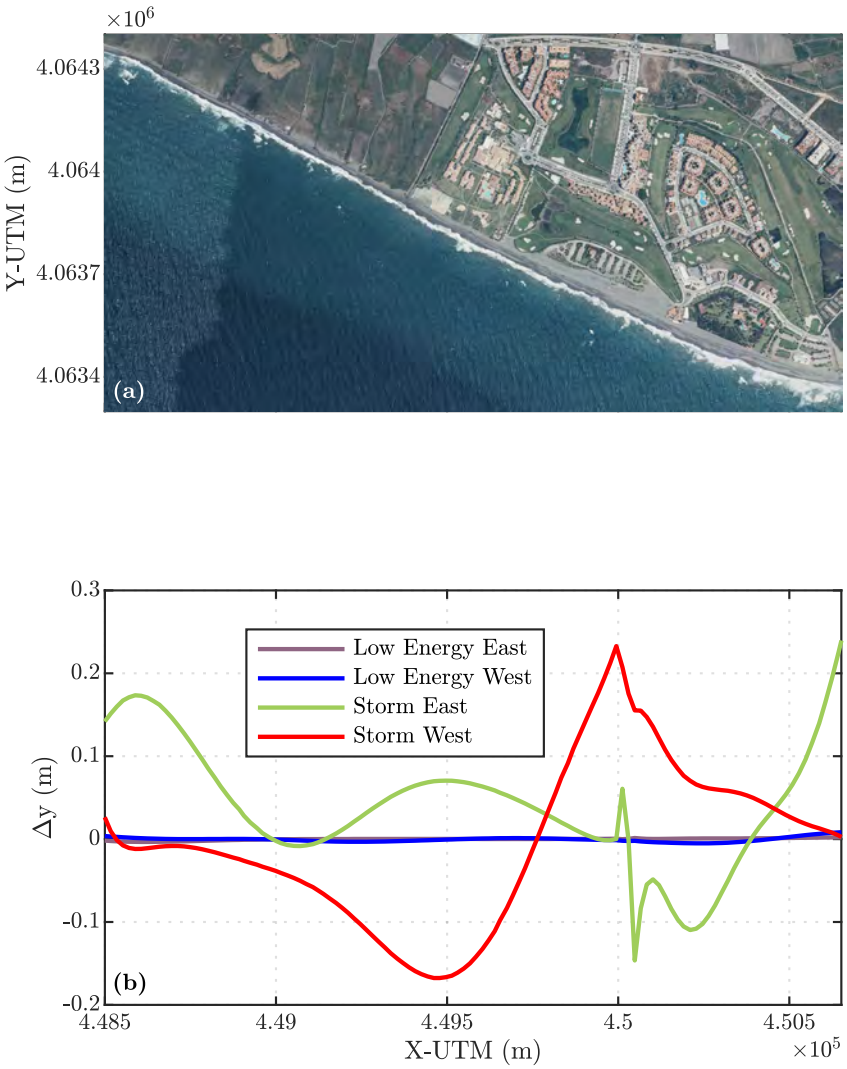

Fig. 5.3 Vertical coordinate difference between the initial position of the shoreline and the final position after 48 h. Positive (Negative) values mean advance (retreat).

In the case of the easterly storm accretion dominates in the stretch of coast. Three areas of accretion are observed, one in the west end of the beach (from X-UTM = 4.485×10^5 to X-UTM = 4.49×10^5), a second in the central part (from X-UTM = 4.49×10^5 to X-UTM = 4.5×10^5) and finally, the third one in the east end. The irregularities observed in the transition between accretion and erosion (X-UTM = 4.5×10^5) are due to the numerical scheme used for the calculation which is very sensitive to changes of alignment of the coast. Maximum accretion is found in the east end (an advance of more than 0.2 m), whereas maximum erosion is about 0.1 - 0.15 m (X-UTM = 4.5×10^5).

Changes in position of the shoreline are lower under low energy conditions and the movements correspond to the beach ends. Under westerly waves the bigger erosion is situated in the east part (from X-UTM = 4.5×10^5 to X-UTM = 4.505×10^5) and the bigger accretion in the east end. Whereas under easterly waves almost no changes in position are observed, with just little erosion in the west end.

In terms of dry beach area, the westerly storms produce a total loss of 16.6 m^2 in the whole stretch of coast. This is because in these conditions the majority sediments are transported inside Playa Granada. However, in the west part of the beach more than 87 m^2 are lost. By contrast, under the easterly storm accretion dominates with an increase of dry beach area of 87.9 m^2. In this case, erosion is concentrated in a narrow stretch of about 500 m, producing a loss of 27.62 m^2 after 48 h. In the rest of Playa Granada accretion produce an increase of 115.5 m^2. The low energy sea states produce a much lower impact, with loss of sediments of 1.6 m^2 and 0.4 m^2 for westerly and easterly waves, respectively.

5.3 Wave farm position impact study

A retreat in the position of the shoreline in coastal areas modifies negatively the available dry beach surface which means a loss of economic, environmental and social value of the zone. Long-term changes in the shoreline position are mainly driven by the longshore sediment transport (LST) of the coastal system. In order to provide an effective coastal protection by means of a wave farm, the effects produced in the LST by the alongshore position of the farm need to be studied. Therefore, the position of the wave farm inside the coastal system should be optimised in order to maximise the dry beach surface area available.

The main objectives of this section are to investigate: (i) the role of the longshore position of the wave farm in the nearshore wave propagation patterns under both storm and low-energy conditions, (ii) the resulting changes in the longshore sediment transport trends and (iii) the consequences for the shoreline evolution and therefore, the dry beach area on a gravel-dominated deltaic coast (Playa Granada, southern Spain). To this end, eight wave farm situated in different alongshore positions were studied. The applied workflow is illustrated in Figure 5.4.

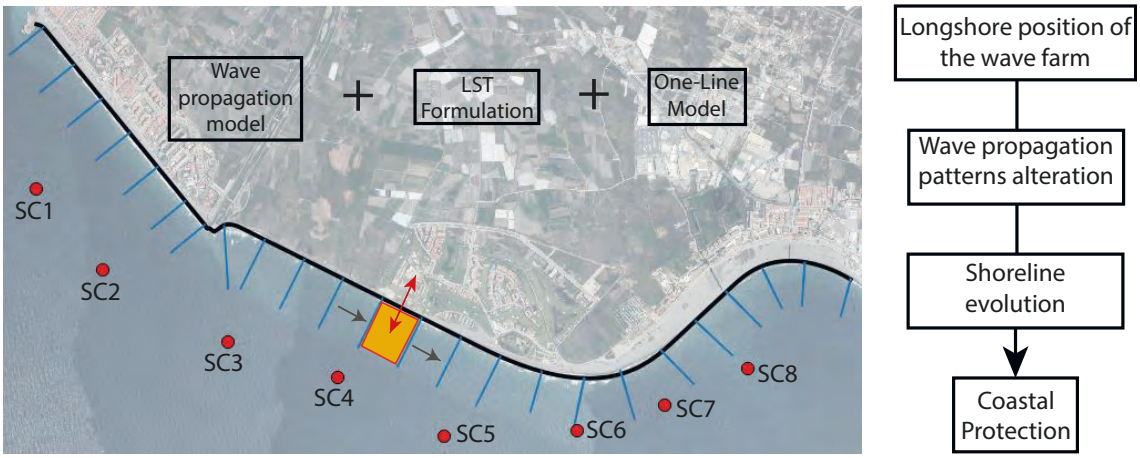

Fig. 5.4 Position sensitivity study workflow. Rodriguez-Delgado et al. (2018b).

5.3.1 Wave propagation patterns

Wave energy extraction by means of the wave farm decreases the significant wave height leewards. The reductions in H_s for scenarios 2, 4, 6 and 8 under both easterly and westerly storms are shown in Figure 5.5. The shape and spread of the reduction are driven by both the wave farm location and the incoming wave direction. Under westerly storm conditions, the effects of the wave farm in scenarios 2 and 4 are concentrated in the Guadalfeo river mouth and Playa Granada. However, the easterly storm spreads the reduction in H_s up to Salobreña Rock (Fig. 5.5). In scenarios 6 and 8, the impact of the farm reaches the Port of Motril under westerly storm conditions; whereas under easterly storms the wave farm leads to a reduction in H_s in the section of Playa Granada for scenario 6, and in Poniente Beach for scenario 8. The trends of the significant wave heights variations are similar under low-energy conditions and for the rest of scenarios, but with changes of lower magnitude and different longshore positions of the beach section affected, respectively.

5.3.2 Grid sensitivity

In order to measure the sensitivity of the model to grid changes, a grid sensitivity analysis was carried out. A greater nested grid, which covers the nearshore area up to a deeper bathymetric line was defined (Fig. 5.6). This greater nested grid coverage allows to assess the irregularities that the interaction between the wave farm shadow and the incoming waves from the south border of the grid could produce in the results of the model. The cell size is kept equal to the smaller nested grid (25x15 m).

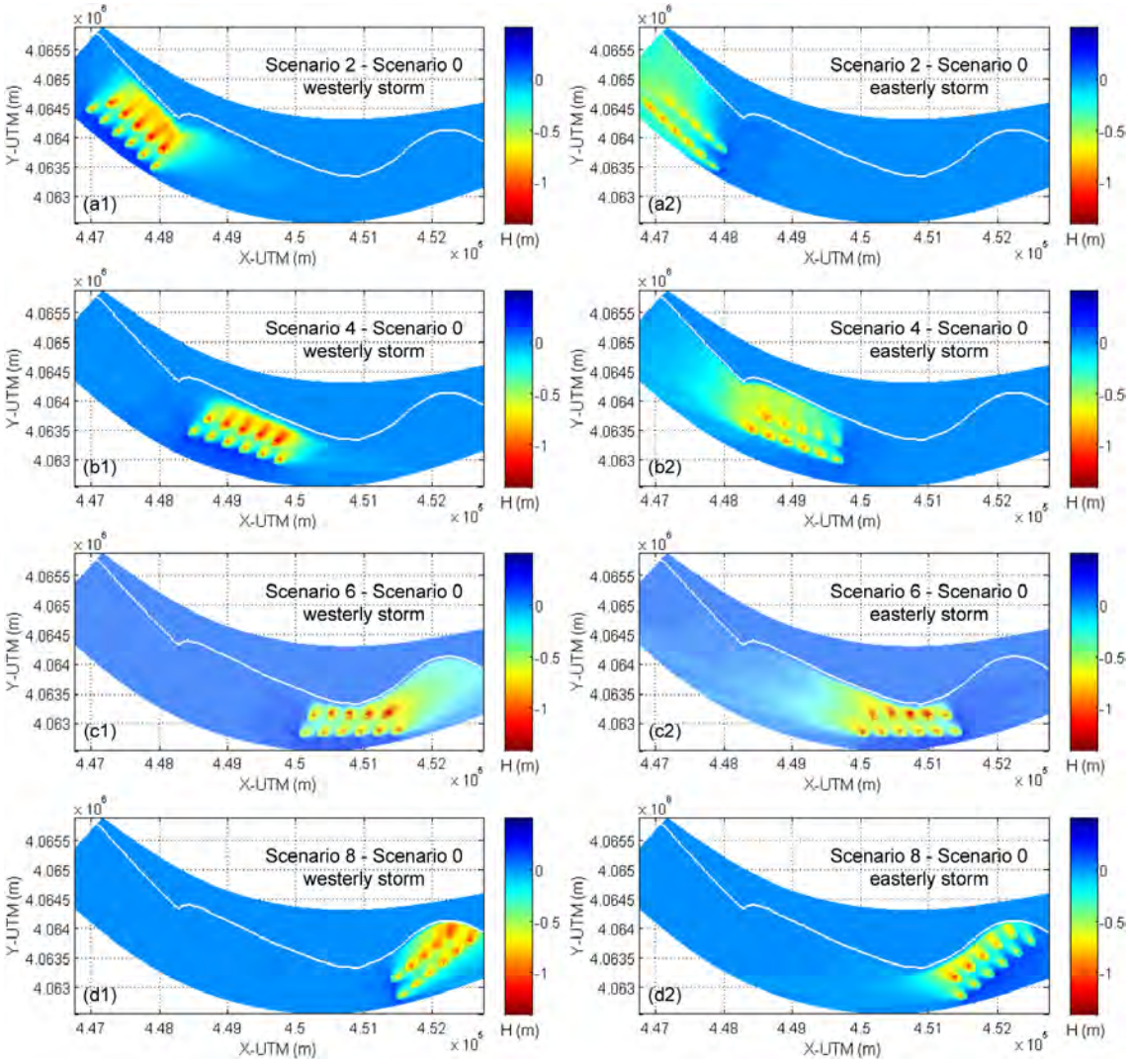

Fig. 5.5 Variation in significant wave height induced by the presence of the wave farm under westerly (1) and easterly (2) storm waves: (a) scenario 2, (b) scenario 4, (c) scenario 6, (d) scenario 8. The shoreline position is indicated with a white line. Rodriguez-Delgado et al. (2018b).

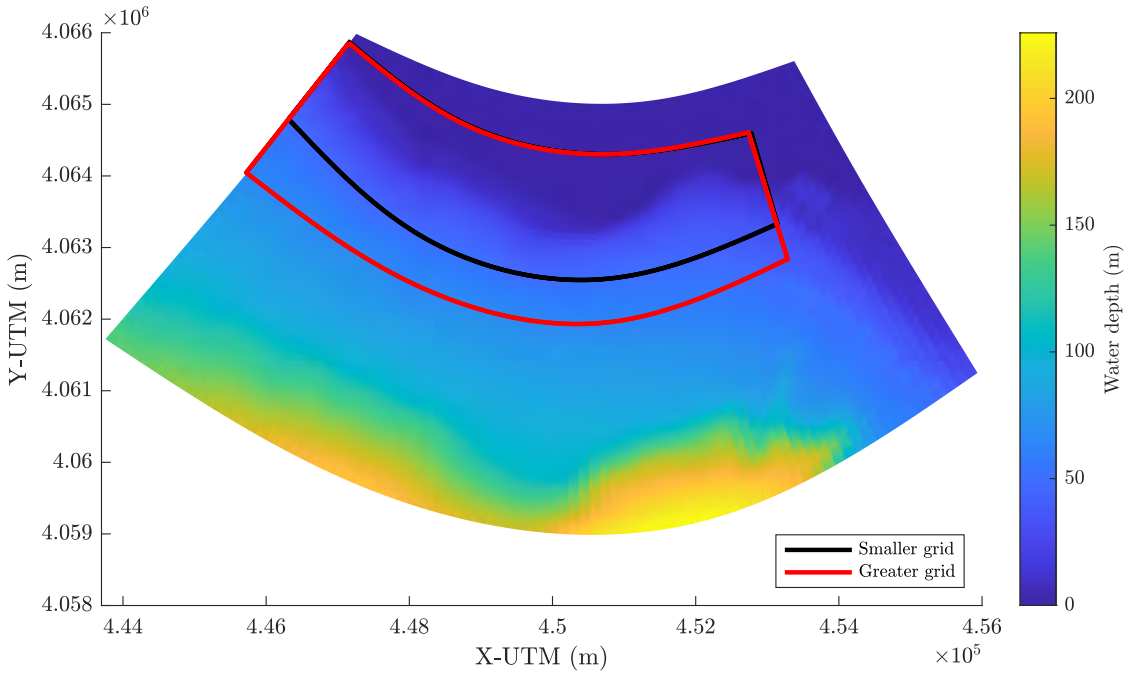

Fig. 5.6 Grid size comparison.

The wave propagation model was run using this new nested grid and the results were compared to the one obtained with the smaller grid. Once the model was run in both nested grids, the results of the greater nested grid were interpolated in the cells of the smaller grid. In order to assess the changes in significant wave height of the results of the model using each nested grid the following equation was used:

$$H_{m0,dif} = \frac{|H_{m0,greater} - H_{m0,smaller}|}{H_{m0,smaller}} \tag{5.1}$$

The results show that the variations are low in the majority of the grid (Fig. 5.7). The greatest variation (about 10%) is found in the east end of the grid due to boundary effects. In the studied stretch of coast variations are much lower, non-exceeding 2 - 3 %. The accuracy of the results is ensured by the calibration carried out (Section 3.2.4). Smaller sizes of the nested grid are discarded because: (i) to ensure a proper nesting it is recommended that the nested grid cell size was at least the coarse grid cell size divided by 5 and (ii) cell sizes smaller than 15 m do not converge in the wave propagation model.

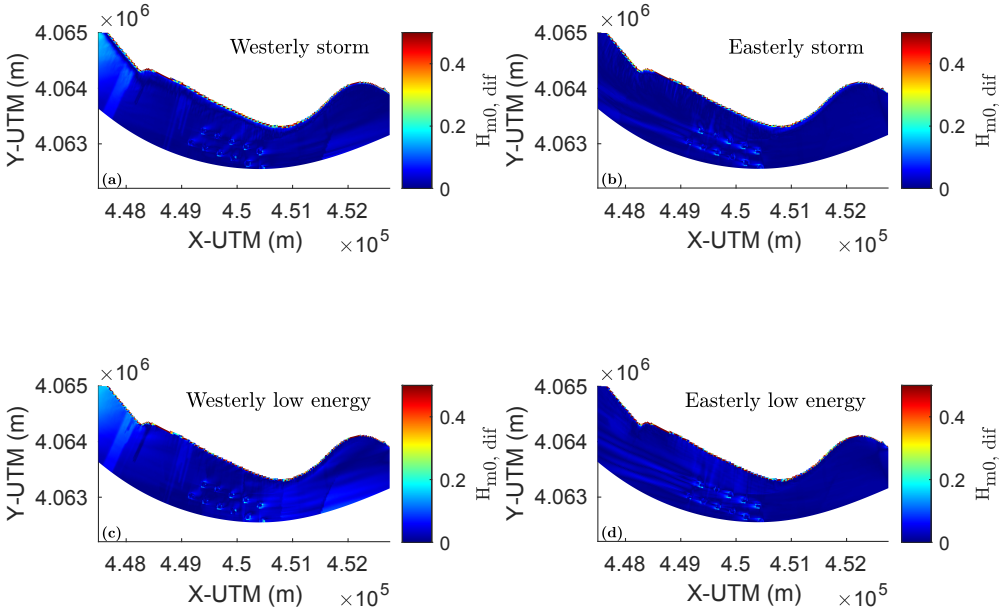

Fig. 5.7 Significant wave height differences between the greater and smaller grids. Scenario 5.

5.3.3 Breaking line

The breaking line is obtained by means of the result of the wave propagation model. The fraction of waves breaking at each cell is calculated by SWAN model based on the depth-induced breaking by means of the bore based model of Battjes and Janssen (1978). The breaking line has been fixed in those cells whose fraction breaking is 5% (Van Rijn, 2014). Once the breaking line has been identified, the breaking parameters (significant wave height and mean direction) are taken from those cells. In order to illustrate the changes in position of the breaking line in the different scenarios, the water depth at breaking has been obtained (Fig 5.8).

Water depth at breaking varies from storm to low energy conditions. Under storm conditions, water depth at breaking ranges from 1.4 m to 1.8 m along Playa Granada. It is minimum at the extremes of the stretch of coast whereas it increases up to 1.8 m in two peaks (X-UTM = 4.487 $\times 10^5$ m and X-UTM = 4.497 $\times 10^5$ m). Under low energy conditions, the water depth at breaking varies between the different scenarios. It is higher under westerly waves, ranging from 0.2 m to 0.8 m whereas it ranges from 0.1 to 0.35 m under easterly waves. Under westerly waves, scenarios 2, 6 and 8 follow a similar pattern.

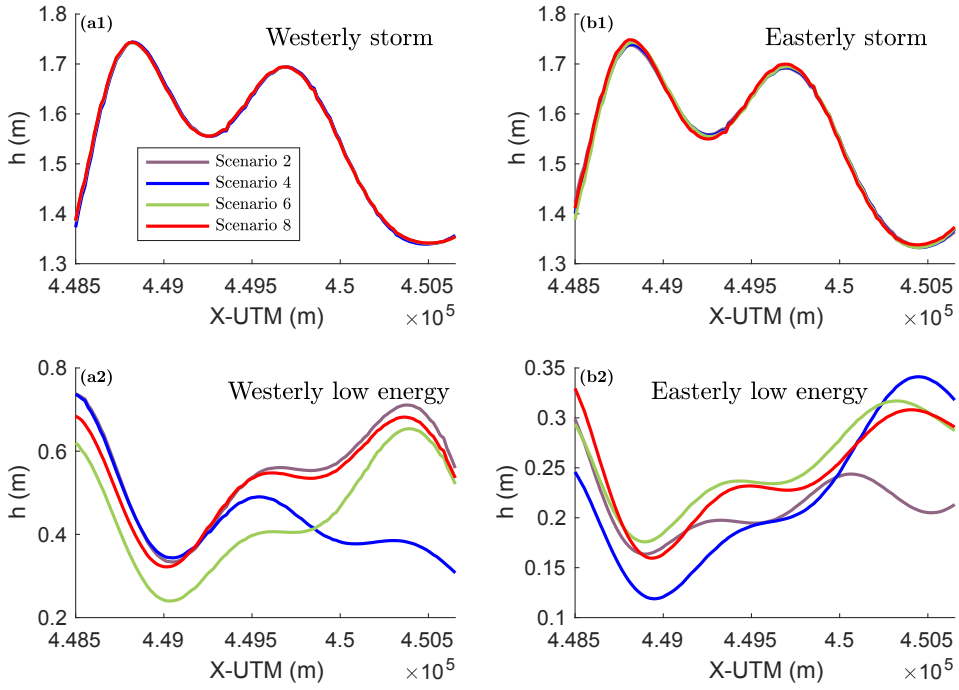

Fig. 5.8 Water depth at breaking for scenarios 2, 4, 6 and 8 under westerly (a) and easterly (b) storms (1) and low energy (2) conditions.

They reach the maximum in the westernmost end of the beach, decreasing up to reach a minimum at X-UTM = 4.49 $\times 10^5$ m, and from then increasing up to the east end. However, scenario 4 follows a similar pattern up to X-UTM = 4.49 $\times 10^5$ m, but from then it reaches a peak at X-UTM = 4.495 $\times 10^5$ m and then decreasing again up to the east end. In this sense, it is clear the influence of the wave farm which in scenario 4 is situated just in front of Playa Granada, decreasing the significant wave height and consequently the water depth at breaking. A similar pattern is observed under easterly low energy conditions, but in this case the reduction of breaking water depth in scenario 4 is observed at the west part of Playa Granada.

5.3.4 Wave height at breaking

The longshore variation of the non-dimensional wave height at breaking along the section of Playa Granada is shown in Figure 5.9. Under the westerly storm, scenarios 3 and 4 produce a non-dimensional alongshore-averaged wave height reduction of 2.1% and 2.3%, respectively. Scenario 5 leads to $\overline{\eta} = 0.6\%$, whereas in scenario 6 this value is a mere 0.3%. The rest of the scenarios do not produce significant changes with respect to the

baseline ($\overline{\eta} < 0.1\%$). Values of the non-dimensional wave height reduction are greater for the easterly storm. Scenario 5 has the best performance in terms of coastal protection with $\overline{\eta} = 16.4\%$, followed by scenario 4 ($\overline{\eta} = 12.4\%$), whereas in scenario 6 it reaches 7.8%. For scenarios 8, 7 and 3 the alongshore-averaged value of the non-dimensional wave height reduction is equal to 1.9%, 1.8% and 1.2% respectively; whereas the impact is considerably weaker in the case of scenarios 1 and 2, with $\overline{\eta}$ below 0.4%. The negative values observed mean an increase of significant wave height at breaking with respect the baseline. These are due to wave reflection by the WECs that makes possible that the wave height is slightly higher than in the baseline scenario.

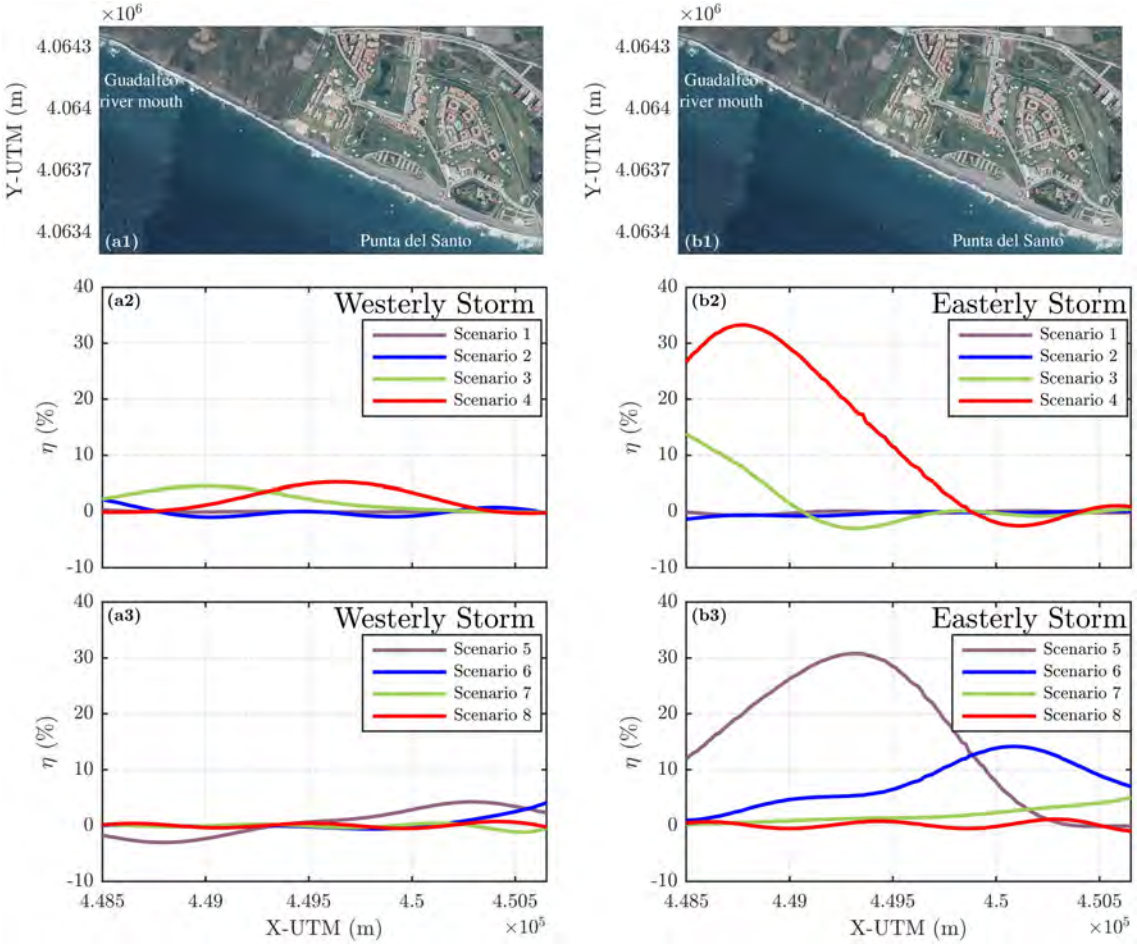

Fig. 5.9 Non-dimensional wave height reduction under westerly (a) and easterly (b) storm conditions: scenarios 1-4 (2), scenarios 5-8 (3). Rodriguez-Delgado et al. (2018b).

Regarding the low-energy conditions, the reduction achieved is higher in relative terms, as shown by the non-dimensional wave height reduction (Fig. 5.10). In the case of the westerly mean direction, scenario 4 presents the highest alongshore-averaged value of η, ($\overline{\eta} = 22.2\%$), followed by scenario 5, with 18.4%. In scenario 3 this value is equal to

17%, whereas scenarios 2 and 6 lead to smaller differences: 6.3% and 5.3%, respectively. Scenarios 1, 7 and 8 do not produce significant changes in $H_{s,br}$. The reductions produced by the wave farm for easterly low-energy waves are similar. Scenarios 6 and 5 produce $\overline{\eta} = 23.9\%$ and $\overline{\eta} = 18.9\%$, respectively, whereas the reduction achieved in scenario 7 is 11.7%, and in scenario 4, 9.5%. The rest of the scenarios have a lower impact, with $\overline{\eta} < 2.5\%$.

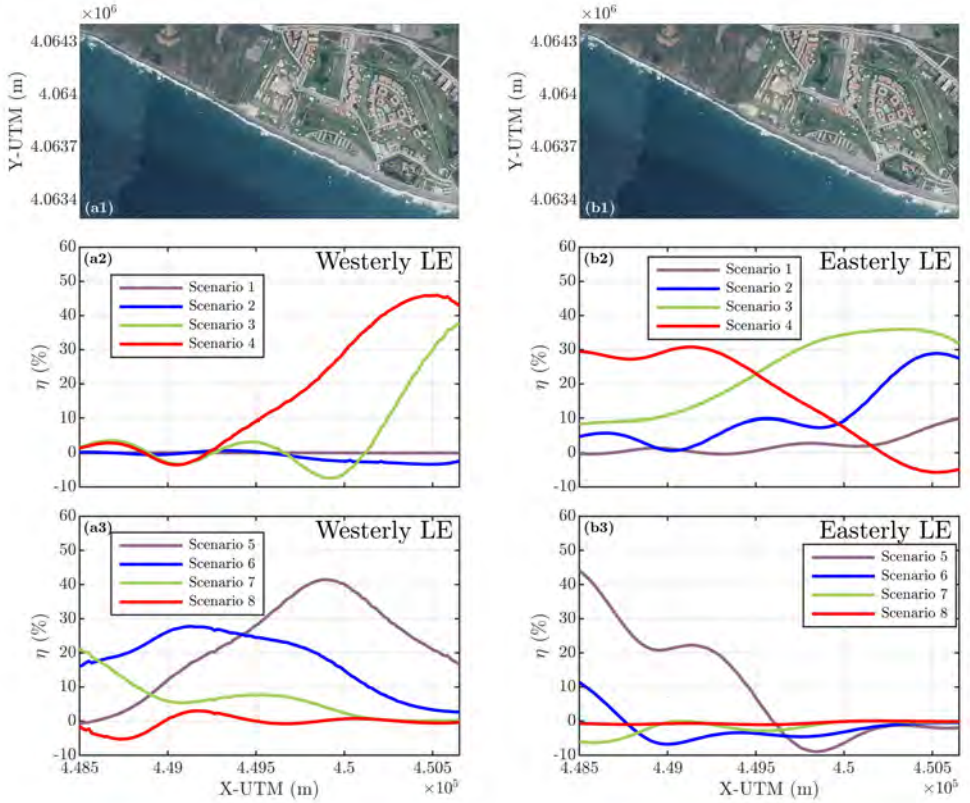

Fig. 5.10 Non-dimensional wave height reduction under westerly (a) and easterly (b) low energy conditions: scenarios 1-4 (2), scenarios 5-8 (3). Rodriguez-Delgado et al. (2018b).

5.3.5 Longshore sediment transport rates

The longshore variations of the LST rates along Playa Granada, modelled with the formulation of Van Rijn (2014) (Eq. 3.3), are described in this section.

Non-dimensional LST rate reduction values under storm conditions are depicted in Figure 5.11. Under the westerly storm, in scenario 4, LST rate reduction increases from the Guadalfeo River mouth to the central part of Playa Granada, and then, decreases towards Punta del Santo, whereas in scenarios 3 and 5 the maximum value of τ is displaced towards

the west and east, respectively. The greatest value of the non-dimensional alongshore-averaged LST reduction is achieved in scenario 4 with a 22%, followed by scenario 3, with a reduction of 20.3%. The values induced by scenarios 2, 5 and 6 were significantly lower (7.6%, 5.3% and 3.2% respectively); whereas in scenarios 1, 7 and 8 there is almost no difference with respect to scenario 0 ($\overline{\tau} < 1\%$). In some scenarios negative values are observed, presumably due to increases in H_s due to the interaction between the wave field and the farms.

Changes in LST rates between the baseline (no-farm) situation and the wave farm scenarios are more pronounced under easterly storm conditions, influenced by the wave height reduction (Fig. 5.9) and the position of the wave farm which increases the shelter under easterly waves. In this case, $\overline{\tau}$ value reaches up to 44.6% in scenario 5; whereas the non-dimensional alongshore-averaged LST rate reduction in scenarios 4 and 6 are 30.2% and 30.5%, respectively. On the other hand, $\overline{\tau}$ values in scenarios 3, 7 and 8 are 5.8%, 9.5% and 1.4%, respectively. Finally, scenarios 1 and 2 do not induce significant changes in LST rates, with $\overline{\tau} < 1\%$.

Following the same trend as the non-dimensional wave height reduction, τ values under low-energy conditions are greater than those under storm conditions (Fig. 5.12). Under westerly waves, scenario 4 experienced the greater value of the non-dimensional alongshore-averaged LST rate reduction ($\overline{\tau} = 64.6\%$), followed by Scenarios 5 and 3, with 40.3% and 39.6%, respectively. For their part, these values in scenarios 6 and 2 are 25.4% and 14.6%, respectively. Scenarios 1, 7 and 8 present the lowest reductions ($\overline{\tau} < 5\%$). In the case of the low-energy conditions with easterly mean wave direction, the most pronounced reduction is achieved in scenario 6 ($\overline{\tau} = 60.6\%$), followed by scenario 5 ($\overline{\tau} = 47.7\%$), scenario 7 ($\overline{\tau} = 34.3\%$) and scenario 4 ($\overline{\tau} = 29.8\%$). Finally, non-dimensional alongshore-averaged LST rate reduction in scenario 8 is 8.9%, whereas the values of this parameter in scenarios 1, 2 and 3 are under 5%.

5.3.6 Shoreline evolution

Changes in the shoreline geometry of Playa Granada under westerly storm conditions, assessed by means of the one-line model, are shown in this section.

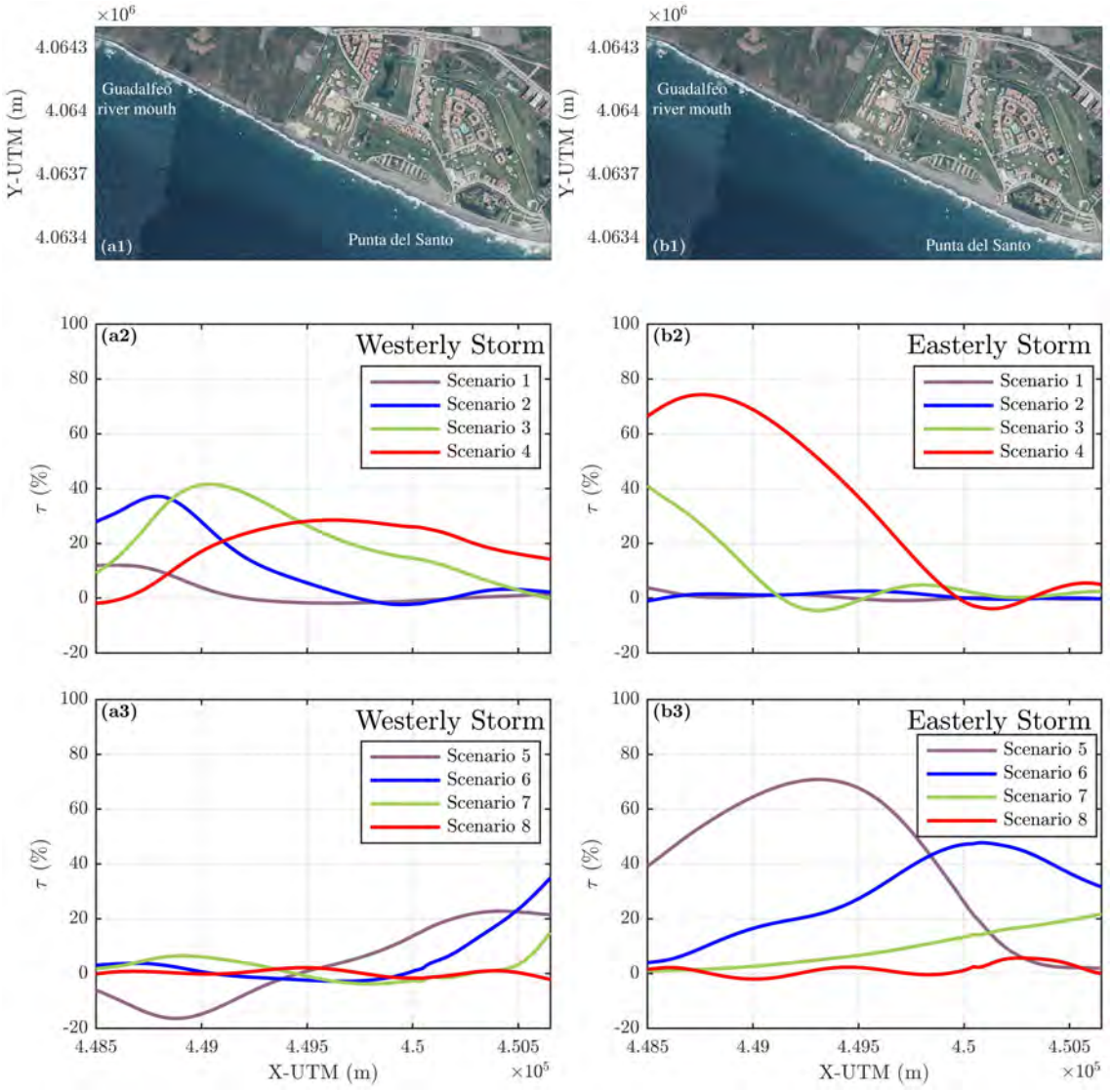

Fig. 5.11 Non-dimensional LST rate reduction under westerly (a) and easterly (b) storm conditions: (2) scenarios 1-4, (3) scenarios 5-8. Rodriguez-Delgado et al. (2018b).

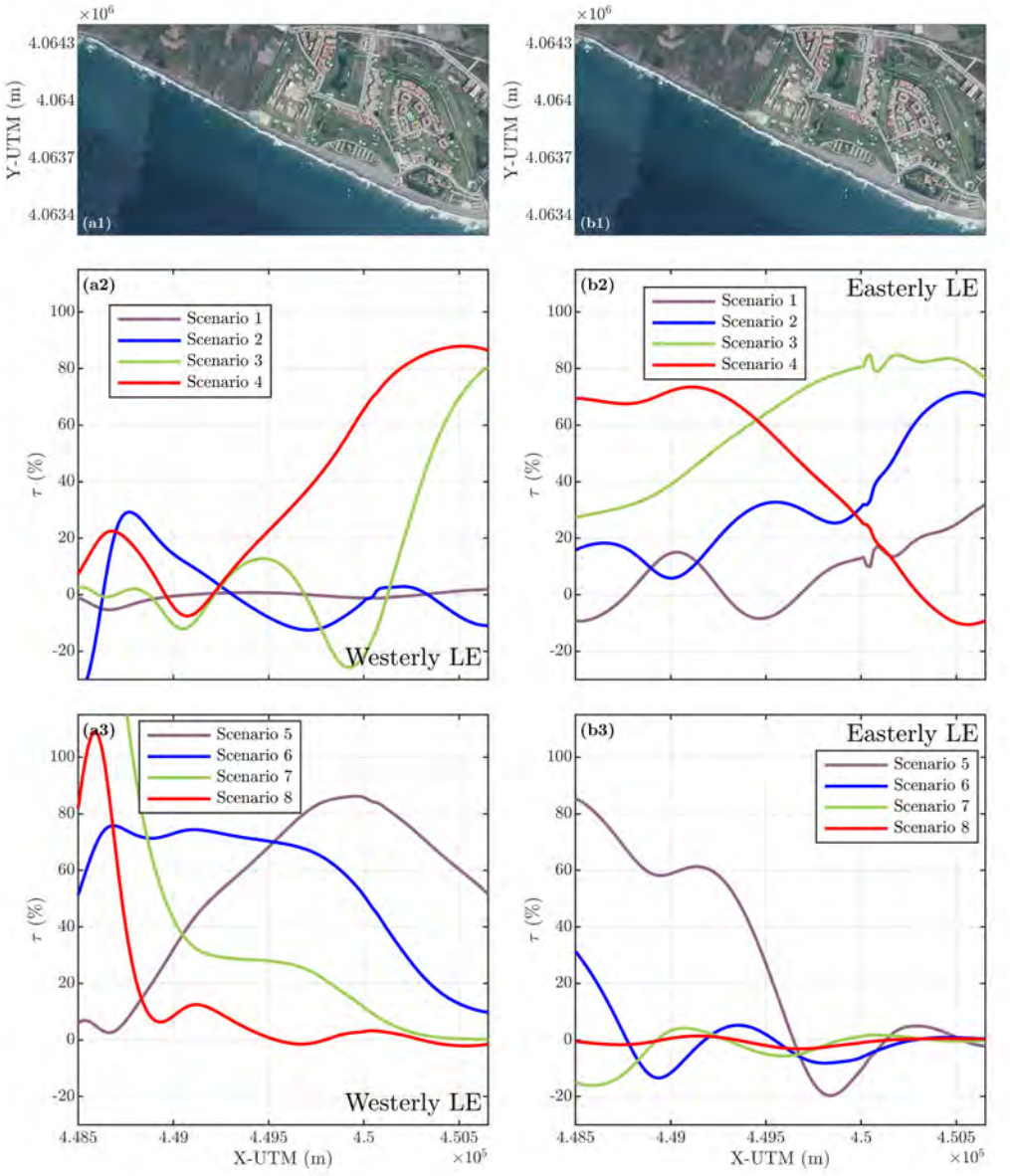

Fig. 5.12 Non-dimensional LST rate reduction under westerly (a) and easterly (b) low energy conditions: (2) scenarios 1-4, (3) scenarios 5-8. Rodriguez-Delgado et al. (2018b).

Under the westerly storm, scenarios 3 and 4 depicts advance with respect to the baseline final shoreline position in the western part of the beach (close to Guadalfeo River mouth) and retreat in the east end of Playa Granada (Fig. 5.13a2-b2). This advanced zone is displaced towards the east in scenarios 5, 6 and 7, whereas the rest of the scenarios do not show significant differences with respect the baseline. Scenarios 5 and 6 stand as the best longshore position reducing the erosion under westerly storms, with $\overline{\upsilon} = 3.2\%$ and $\overline{\upsilon} = 2.9\%$, respectively; followed by scenarios 4 ($\overline{\upsilon} = 2.3\%$) and 7 ($\overline{\upsilon} = 1.3\%$). However, the variations induced by the alongshore location of the wave farm in scenarios 1, 2, 3 and 8 increase the erosion with respect to scenario 0, with negative values of the non-dimensional alongshore-averaged shoreline advance (-0.7%, -1.8%, -1.2% and -0.3%, respectively). As explained in Section 5.2.3 the irregularities observed in X-UTM = 4.5×10^5 m are due to the numerical scheme applied, which is very sensitive to changes in alignment of the coast and, because of that, the curvature of Punta del Santo at this point could produce variations in LST rates.

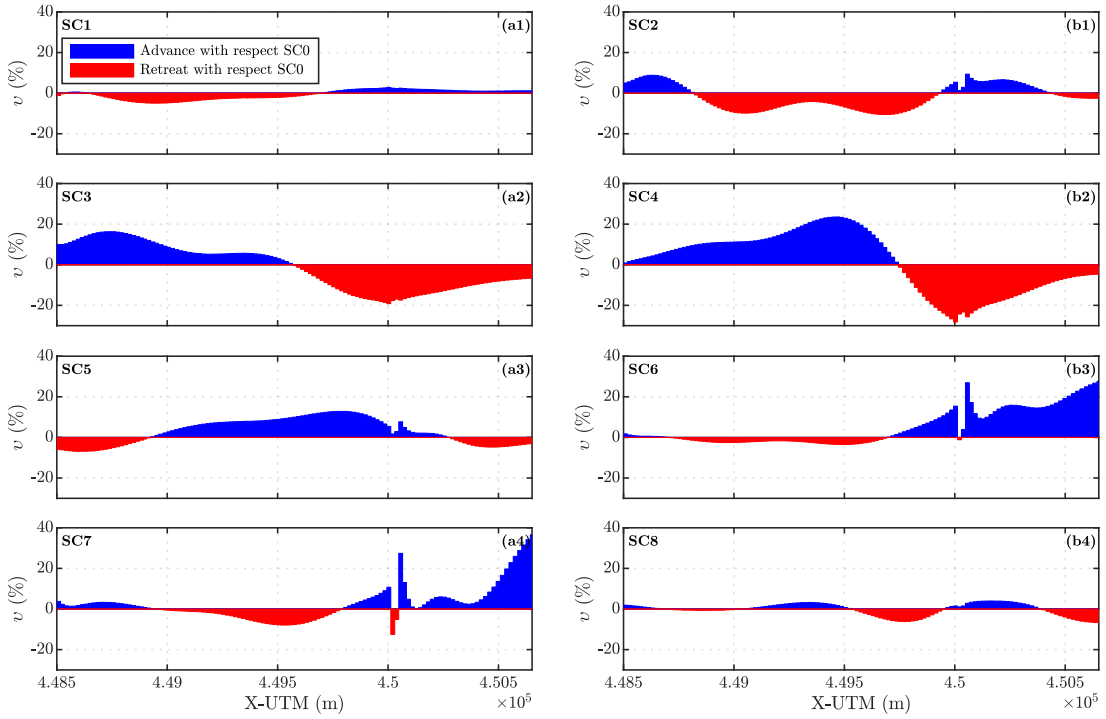

Fig. 5.13 Non-dimensional shoreline advance under westerly storm conditions. Rodriguez-Delgado et al. (2018b).

In the case of the easterly storm conditions, scenarios 1 and 2 do not produce significant changes with respect the baseline (Fig. 5.14a1-b1). Scenario 3 shows some advance with respect the final position of the baseline, especially in the west part of the beach, whereas

a larger advance stretch is depicted in the central part of Playa Granada in scenario 4 (Fig. 5.14a2-b2). In scenario 5 the advance is displaced towards the east, whereas in scenario 6 and 7 the stretch showing retreat with respect the baseline is longer. Scenario 4 show the best performance in terms of coastal protection with a non-dimensional alongshore-averaged shoreline advance of 7.6%, followed by scenario 5 ($\overline{\upsilon} = 6\%$) and scenario 3 ($\overline{\upsilon} = 5.1\%$), whereas scenarios 1, 2 and 8 do not produce significant changes with respect the baseline ($\overline{\upsilon} < 1\%$). However, the rest of the scenarios have negative effects on the shoreline protection; scenario 6 induces the worst impact ($\overline{\upsilon} = -8.3\%$) followed by scenario 7 ($\overline{\upsilon} = -7.3\%$).

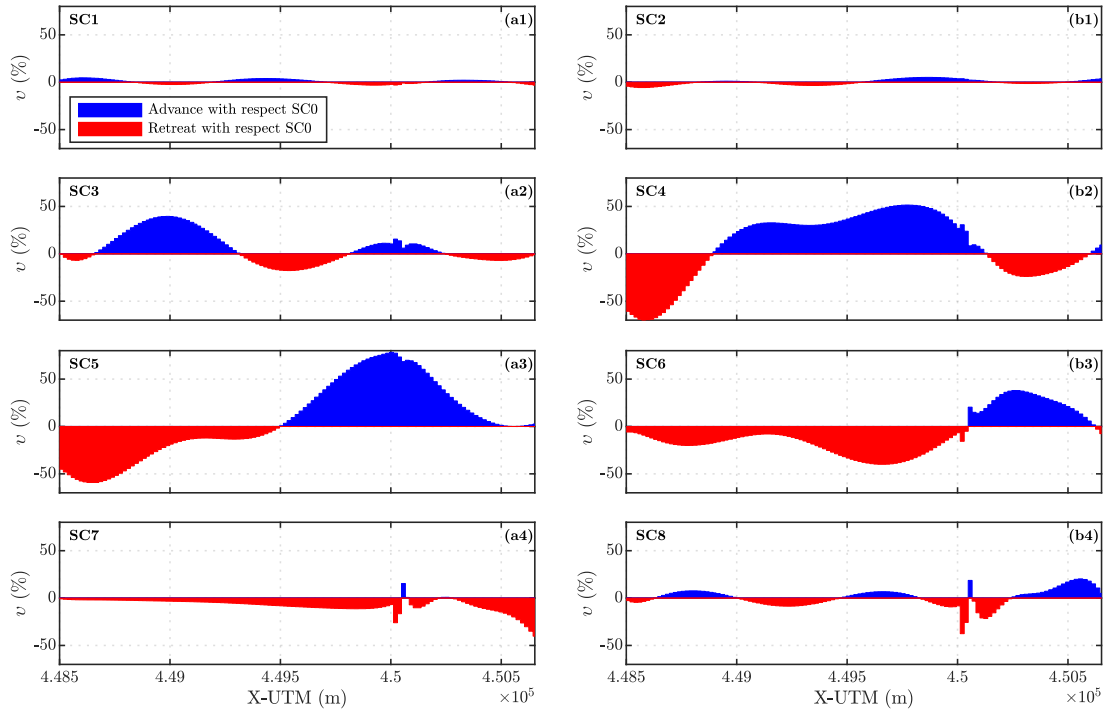

Fig. 5.14 Non-dimensional shoreline advance under easterly storm conditions. Rodriguez-Delgado et al. (2018b).

Under westerly low-energy conditions, scenario 6 has the best performance with $\overline{\upsilon} = 9\%$ (Fig. 5.15). Scenarios 4 and 5 achieve alongshore-averaged values of $\overline{\upsilon} = 4.6\%$ and $\overline{\upsilon} = 8.7\%$, respectively. Scenarios 3, 7 and 8 have a lower impact, with $\overline{\upsilon} < 1\%$. However, scenarios 1 and 2 produce a negative impact in the shoreline, with negative alongshore-averaged values of the non-dimensional shoreline advance ($\overline{\upsilon} = -2.8\%$ and $\overline{\upsilon} = -5.2\%$, respectively).

Finally, scenario 4 has the best performance under easterly low-energy conditions with $\overline{\upsilon} = 13.1\%$, followed by scenarios 5 ($\overline{\upsilon} = 10\%$) and 3 $\overline{\upsilon} = 4\%$ (Fig. 5.16). In the rest of

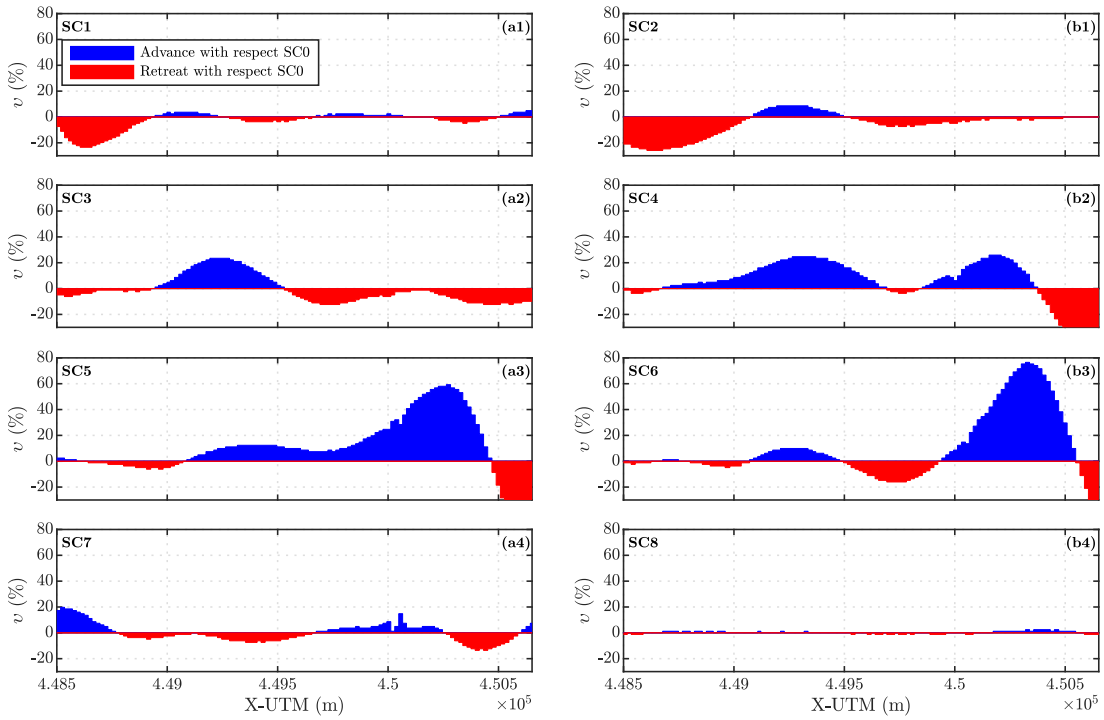

Fig. 5.15 Non-dimensional shoreline advance under westerly low energy conditions.

the scenarios, retreat with respect the shoreline position in the base scenario dominates. Scenario 7 lead to the worst impact ($\overline{v} = -5.5\%$), followed by scenario 6 ($\overline{v} = -5.3\%$). Scenarios 2 and 8 yield $\overline{v} = -1.6\%$ and $\overline{v} = -4.4\%$, respectively, whereas the changes produced by scenario 1 are lower ($\overline{v} = -0.2\%$).

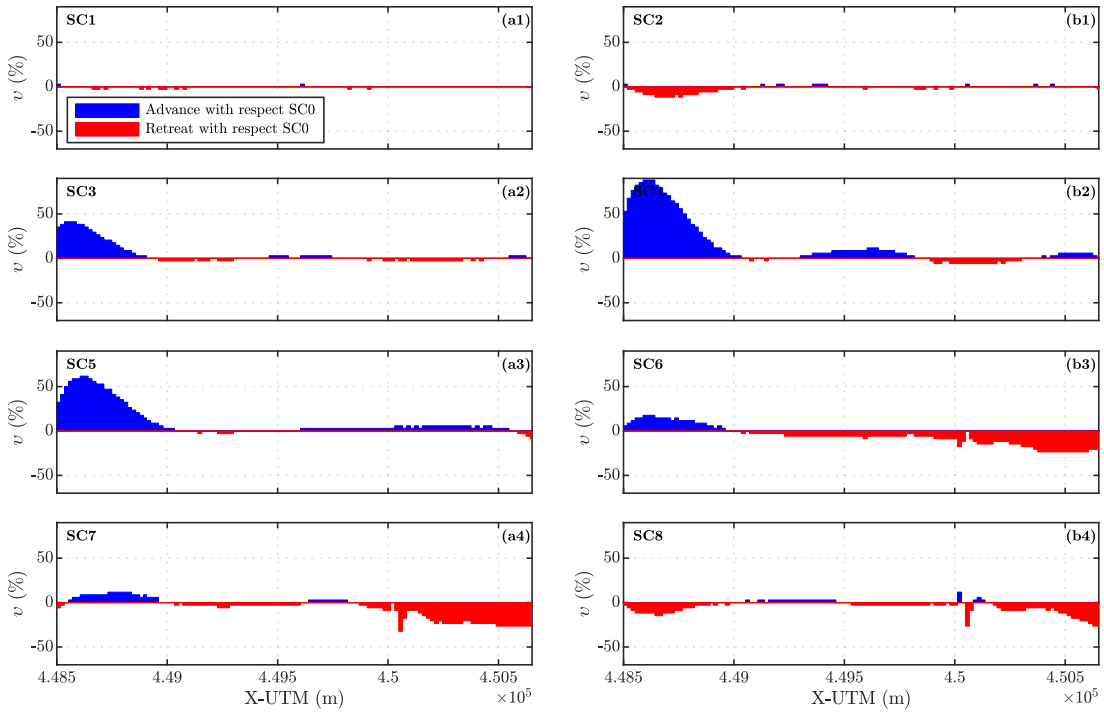

Fig. 5.16 Non-dimensional shoreline advance under easterly low energy conditions.

5.3.7 Dry beach surface

Differences in dry beach surface between each scenario and scenario 0 (ΔA) are depicted in Figure 5.17. The best results in terms of coastal protection (increase in dry beach area) are obtained for those scenarios with the wave farm closest to Playa Granada, although there are important differences between easterly and westerly waves.

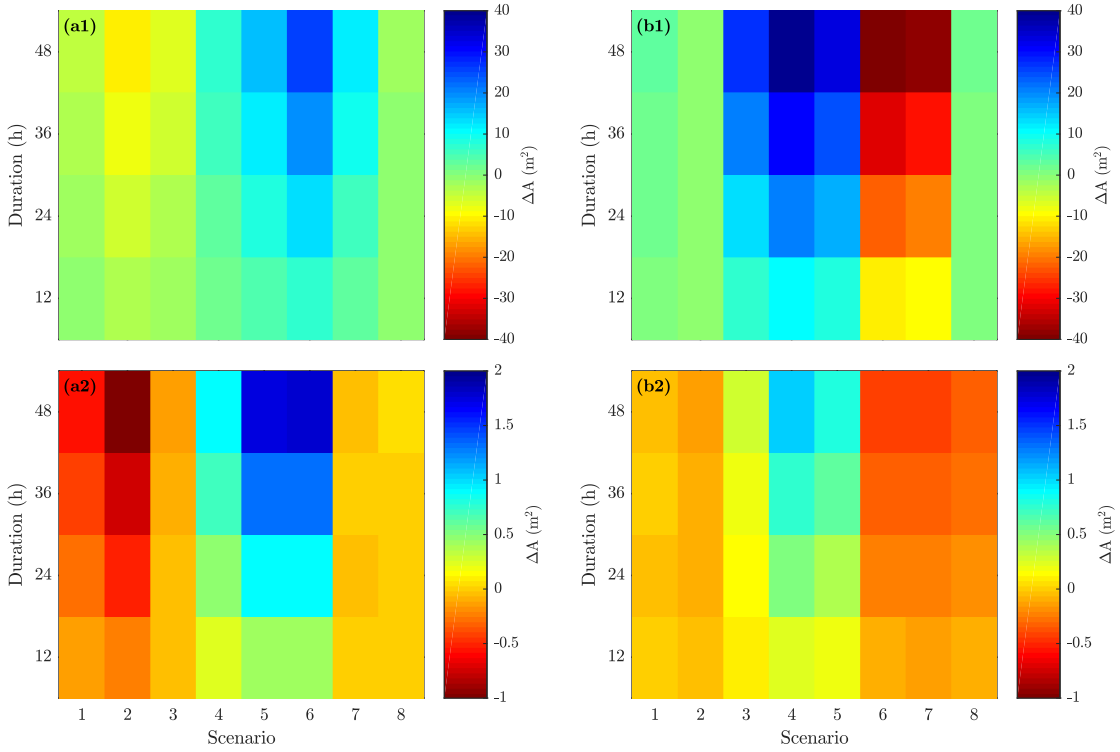

Fig. 5.17 Temporal evolution of the dry beach area for westerly (a) and easterly (b) waves under storm (1) and low energy conditions (2). ΔA = difference in beach surface between each scenario and scenario 0 (no-wave farm). Rodriguez-Delgado et al. (2018b).

Under westerly storm conditions, scenarios 4 to 7 show a positive difference in dry beach area, i.e. advance with respect the final shoreline position in the natural scenario dominates (Fig. 5.17a1). Scenarios 6 and 5 lead to the greatest gain in dry beach surface (26 m^2 and 17 m^2, respectively). However, scenarios 1, 2, 3 and 8 induce a loss of dry beach area with respect to scenario 0; the greatest surface loss is obtained for scenario 2 (-10 m^2). Variations in dry beach surface are more acute under easterly storm conditions (Fig. 5.17b1). Positive surface balances (i.e., greater dry beach surface than in the no-wave-farm scenario) are obtained with scenarios 3, 4 and 5 (27 m^2, 41 m^2 and 34 m^2, respectively). On the contrary, scenarios 6 and 7 induce an important loss of sediment under easterly storm conditions with respect to scenario 0 (-43 m^2 and -38 m^2, respectively).

Results under low-energy westerly waves show a similar behaviour to these under storm conditions, but with smaller differences between wave farm and no-wave farm scenarios (Fig. 5.17a2). Again, the best results in terms of gain in dry beach area are obtained with scenarios 4, 5 and 6 (differences with respect to scenario 0 of 0.9 m^2, 1.7 m^2 and 1.8 m^2, respectively). On the other hand, scenarios 1, 2 and 3 are the worst for coastal protection purposes (differences of -0.5 m^2, -1 m^2 and -0.13 m^2, respectively); whereas scenarios 7 and 8 do not show relevant differences compared to scenario 0 (Fig. 5.17a2). Under easterly low-energy conditions, the loss of sediment extends to scenarios 6, 7 and 8, whereas scenarios 4 and 5 keep the maximum ΔA (1 m^2 and 0.8 m^2 respectively). Finally, changes in dry beach area are insignificant with scenarios 1 and 2 (Fig. 5.17b2).

In order to assess the effects of each scenario on the dry beach variation under storm conditions, the weighted values of dry beach area differences between each scenario with wave farm and scenario 0 were computed (Table 5.1), considering the number of westerly/easterly and low-energy/storm sea states during the last 25 years, which is a typical lifetime of wave farms according to Margheritini et al. (2009), Guanche et al. (2014) and Alonso et al. (2015), among others. The limit between low energy and storm cases was fixed in $H_s = 2.1$ m (99% non-exceeding probability). The weightings in this case represents the percentage of hours with low energy/storm easterly/westerly wave conditions. In order to obtain the results of Table 5.1, the weightings have been kept constant for the different durations. This results are considered as an indicator of which scenario would produce a better impact on the coast but they are not absolute values.

Scenarios 3, 4 and 5 induce a positive balance, while in the rest of scenarios the presence of the wave farm leads to a reduction in the dry beach surface. Scenarios 4 and 5 provide the best results in terms of coastal protection, with an increase in dry beach area of 24.12 m^2 and 25.58 m^2 after 48 h. On the contrary, the beach surface is reduced by 5.1 m^2, 8.68 m^2 and 13.17 m^2 in scenarios 2, 6 and 7, respectively. The changes in beach surface are comparatively insignificant for scenarios 1 and 8 (Table 5.1).

Figure 5.18 depicts the weighted variation of the different parameters analysed for scenarios 4 and 5, which have been demonstrated to be the best locations in terms of coastal protection. The non-dimensional alongshore-averaged weighted values are greater

Table 5.1 Weighted average difference (considering the number of both westerly/easterly and low energy/storm sea states) in dry beach surface for each scenario [m^2]. Rodriguez-Delgado et al. (2018b).

Duration	SC1	SC2	SC3	SC4	SC5	SC6	SC7	SC8
12 h	-0.09	-1.27	2.53	6.01	6.14	-2.17	-3.28	0.02
24 h	-0.18	-2.55	5.07	12.05	12.28	-4.31	-6.56	0.03
36 h	-0.26	-3.81	7.62	18.08	18.43	-6.48	-9.84	0.03
48 h	-0.37	-5.1	10.15	24.12	25.58	-8.68	-13.17	-0.01

in scenario 5 ($\overline{\eta_w} = 8.5\%$) than in scenario 4 ($\overline{\eta_w} = 7.5\%$), i.e. scenario 5 achieves a greater reduction in significant wave height at breaking than scenario 5. Regarding the LST, alongshore-averaged values of τ_w show that the reduction in LST rates is larger in scenario 4 ($\overline{\tau_w} = 26.6\%$) than scenario 5 ($\overline{\tau_w} = 24.8\%$). In this case, the maximum reduction in scenario 5 is found in the central part, while in scenario 4 the maximum decrease is displaced towards the west (Fig. 5.18b). Finally, differences in the shoreline geometries show that, in scenario 5, the shoreline retreats with respect to the no-wave farm scenario on the west side, and dry beach surface is gained in the east part (Fig. 5.18c). On the other hand, in scenario 4, loss of dry beach surface occurs in the west and east sections of the beach (negative values mean a retreat of the shoreline with respect the baseline); while the dry beach area increases with respect to scenario 0 in the central part of the shoreline.

Beach surface differences and reduction in LST rates and wave height are similar in both scenarios, so that the final election between these two wave farm locations should be on the wave resource potential wave energy. López-Ruiz et al. (2016) studied the energy resource in Playa Granada and found that the best location for a wave farm maximising the energy extracted and allowing a good accessibility for maintenance corresponds to scenario 5, followed by scenario 6, in other words, scenario 5 represents the most promising location considering both coastal protection and wave resource criteria.

5.4 Wave farm layout and coastal defence

In the previous section, the importance of the alongshore position of the wave farm in order to achieve an adequate performance as a coastal protection element has been highlighted. Once the position is fixed, the positive effects produced by the wave farm can be modified

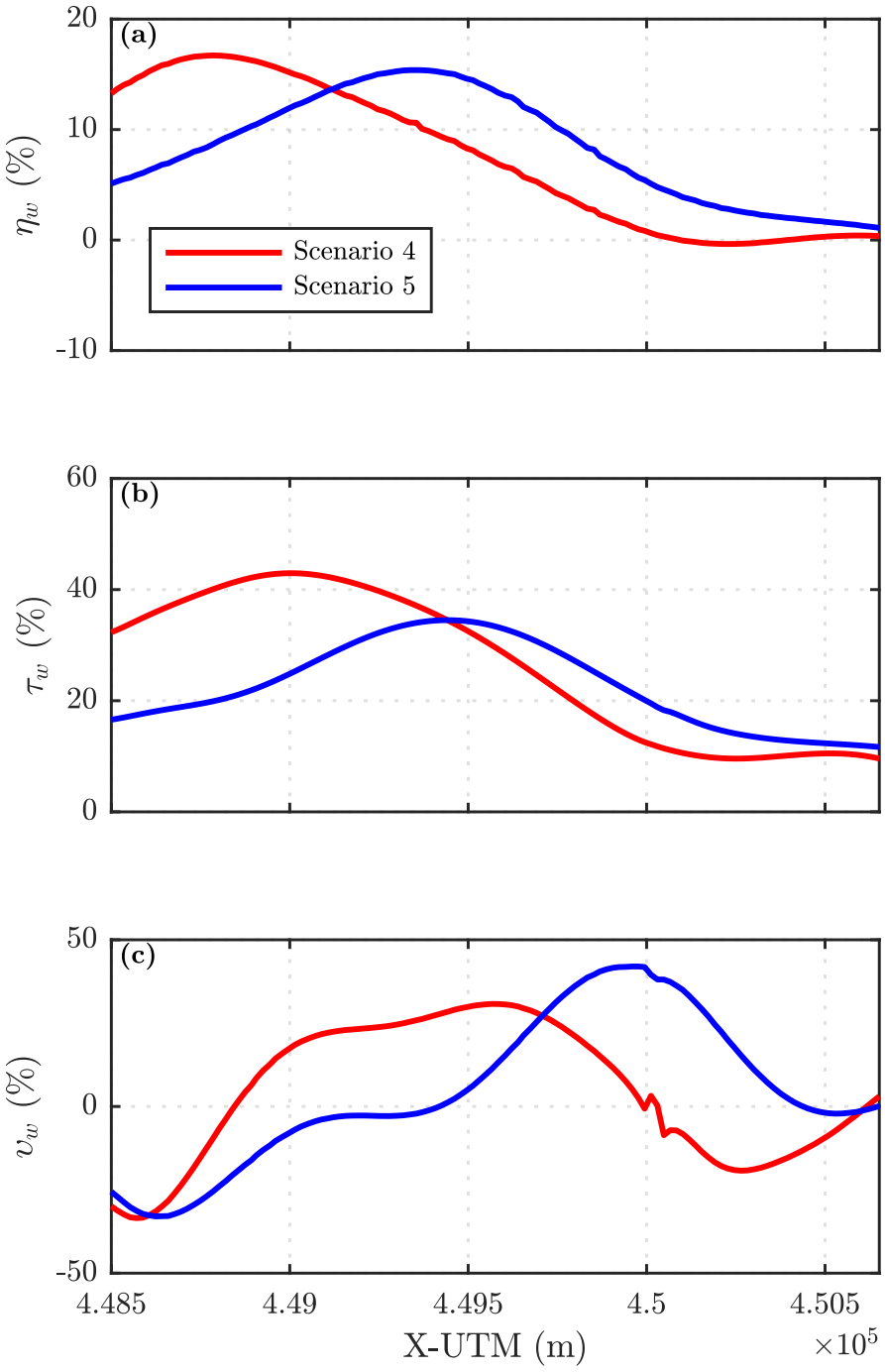

Fig. 5.18 (a) Weighted values of the non-dimensional wave height reduction (η_w), (b) LST rate reduction (τ_w) and (c) shoreline advance (υ_w). Rodriguez-Delgado et al. (2018b).

by the geometry selected for the farm. In this sense, the impact of the configuration of the wave farm needs to be studied. This section deals with different wave farm layouts, more specifically, the number of rows in which the WEC are sorted is analysed. The impact produced by the different layouts studied on the dry beach surface is obtained in order to select the optimum configuration in terms of reduction of the coastal erosion (Fig. 5.19).

The objectives of this section are: (i) to characterise the role of the wave farm layout on coastal protection; (ii) to study the farm-induced changes on wave propagation patterns and, consequently, on longshore sediment transport (LST) rates; and (iii) to investigate the evolution of the shoreline and dry beach surface area on a gravel-dominated deltaic coast (Playa Granada, southern Spain). To this end, changes produced in wave propagation patterns by four wave farm layouts with different number of rows were studied. All the results were compared with the baseline (no-wave farm) situation.

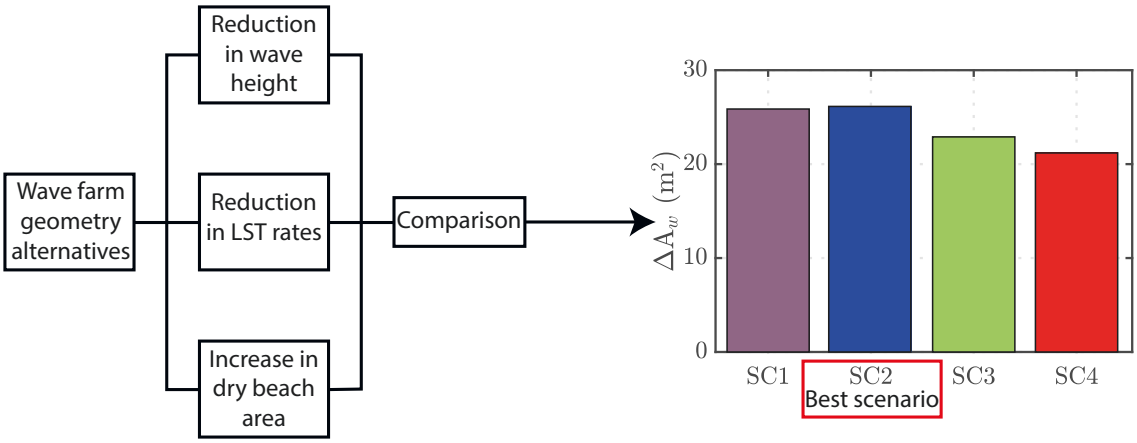

Fig. 5.19 Wave farm layout sensitivity study workflow. Rodriguez-Delgado et al. (2018a).

5.4.1 Wave propagation patterns

The WECs forming a wave farm act like partially transmitting obstacles, altering wave propagation patterns in their lee. The role played by the number of WEC rows in the significant wave height variations is analysed in this section. Under westerly waves, the reduction in significant wave height produced in the lee of the wave farm extends up to Poniente Beach in scenarios 1 and 2 (Fig. 5.20a1-a2). However, scenarios 3 and 4, with the same number of WEC but distributed on more rows, induce a greater reduction but concentrated in the vicinity of the wave farm (Fig. 5.20a3-a4). Under easterly waves, these

differences between the shadows produced by each scenario are less noticeable, covering the whole coastline section of Playa Granada in all cases (Fig. 5.20b1-b4).

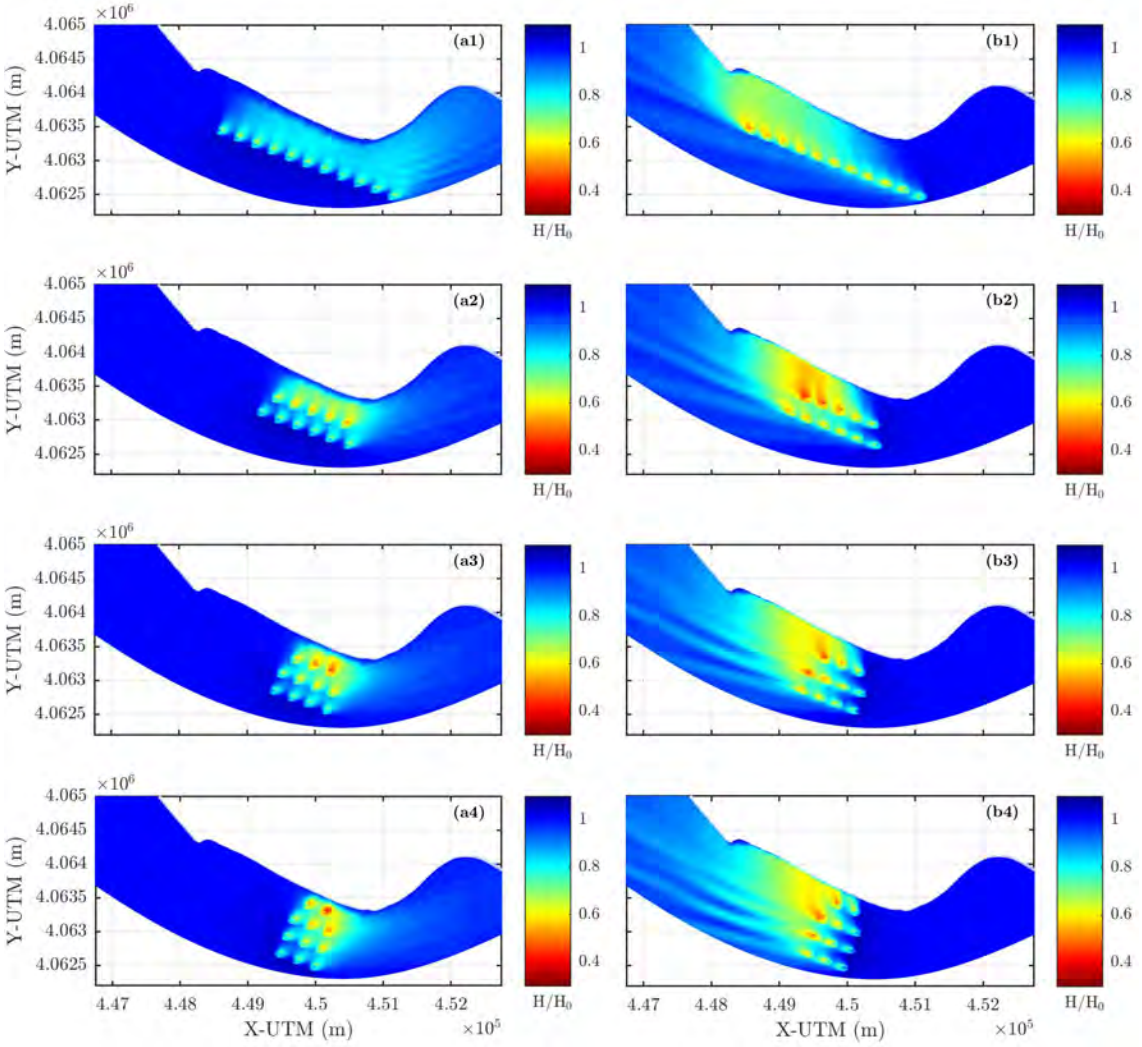

Fig. 5.20 Changes in wave propagation patterns induced by the presence of the wave farm under westerly (a) and easterly (b) storm conditions for scenarios 1, 2, 3 and 4. Rodriguez-Delgado et al. (2018a).

5.4.2 Breaking line

Based on the results of the wave propagation model the breaking line has been obtained as explained in the previous chapters. The results in the case of the storm conditions are similar to those previously obtained (Fig. 5.21). There are no significant differences between the four scenarios studied, which indicates that under high significant wave heights the layout of the wave farm does not affect the position of the breaking line as was already observed in the position sensitivity study.

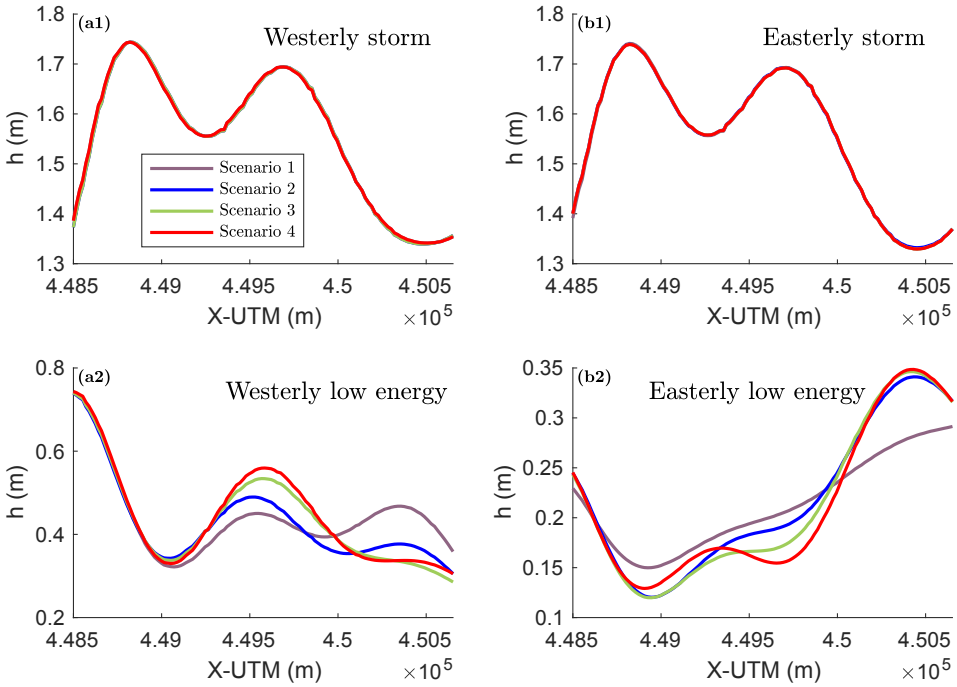

Fig. 5.21 Water depth at breaking under westerly (a) and easterly (b) storms (1) and low energy (2) conditions.

The situation is different in the case of the low energy conditions where appreciable differences may be observed. Under westerly waves, the water depth at breaking varies from 0.3 m to 0.75 m. The maximum water depth is found at the west end of Playa Granada (X-UTM = 4.485 $\times 10^5$ m) and then decrease up to X-UTM = 4.49 $\times 10^5$ m. Then, a peak is found at X-UTM = 4.495 $\times 10^5$ m for scenarios 2, 3 and 4 with scenario 4 reaching the maximum value, followed by scenario 3 and 2. In the case of scenario 1, this peak is found eastwards, at X-UTM = 4.505 $\times 10^5$ m, approx. Under easterly waves the water depth at breaking ranges from 0.12 m to 0.35 m. In this case, again it decreases from the west end up to X-UTM = 4.49 $\times 10^5$ m and then starts to raise. Under these wave conditions the peak is achieved close to the east end (X-UTM = 4.505 $\times 10^5$ m) with a similar value for scenarios 2, 3 and 4.

5.4.3 Wave height at breaking

The non-dimensional wave height at breaking has been calculated in order to assess the impact of each scenario with respect the natural, no-wave farm, scenario. The values for both low-energy and storm conditions are presented in Figure 5.22. In order to assess

the effects of the wave farm on the entire beach, the alongshore-averaged value of the non-dimensional wave height reduction were also computed ($\overline{\eta}$, Table 5.2). To obtain this value the non-dimensional wave height reduction has been averaged along the cross section profiles defined at Playa Granada. This allows to benchmark the performance in the overall stretch of the beach with a simple indicator and compare the impact of the different studied scenarios. The greatest reductions occur under low energy conditions (Table 5.2). Under westerly waves, the significant wave height is reduced in the east part of Playa Granada, the area closer to Punta del Santo, with less pronounced changes near the mouth of the Guadalfeo River (Fig. 5.22a2). This impact extends westward in scenarios 1 and 2; therefore, the greatest reductions are obtained for scenarios 2 ($\overline{\eta} = 18\%$) and 1 ($\overline{\eta} = 17\%$), whereas scenarios 3 and 4 lead to average wave height reductions of 16% and 15%, respectively (Table 5.2). In the case of easterly waves, the reduction covers most of the breaking line along the section of Playa Granada, with maximum reduction in the central and west parts of the beach (Fig. 5.22b2). Alongshore-averaged reductions are similar in the four scenarios, but the maximum reduction is obtained for scenario 3 (Table 5.2).

The reduction in significant wave height at breaking is less noticeable under westerly storms (Fig 5.22a3). The greatest reduction is achieved eastward. Scenario 1 leads to the greatest alongshore-averaged reduction ($\overline{\eta} = 2\%$), whereas for the rest of the scenarios this reduction is slightly smaller (Table 5.2). Under easterly storms, the alongshore distribution of the significant wave height at breaking is similar to the low energy conditions. The maximum reduction is concentrated in the central part of Playa Granada (Fig. 5.22b3). Focusing on the reduction along the entire length of the beach, an alongshore-averaged reduction of 17% is obtained for scenario 2 whereas the lowest reduction is provided by scenario 1 (Table 5.2).

5.4.4 Longshore sediment transport

Wave propagation patterns altered by the presence of the wave farm modify the LST rates, calculated by means of the formulation of Van Rijn (2014). Due to the strong correlation

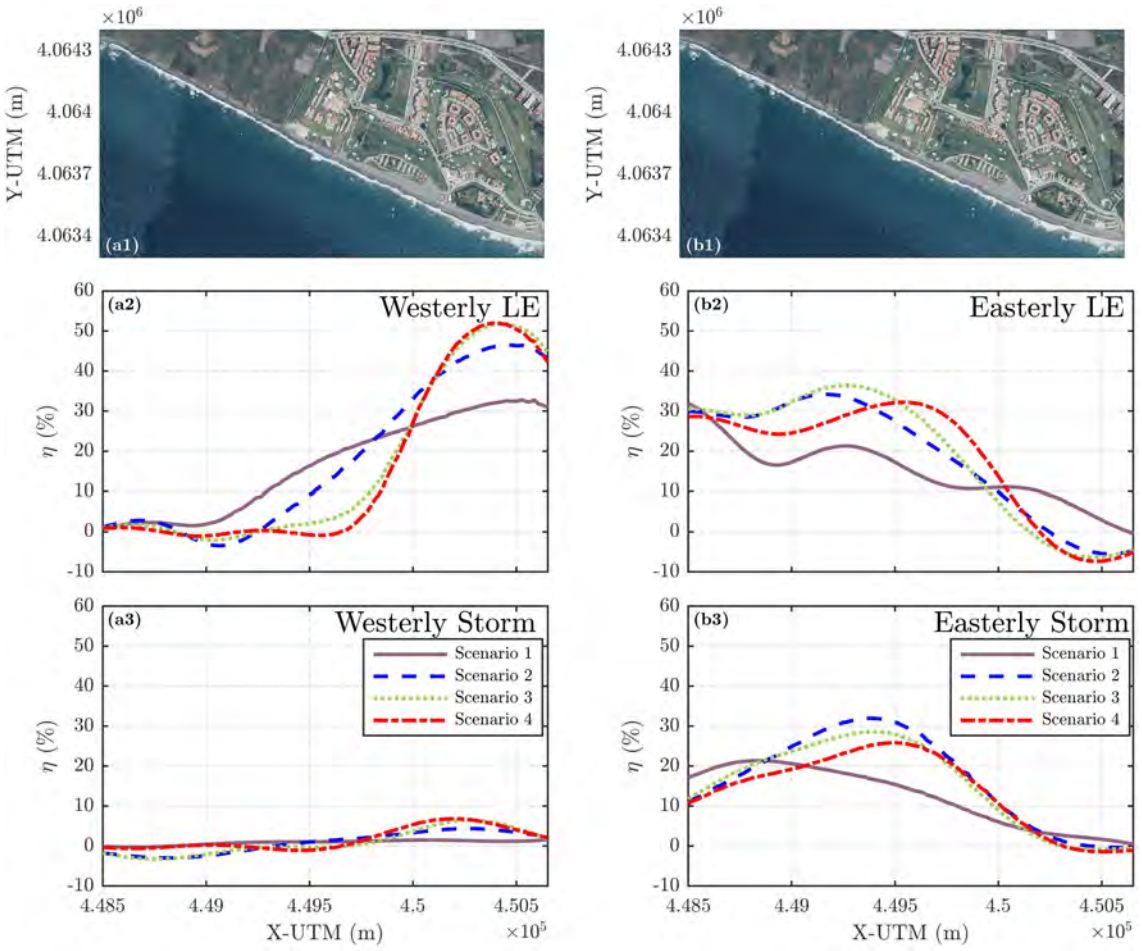

Fig. 5.22 (a1) (b1) Aerial photograph of study site. Non-dimensional wave height reduction (η) for westerly low-energy (a2), easterly low-energy (b2), westerly storm (a3) and eaterly storm (b3) conditions. Rodriguez-Delgado et al. (2018a).

Table 5.2 Non-dimensional alongshore-averaged wave height reduction ($\overline{\eta}$) [%]. Rodriguez-Delgado et al. (2018a).

	Low energy		Storm	
	West	East	West	East
SC1	17	15	**2**	12
SC2	**18**	19	1	**17**
SC3	16	**20**	1	16
SC4	15	19	1	14

between LST rates and significant wave height at breaking (power of 3.1), the reduction of the latter induced by the wave farm leads to a strong reduction in LST rates.

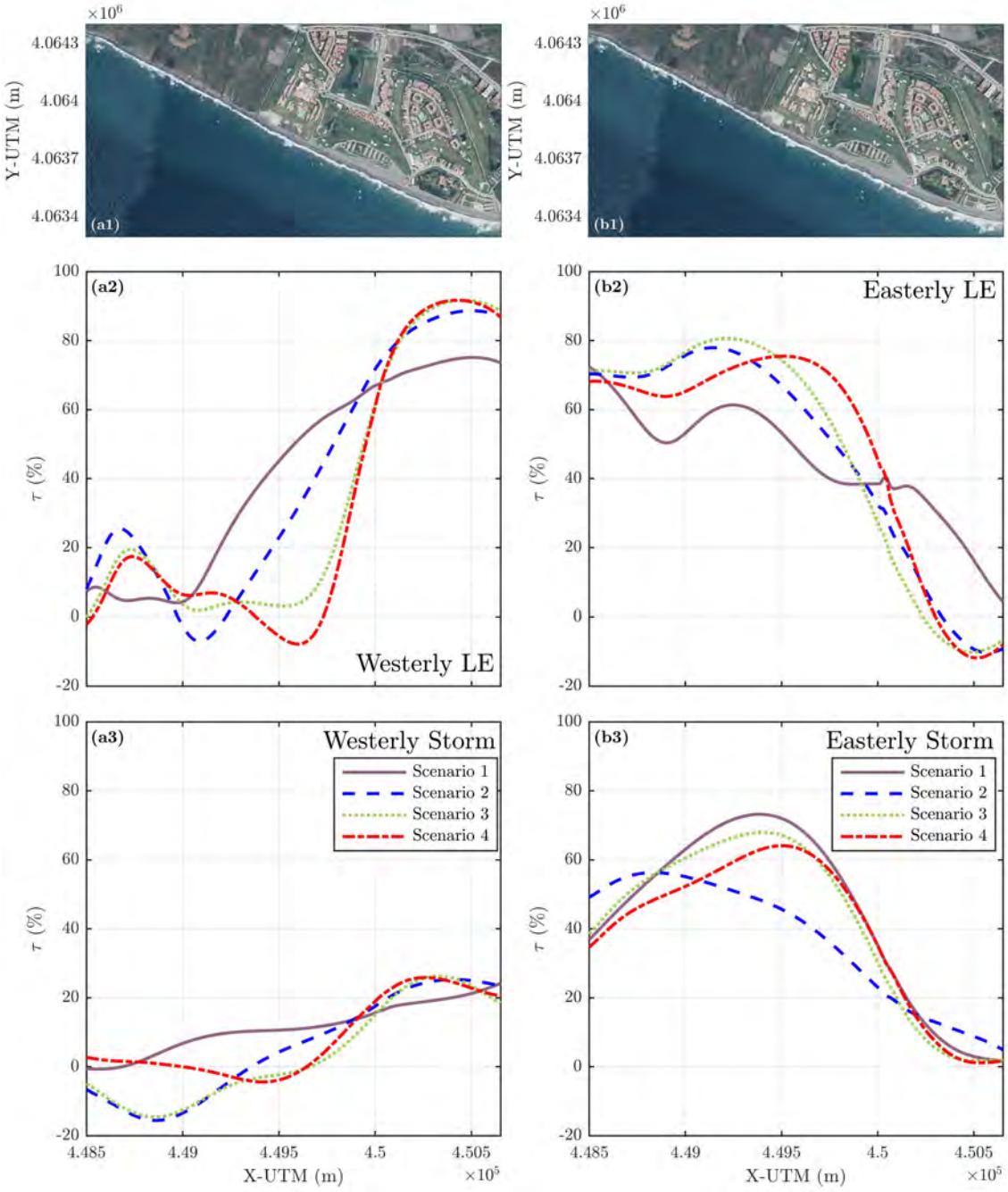

Fig. 5.23 Non-dimensional LST rate reduction (τ). Rodriguez-Delgado et al. (2018a).

Under low energy conditions and westerly waves LST rates are reduced mainly in the eastern part of Playa Granada in scenarios 2, 3 and 4. However, scenario 1 extends the impact up to the western limit of the beach (Fig. 5.23a2). Thus, considering the entire length of Playa Granada, scenario 1 produces the highest alongshore-averaged reduction ($\overline{\tau} = 42\%$), followed by scenario 2 (Table 5.3). Under easterly waves, the reduction in the LST rates induced by the wave farms covers most of the section of Playa Granada (Fig.

5.23b2). The maximum values (highest protection) are obtained close to the Guadalfeo River mouth, i.e. in the western part of the beach. Focusing on the total impact on Playa Granada, scenario 4 induces an alongshore-averaged reduction of 50%, whereas scenarios 2 and 3 provide a reduction of 49% and 48%, respectively. Finally, scenario 1 accomplishes the lowest alongshore-averaged reduction ($\overline{\tau} = 46\%$, Table 5.3).

The wave farm effects under westerly storm conditions with respect to scenario 0 are less pronounced. The same trends as under westerly low energy conditions is observed, so that scenarios 2, 3 and 4 concentrate the reduction in LST rates eastwards, while scenario 1 extends the effect over the whole stretch of beach (Fig. 5.23a3). The best alongshore-averaged reduction ($\overline{\tau} = 11\%$) is obtained for scenario 1 due to its impact in the western part of the stretch of beach. Scenario 4 is the second one with a highest reduction ($\overline{\tau} = 8\%$), whereas scenarios 2 and 3 provide values of the reduction equal to 5% and 3%, respectively (Table 5.3). Under easterly storm conditions, LST rates reduction is maximum in the central part of the beach (Fig. 5.23b3). Attending to the results along the whole stretch of Playa Granada, the best reductions are obtained for scenario 2, with $\overline{\tau} = 45\%$, followed by scenarios 3 and 4. Finally, the lowest alongshore-averaged reduction (worst protection) is obtained with scenario 1 (Table 5.3).

Table 5.3 Non-dimensional alongshore-averaged LST rate reduction ($\overline{\tau}$) [%]. Rodriguez-Delgado et al. (2018a).

	Low energy		Storm	
	West	East	West	East
SC1	**42**	46	**11**	37
SC2	40	48	5	**45**
SC3	34	49	3	43
SC4	31	**50**	8	40

5.4.5 Shoreline evolution

This section analyses the shoreline changes after 48 hours, obtained by means of the one-line model (Eq. 3.7) based on the LST rates explained in Section 5.4.4. As a representation of the advance of the shoreline with respect the baseline along the entire beach, the alongshore-averaged values of the non-dimensional shoreline advance ($\overline{\upsilon}$) were computed for each scenario and wave condition (Table 5.4).

Under westerly low energy conditions, in every scenario, advance in the final shoreline position with respect the baseline (coastal protection induced by the farms) occurs along most of the coastline except in the vicinity of Punta del Santo, i.e., in the eastern part of Playa Granada (Fig. 5.24a). In terms of alongshore-averaged shoreline advance, positive effect dominates in all scenarios, highlighting the efficiency of wave farms as coastal defence elements (Table 5.4). The best results under these conditions are obtained for scenario 3 ($\overline{\upsilon} = 9.2\%$), followed by scenarios 2 and 4 ($\overline{\upsilon} = 8.8\%$); whereas the worst non-dimensional shoreline advance is provided by scenario 1 ($\overline{\upsilon} = 7.2\%$).

Regarding the easterly low energy conditions, results show advance with respect the baseline mainly in the western part of the beach (Fig. 5.24b). In terms of alongshore-averaged shoreline advance, positive effect dominates again for all scenarios. The best results for shoreline protection purposes are achieved with scenario 1 ($\overline{\upsilon} = 10.5\%$), followed by scenarios 2 and 3 ($\overline{\upsilon} = 10.2\%$) and, finally, by scenario 4 ($\overline{\upsilon} = 9.6\%$).

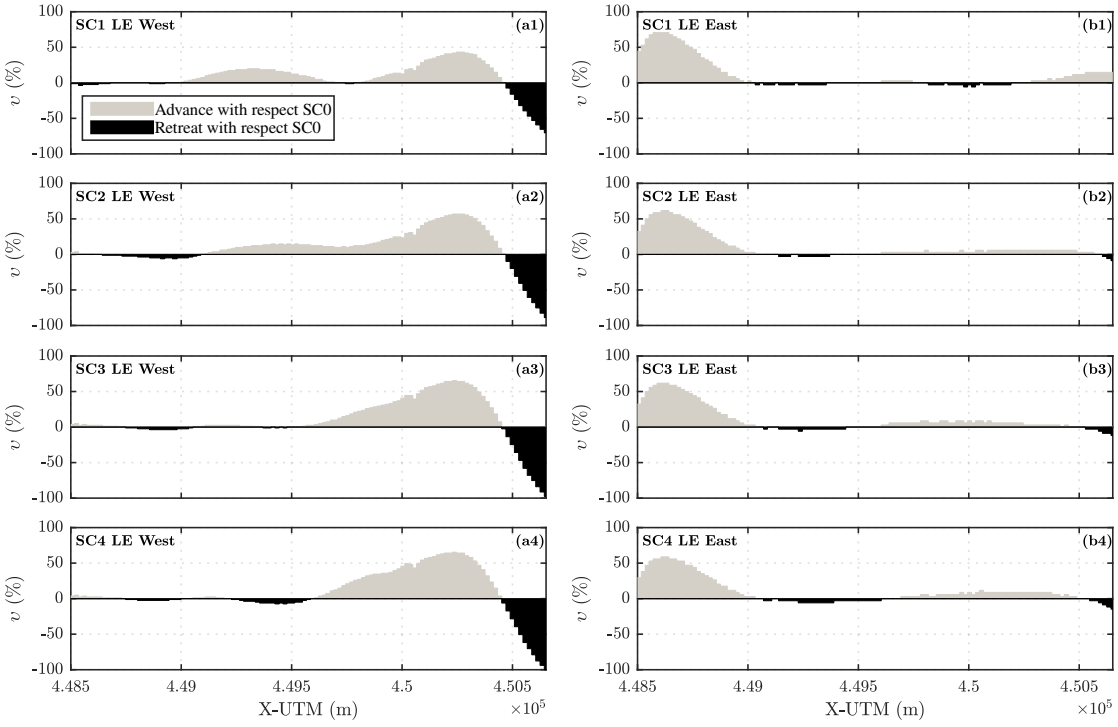

Fig. 5.24 Non-dimensional shoreline advance (υ) under low-energy conditions. Rodriguez-Delgado et al. (2018a).

Under westerly storm conditions, scenarios 2, 3 and 4 induce advance with respect the no-wave-farm scenario in the central area of the beach, and retreat in the western and eastern parts (Fig. 5.25a). Scenario 1 leads to advance in both limits of the beach, whereas retreat is only found in a narrow stretch of beach in the central zone. In terms of alongshore-

averaged shoreline advance (Table 5.4), positive effect is dominant: the best results are obtained for scenario 2 ($\overline{\upsilon} = 3.2\%$), followed by scenarios 1 ($\overline{\upsilon} = 3.0\%$), 3 ($\overline{\upsilon} = 2.2\%$) and 4 ($\overline{\upsilon} = 1.9\%$). Finally, shoreline geometry changes with respect to the natural scenario under the easterly storms show a similar pattern for all scenarios, with advance (retreat) in the eastern (western) part of Playa Granada (Fig. 5.25b). Focusing on the alongshore-averaged shoreline advance, the best results in terms of coastal protection are obtained with scenario 1 ($\overline{\upsilon} = 6.5\%$), followed by scenarios 2 ($\overline{\upsilon} = 6.3\%$), 3 ($\overline{\upsilon} = 6.0\%$) and 4 ($\overline{\upsilon} = 5.8\%$).

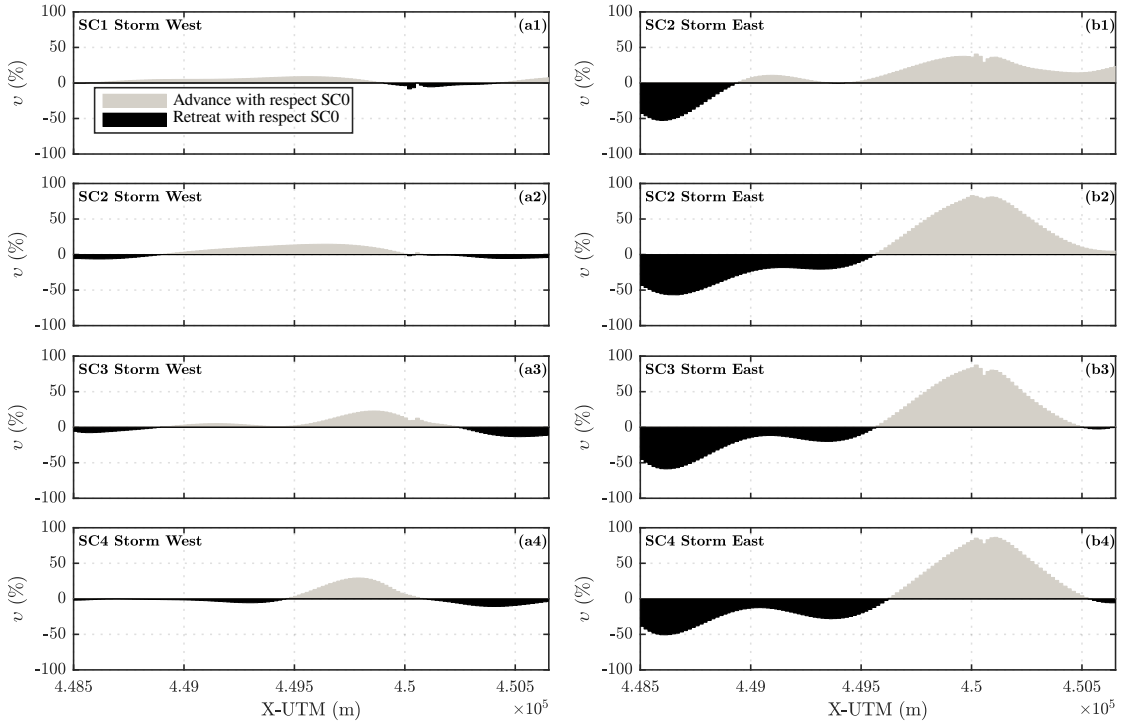

Fig. 5.25 Non-dimensional shoreline advance (υ) under storm conditions. Rodriguez-Delgado et al. (2018a).

Table 5.4 Non-dimensional alongshore-averaged shoreline advance ($\overline{\upsilon}$ [%].). Rodriguez-Delgado et al. (2018a).

	Low energy		Storm	
	West	East	West	East
SC1	7.2	**10.5**	3.0	**6.5**
SC2	8.8	10.2	**3.2**	6.3
SC3	**9.2**	10.2	2.2	6.0
SC4	8.8	9.6	1.9	5.8

5.4.6 Dry beach surface

On the basis of the results described in Section 5.4.5 concerning the shoreline evolution, farm-induced changes in dry beach surface were computed. The differences between each scenario and the baseline scenario are depicted in Figure 5.26. Positive differences in dry beach area are obtained for all the scenarios, confirming the advance of the shoreline position caused by the wave farm. Under westerly low energy conditions (Fig. 5.26a1), scenario 3 provides the largest increase in dry beach area, followed by scenarios 4, 2 and 1. On the contrary, under easterly low energy conditions (Fig. 5.26b1), the best alternative in terms of gained dry beach surface is scenario 1, followed by scenarios 2, 3 and 4.

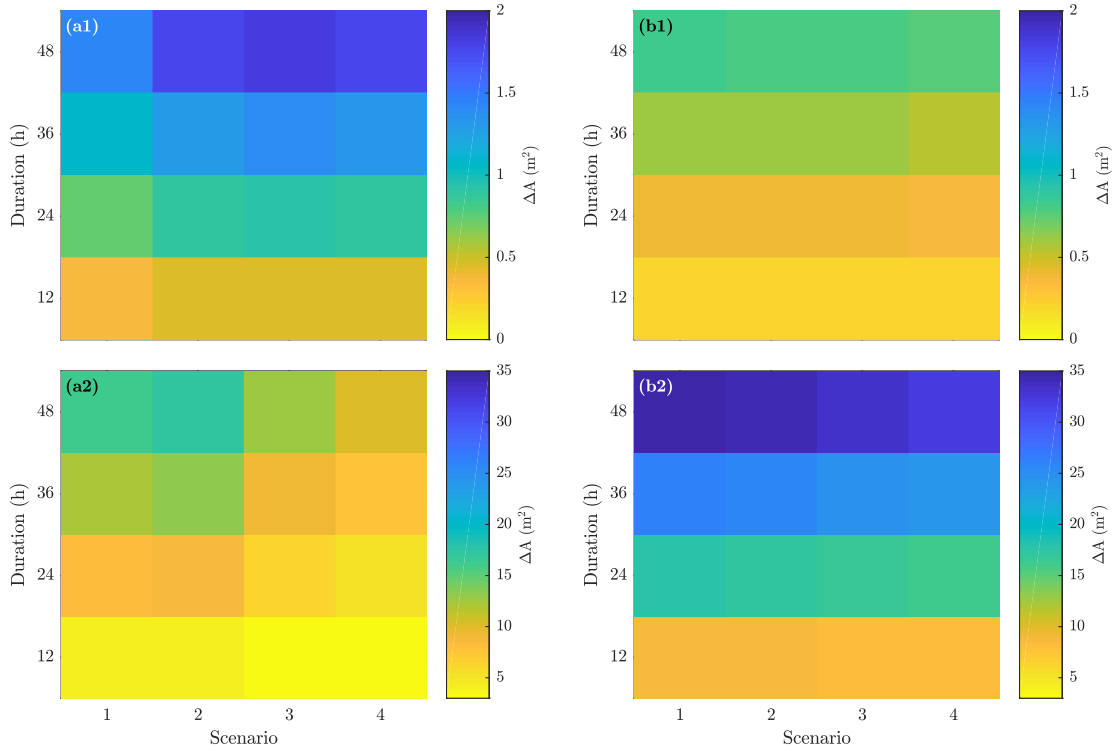

Fig. 5.26 Changes in dry beach area between each scenario and the baseline scenario under westerly (a) and easterly (b) low energy (1) and storm (2) conditions. Rodriguez-Delgado et al. (2018a).

Under storm conditions, differences in beach surface are higher for easterly waves than for westerly ones. In the case of the westerly waves (Fig. 5.26a2), scenario 2 provides the best results (with a positive relative difference of 17.43 m^2 after 48 hours) followed by scenario 1 (16.05 m^2). Scenario 3 induces an increase in beach surface of 12.58 m^2 and, finally, scenario 4 leads to the lowest gain in dry beach area. On the contrary, under easterly storm conditions (Fig. 5.26b2), scenario 1 yields the highest surface difference,

with an increase of 35.29 m^2 with respect to the baseline scenario. Scenario 2 is the second best for coastal protection purposes, with a dry beach gain of 34.46 m^2. Finally, dry beach surface gains with respect to the natural scenario are equal to 33.21 m^2 and 32.09 m^2 for scenarios 3 and 4, respectively.

5.4.7 Overall performance of the wave farm scenarios

As shown in the previous sections, the efficiency of each scenario for coastal protection purposes varies depending on the sea state (Tables 5.2, 5.3 and 5.4). For this reason, in order to assess the overall performance of each scenario under varying wave conditions, weighted values of the different variables analysed in this section were computed, considering the number of westerly/easterly and low energy/storm sea states during the last 25 years – a typical life-cycle for WEC devices (Alonso et al., 2015; Guanche et al., 2014; Margheritini et al., 2009) as referred in Section 5.3.7.

The weighted values of the non-dimensional wave height reduction (η_w) indicate that the highest effects are concentrated in the central part of the beach for scenarios 2, 3 and 4 (Fig. 5.27c). In scenario 1, the impact varies less along the beach, with the minimum value in the western part. The weighted values of the non-dimensional alongshore-averaged wave height reduction ($\overline{\eta_w}$) are 7% (scenario 1), 9% (scenarios 2) and 8% (scenarios 3 and 4).

Similar patterns are obtained for the weighted values of the non-dimensional LST rate reduction (τ_w), with the maximum values located in the central part of the beach for scenarios 2, 3 and 4 (Fig. 5.27 d). Again, the maximum τ_w in scenario 1 is located in the western part of the beach. The highest reduction is obtained with scenario 2 ($\overline{\tau_w} = 25\%$), followed by scenario 1 ($\overline{\tau_w} = 24\%$), 4 ($\overline{\tau_w} = 24\%$) and 3 ($\overline{\tau_w} = 23\%$).

Weighted values of non-dimensional shoreline advance (υ_w) show that advance with respect to the baseline scenario dominates, mainly, in the eastern part of Playa Granada, although scenario 1 also induces an advance with respect to the baseline in the western part (Fig. 5.27e). In terms of alongshore-averaged weighted values ($\overline{\upsilon_w}$), scenarios 2 and 1 yield the best results with $\overline{\upsilon_w} = 4.7$ and $\overline{\upsilon_w} = 4.6$, respectively, whereas $\overline{\upsilon_w} = 4.1$ in scenario 3 and $\overline{\upsilon_w} = 3.8$ in scenario 4. Scenario 2 not only provides a slightly higher

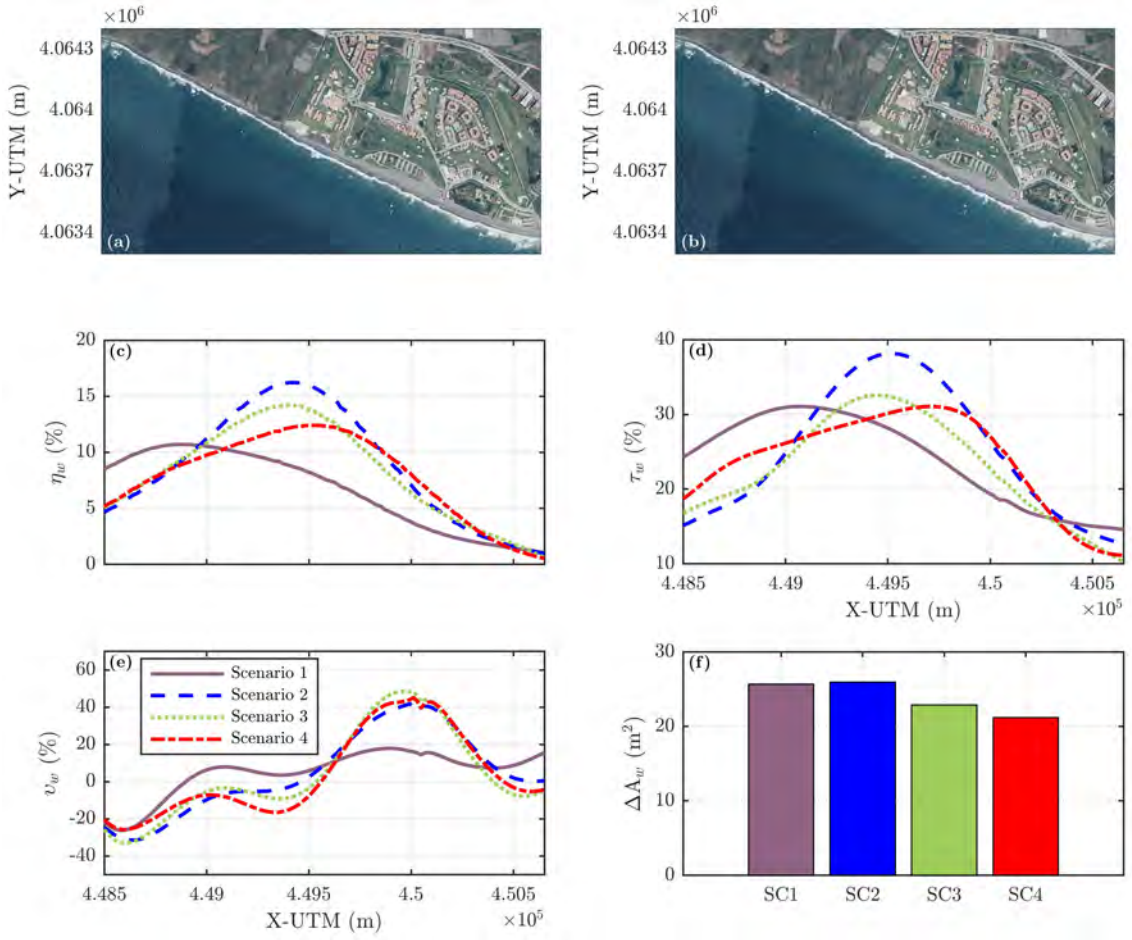

Fig. 5.27 Weighted values of the non-dimensional wave height reduction (c), LST rate reduction (d), shoreline advance (e) and dry beach area (f). Rodriguez-Delgado et al. (2018a).

alongshore-averaged shoreline advance ratio than scenario 1, but also concentrates the protection on the eastern part of Playa Granada, where most of the residential buildings and hotel complex are located.

Finally, the overall coastal protection performance of each scenario is analysed by means of the weighted dry beach surface difference (Figure 5.27f). The best coastal protection performance (highest weighted dry beach surface difference with respect to scenario 0) is provided by scenario 2 (25.94 m^2), followed by scenario 1 (25.67 m^2). Scenarios 3 and 4, with more WEC rows, yield smaller differences in dry beach area (22.9 m^2 and 21.19 m^2, respectively).

5.5 Inter-device spacing interaction with the wave field

In previous sections, the impact of the alongshore position of the wave farm and its layout has been studied in order to optimise the performance of the wave farm in terms of coastal protection. In dual wave farms, i.e., arrays of wave energy converters with a dual function – generation of renewable power and mitigation of coastal erosion – the spacing between the WECs is a fundamental design parameter. The wave farm interaction with the wave field is modified and therefore, the energy absorption capabilities and the coastal protection performance varies depending on the space between devices. The optimum alongshore position and layout obtained in the previous sections are kept whereas different inter-device spacings are tested in order to optimise this design parameter (Fig. 5.28).

In this next section the present research has the objective of establishing how this parameter affects the shoreline evolution behind the array and, on this basis, to propose and apply a method to determine the optimum spacing for coastal protection. Four scenarios are considered modelling different inter-WEC spacings.

5.5.1 Wave propagation patterns

In this section, the impacts caused by the dual WEC array on wave transmission are analysed. The inter-WEC spacing is found to play a relevant part (Figure 5.29). Under the westerly storm, a more compact array results in a more pronounced and narrower wake,

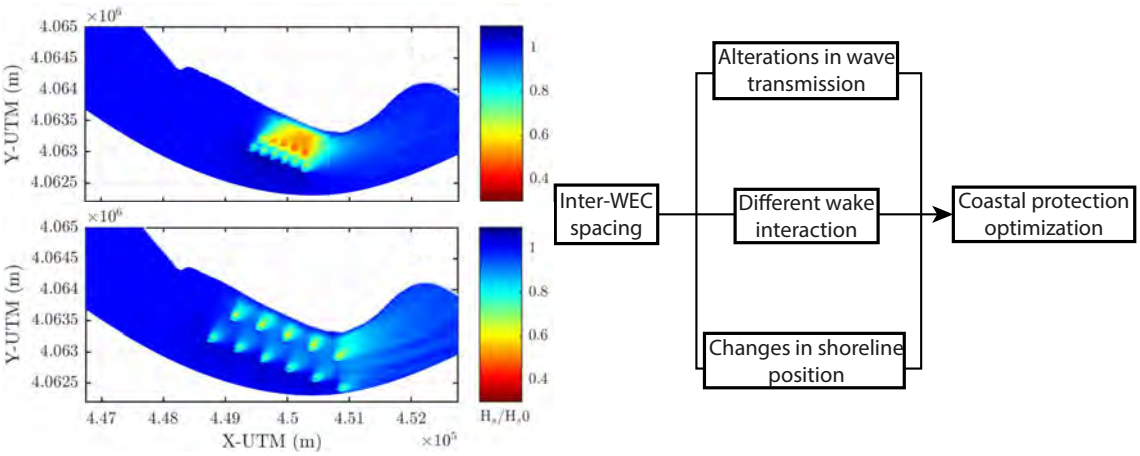

Fig. 5.28 Workflow applied in the inter-device spacing impact study. Rodriguez-Delgado et al. (2019).

i.e., smaller wave heights but concentrated near Punta del Santo (Figure 5.29a1-a2). When the inter-WEC spacing is larger, the wake of the array is less pronounced, for the wakes of the individual WECs do not merge with one another (Figure 5.29a3-a4).

Under the easterly storm, a similar behaviour is observed, with a higher reduction in wave height for the first two scenarios, in particular in the vicinity of the Guadalfeo River mouth (Figure 5.29b1-b2). The wakes of the individual WECs merge under easterly waves, resulting in a more pronounced wake (Figure 5.29b1-b4).

Under westerly waves, the greatest reduction is achieved in the east part of the beach, near Punta del Santo, with SC1 producing the highest impact in this zone for both low and storm conditions (Figure 5.30a2-a3). However, SC2 to SC4 lead to a more pronounced attenuation mid-beach under low energy conditions.

Considering each case in turn, the overall impact on Playa Granada may be quantified in relative terms (relative to the breaking wave height in the baseline) by means of the alongshore average of the non-dimensional significant wave height reduction, η (Table 5.5). Under westerly waves the impact is considerably greater in low energy sea states than in storm conditions. In low energy conditions, SC2 leads to the greatest wave height reduction, with $\overline{\eta} = 18\%$, whereas SC4 produces the lowest impact ($\overline{\eta} = 16\%$). Under storm conditions, $\overline{\eta}$ values are significantly lower, with SC1 leading to the highest reduction ($\overline{\eta} = 1.3\%$), followed by SC3 ($\overline{\eta} = 1.15\%$).

By contrast, under easterly waves there is little difference in the overall impact between the low and storm conditions. For low energy sea states, a greater attenuation is achieved

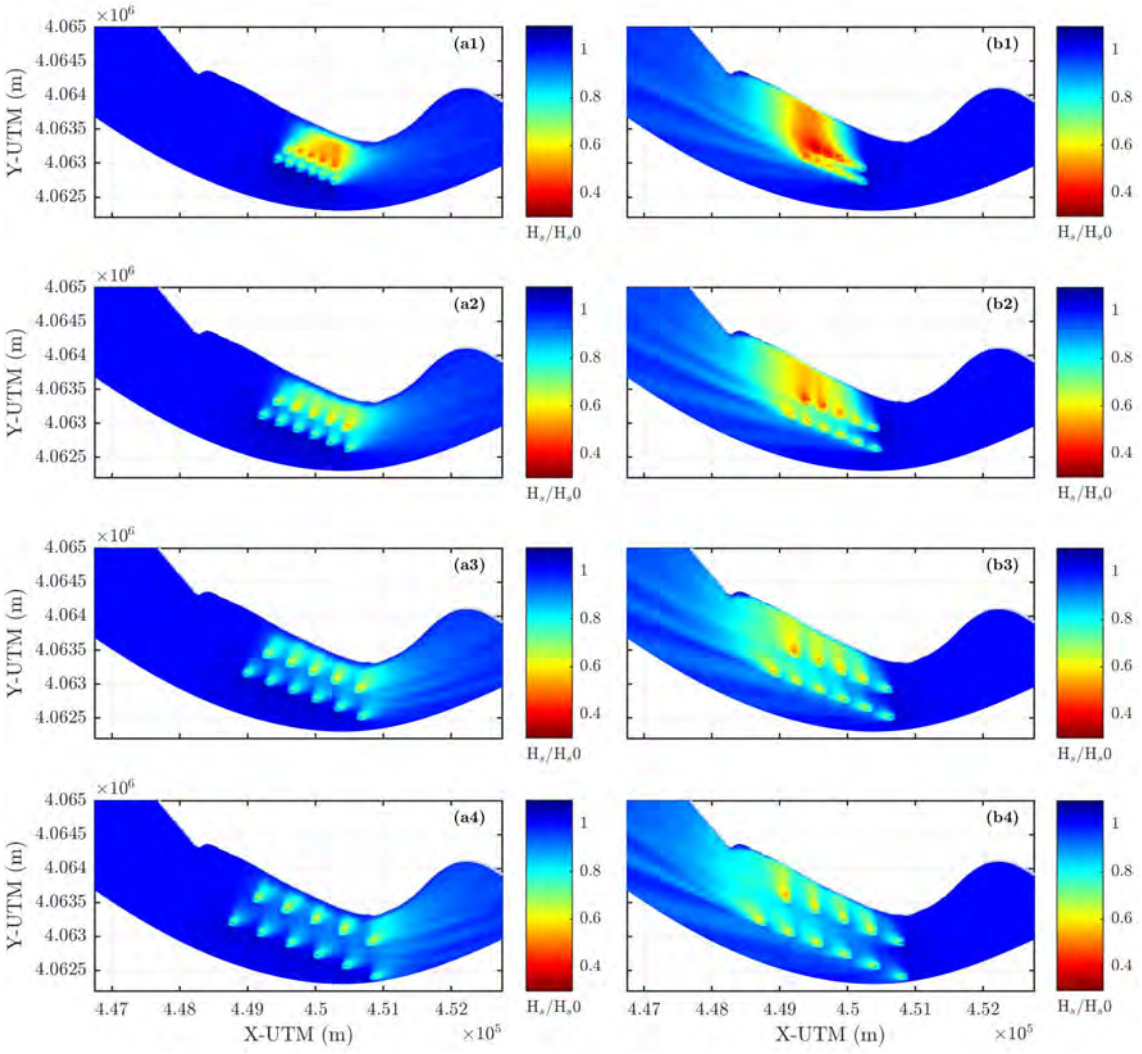

Fig. 5.29 Ratio of the significant wave height in each of the wave farm cases (H_s) to the baseline (H_{s0}); from top to bottom, scenarios 1 - 4; westerly (a, left) and easterly (b, right) storm conditions. Rodriguez-Delgado et al. (2019).

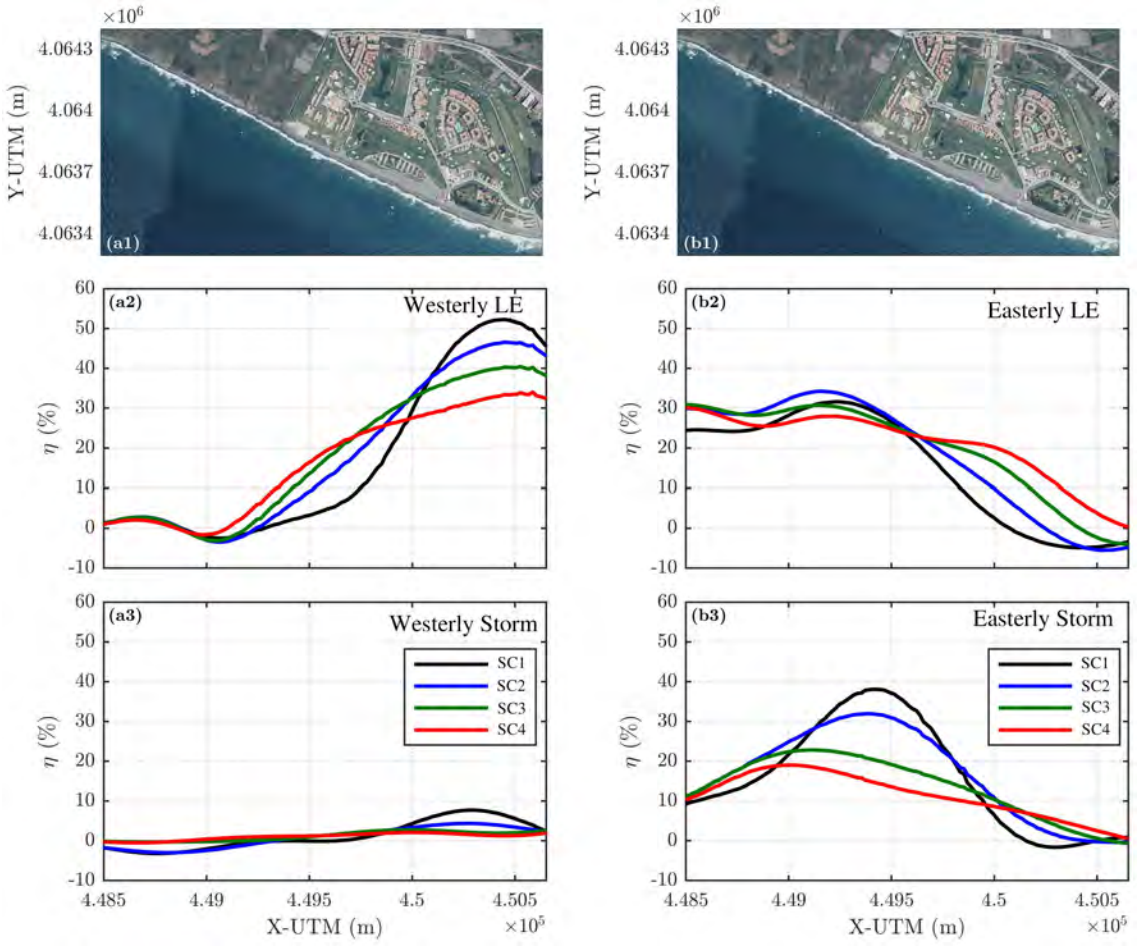

Fig. 5.30 Aerial photograph of Playa Granada (a1-b1). Alongshore variation of the non-dimensional significant wave height reduction under westerly (a) and easterly (b), low energy (2) and storm (3) conditions. Rodriguez-Delgado et al. (2019).

in the western part of the beach, with the impact decreasing eastwards (Figure 5.30b2). The highest alongshore-averaged reduction under low energy conditions is induced by SC4 ($\overline{\eta} = 21\%$, Table 5.5), since in this case the reduction is extended until Punta del Santo (Figure 5.30b2). On the contrary, SC1 leads to the lowest value of the alongshore-averaged reduction ($\overline{\eta} = 16\%$). Under storm conditions, the highest impact is produced in the central part of Playa Granada, decreasing both eastwards and westwards (Figure 5.30b3). The highest alongshore-averaged reduction ($\overline{\eta} = 17\%$) is obtained for SC2, followed by SC1 ($\overline{\eta} = 16\%$), whereas SC3 and SC4 produce the lowest impact, with $\overline{\eta} = 14\%$ and $\overline{\eta} = 12\%$, respectively.

Table 5.5 Longshore average of the non-dimensional significant wave height reduction ($\overline{\eta}$) [%]. Rodriguez-Delgado et al. (2019).

	Low energy		Storm	
	West	East	West	East
SC1	17	16	**1.3**	16
SC2	**18**	19	1	**17**
SC3	17	20	1.15	14
SC4	16	**21**	1	12

5.5.2 Longshore sediment transport

As for the wave height at breaking, under westerly waves the wave farm causes LST rates to decline primarily in the vicinity of Punta del Santo (Figure 5.31a2-a3), in particular under low energy conditions. In fact, under storm conditions the attenuation in wave heights around the Guadalfeo mouth is negligible (SC3 and SC4) or even negative (SC1 and SC2).

The overall impact of the wave farm on the sediment transport patterns may be quantified by means of the alongshore average of the non-dimensional LST rate reduction (τ), hereafter denoted by $\overline{\tau}$ (Table 5.6). In low energy conditions, the greatest decline in LST rates ($\overline{\tau} = 42\%$) occurs in SC3, followed by SC4, SC2 and SC1 ($\overline{\tau} = 33\%$). Under the westerly storm, the wave farm is less effective at attenuating longshore sediment transport. The most pronounced attenuation occurs in SC4 ($\overline{\tau} = 11\%$) and SC3 ($\overline{\tau} = 10\%$), with a mere $\overline{\tau} = 2\%$ in SC1.

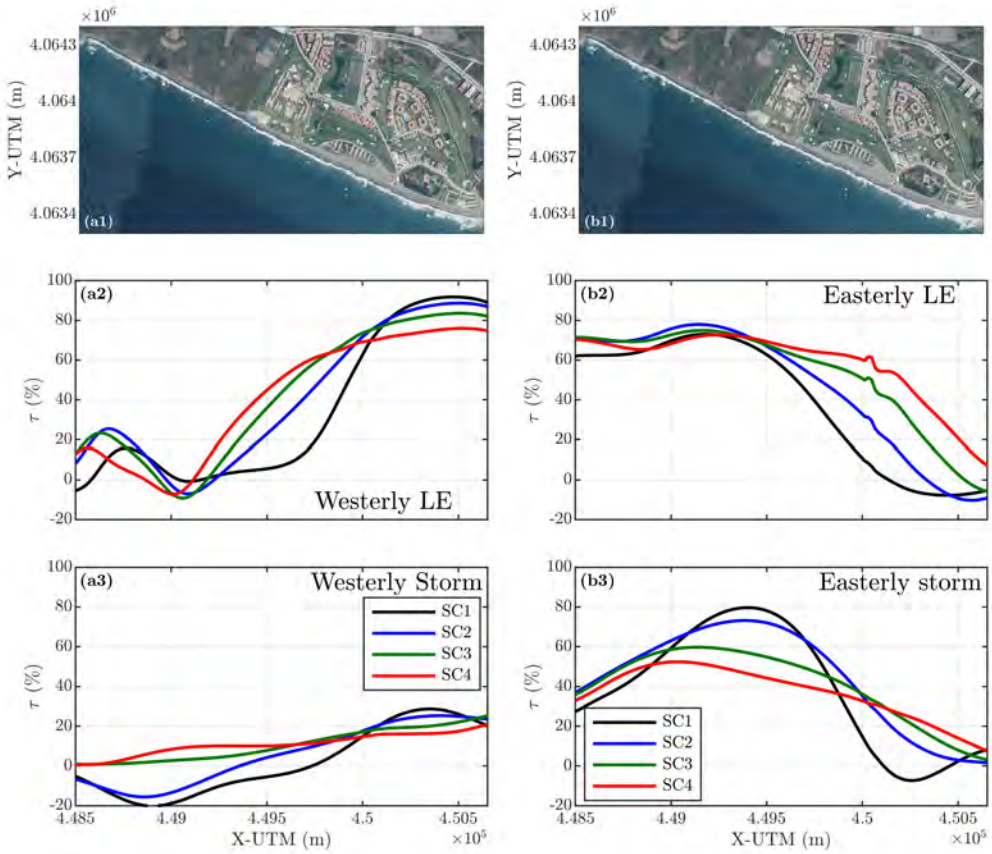

Fig. 5.31 Aerial photograph of Playa Granada (a1-b1). Alongshore variation of the non-dimensional LST rate reduction (τ) under westerly (a) and easterly (b), low energy (2) and storm (3) conditions. Rodriguez-Delgado et al. (2019).

Under easterly waves, LST rate reduction patterns follow the trends of the significant wave height in the surf zone, with maximum reductions in the west part of the beach, decreasing eastwards in low energy conditions; by contrast, under storm conditions this most pronounced reduction occurs in the central area of the beach (Figure 5.31b2-b3). Considering the entire beach, SC4 generates the best overall results under low energy conditions ($\overline{\tau} = 59\%$, Table 5.6), followed by SC3 ($\overline{\tau} = 54\%$), SC2 ($\overline{\tau} = 48\%$) and SC1 ($\overline{\tau} = 40\%$). Under storm conditions, the best scenario in terms of coastal protection is SC2 ($\overline{\tau} = 45\%$), followed by SC3 and SC1, whereas SC4 provides the worst protection ($\overline{\tau} = 37\%$).

Table 5.6 Longshore average of the non-dimensional LST rate reduction ($\overline{\tau}$) [%]. Rodriguez-Delgado et al. (2019).

	Low energy		Storm	
	West	East	West	East
SC1	33	40	2	40
SC2	40	48	5	**45**
SC3	**42**	54	10	42
SC4	41	**59**	**11**	37

5.5.3 Shoreline position

In this section, the results concerning the changes in the shoreline position, obtained by means of the LST rates presented in the previous section and the one-line model, are analysed. Advance of the final shoreline position with respect to the natural scenario dominate under low energy conditions (Figure 5.32). SC1 and SC2, with a smaller spacing between WECs, lead to the maximum advance with respect the baseline in the east part of the beach (Figure 5.32a1-a2). However, in SC3 and SC4, formed by WECs with a longer spacing between them, the advance with respect to the natural scenarios is lower at the east of the beach, but a positive effect is also observed in the central part of Playa Granada (Figure 5.32a3-a4).

The alongshore averages of the non-dimensional shoreline advance ($\overline{\upsilon}$) were also computed (Table 5.7). Results show that under western low energy conditions, SC1 provides the best performance with $\overline{\upsilon} = 9.6\%$, followed by SC2 and SC3. Finally, the worst results are obtained with SC4 ($\overline{\upsilon} = 7.3\%$). Under eastern waves, results are similar

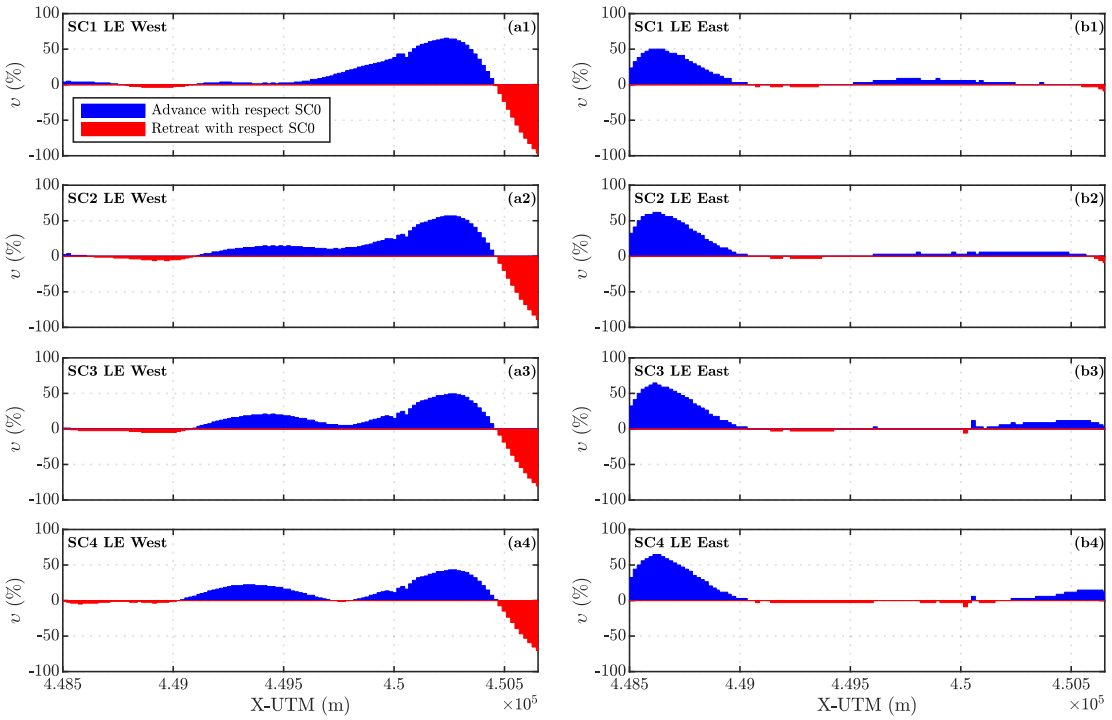

Fig. 5.32 Alongshore variation of the non-dimensional shoreline advance, westerly (a) and easterly (b) low energy conditions. Rodriguez-Delgado et al. (2019).

in the four scenarios, with advance dominating in the westernmost area of Playa Granada and less important changes in the rest of the beach (Figure 5.32b1-b4). Regarding the alongshore-averaged values, SC3 and SC2 lead to the best performance in terms of coastal protection with $\overline{\upsilon} = 10.6\%$ and $\overline{\upsilon} = 10.2\%$, respectively, whereas SC1 and SC4 provide the worst results (Table 5.7).

Non-dimensional shoreline advance values are lower under westerly storm conditions (Figure 5.33a1-a4). Advace dominates in mid-beach, with retreat at both the eastern and western boundaries of the beach for SC1 and SC2. In SC3 and SC4, with greater inter-WEC spacings, some advance occurs also in the east section. The greatest advance occurs in SC2 ($\overline{\upsilon} = 3.2\%$), followed by SC3, whereas in cases SC1 and SC4 the wave farm is slightly less effective (Table 5.7).

Under easterly storm conditions, in SC1 the wave farm leads to mid-beach advance and retreat to the east and west (Figure 5.33b1). In the other scenarios, the advance zone reaches the east limit of the beach (Punta del Santo). In SC2 and SC3 the greatest alongshore-averaged values are obtained, with $\overline{\upsilon} = 6.3\%$ and $\overline{\upsilon} = 6.0\%$, respectively (Table 5.7); conversely, in SC1 the wave farm performance is rather discrete ($\overline{\upsilon} = 1\%$).

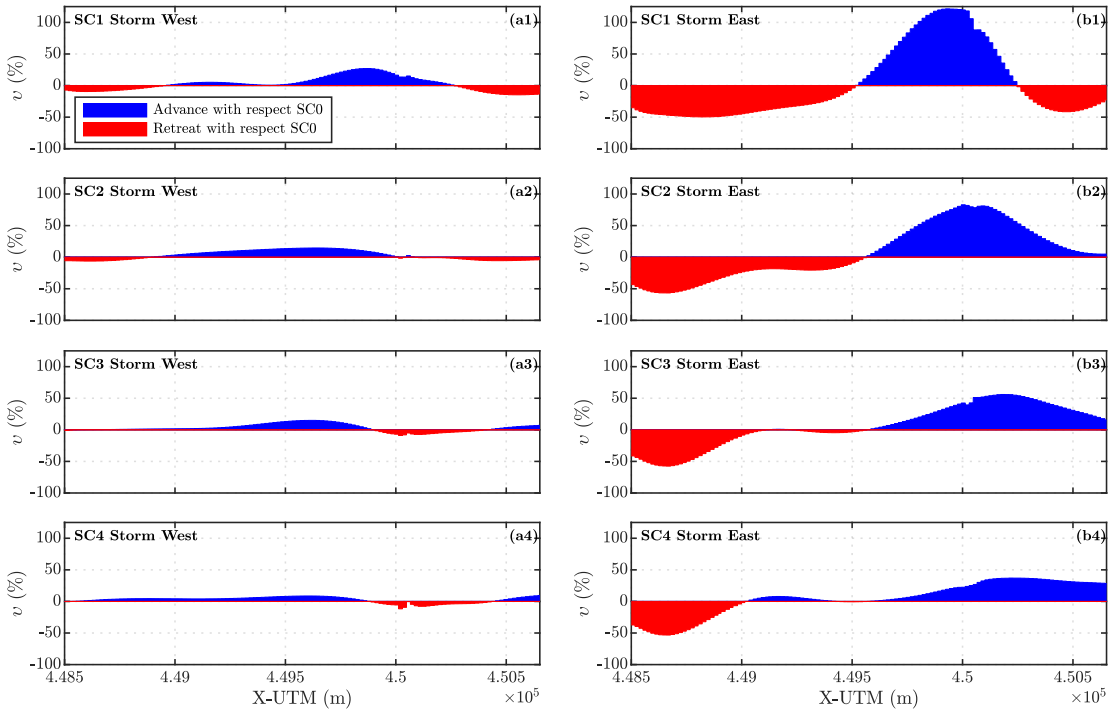

Fig. 5.33 Alongshore variation of the non-dimensional shoreline advance, westerly (a) and easterly (b) storm conditions. Rodriguez-Delgado et al. (2019).

Table 5.7 Longshore average of the non-dimensional shoreline advance ($\overline{\upsilon}$) [%]. Rodriguez-Delgado et al. (2019).

	Low energy		Storm	
	West	East	West	East
SC1	**9.6**	8.5	2.5	1
SC2	8.8	10.2	**3.2**	**6.3**
SC3	8.0	**10.6**	2.9	6.0
SC4	7.3	9.5	2.4	4.0

5.5.4 Dry beach surface

The shoreline position changes, obtained by means of the one-line model and presented in the previous section, may be used to establish the trends of the dry beach surface respect to the baseline scenarios (Figure 5.34), so that positive values of the dry beach surface represent coastal protection induced by the wave farm. Under low energy westerly waves, SC1 provides the best results in terms of coastal protection, with an additional surface area of 1.9 m^2; at any rate, the protection is of the same order of magnitude in the other cases: SC2 (1.8 m^2), SC3 (1.6 m^2) and SC4 (1.4 m^2). Under low energy easterly conditions, the differences are lower and the maximum values – best protection – are obtained for SC2 and SC3.

As expected, the greatest dry beach area differences are obtained under storm conditions (Figure 5.34a2-b2). Under westerly waves, SC2 provides the greatest difference (17.4 m^2), followed by SC3 (15.9 m^2), whereas SC1 and SC4 lead to the worst results (14.2 m^2 and 13.3 m^2, respectively). Regarding the easterly storm conditions, SC2 and SC3 induce similar area differences (34.5 m^2 and 33.1 m^2, respectively), SC4 produces a dry beach surface difference of 22 m^2 and, finally, the worst results are obtained with SC1 (6.2 m^2).

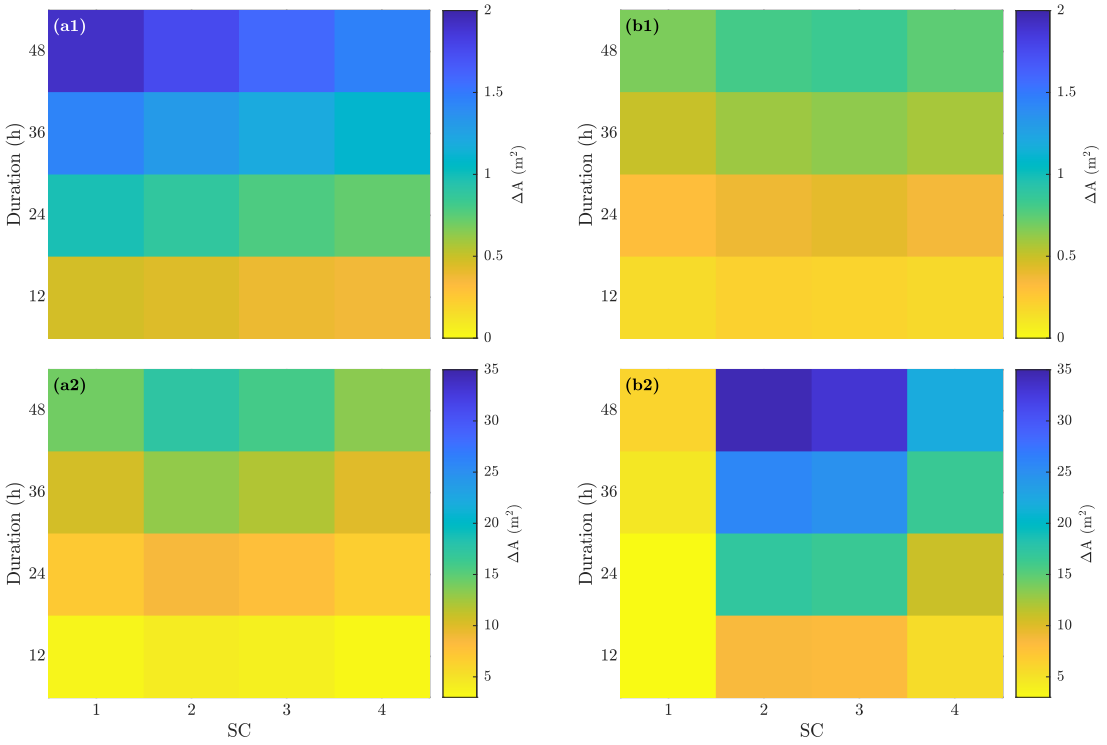

Fig. 5.34 Temporal evolution of the dry beach surface difference between each scenario and the baseline for low energy (1), storm (2), westerly (a) and easterly (b) conditions. Rodriguez-Delgado et al. (2019).

The duration has been included in this study in order to assess the influence of the storm persistence on the shoreline evolution of the study site. However, for the four scenarios studied and under the four conditions modelled, the dry beach area difference is almost linear with the duration. This is especially remarkable in the case of the storm conditions. This effect is due to two facts. First, the geometry of Playa Granada, almost completely rectilinear excepts for the two ends (Punta del Santo to east and Guadalfeo river mouth to the west) which produce almost no changes in the mean direction at breaking and therefore, in the LST rates. And second, the period studied is no sufficiently long to produce significant changes in this rectilinear shape.

5.5.5 Overall performance of the wave farm

On the basis of the previous data, the effectiveness of the dual wave farm depends on the energy content of the sea state (storm vs. low energy) and, even more importantly, on its mean direction (eastern vs. western). For the purpose of quantifying the coastal protection effectiveness of the farm in the different scenarios, in this section the indicators concerned are pondered according to the occurrence of easterly and westerly, low energy and storm conditions, over the last 25 years. This period of time was chosen as representative of the typical life cycle of a wave farm, following Margheritini et al. (2009) or Alonso et al. (2015), among others. The indicators weighted by the occurrence of the respective wave conditions are denoted by the subindex w (η_w, τ_w, υ_w, ΔA_w).

The maximum values of the weighted non-dimensional significant wave height reduction (η_w) occur in the central part of the beach for SC1 and SC2 (Figure 5.35c), and in the west part for SC3 and SC4, with a greater spacing between WECs. In all scenarios, the minimum values are observed in the east end of Playa Granada. Alongshore-averaged weighted values show that SC2 and SC1 have the best overall performance, with $\overline{\eta_w} = 9\%$ and $\overline{\eta_w} = 8.9\%$, respectively. SC3 achieves an alongshore-averaged weighted value of 7.5%, whereas SC4 leads to the worst performance ($\overline{\eta_w} = 6.3\%$).

A similar behaviour is obtained for the weighted non-dimensional LST reduction (τ_w). Again, in cases SC1 and SC2 the largest values occur in the central part of the beach, while in SC3 and SC4 the maxima occur towards the west (Figure 5.35d). In this case, SC3 provides the best overall performance with $\overline{\tau_w} = 26\%$, followed by SC2 and SC4 ($\overline{\tau_w} = 25\%$ and $\overline{\tau_w} = 24\%$). Finally, the lowest alongshore-averaged weighted value is obtained for SC1 ($\overline{\tau_w} = 21\%$).

According to the values of the weighted non-dimensional shoreline advance (υ_w), in SC1 advance with respect the baseline dominates in the central stretch, whereas retreat prevails in both east and west ends (Figure 5.35e). In the other cases retreat is limited to the west part of the beach. This retreat zone is narrower in SC3 and SC4, although the maxima of the weighted non-dimensional shoreline advance are lower in these cases than in SC1 and SC2. Alongshore-averaged values show that the best performance in terms

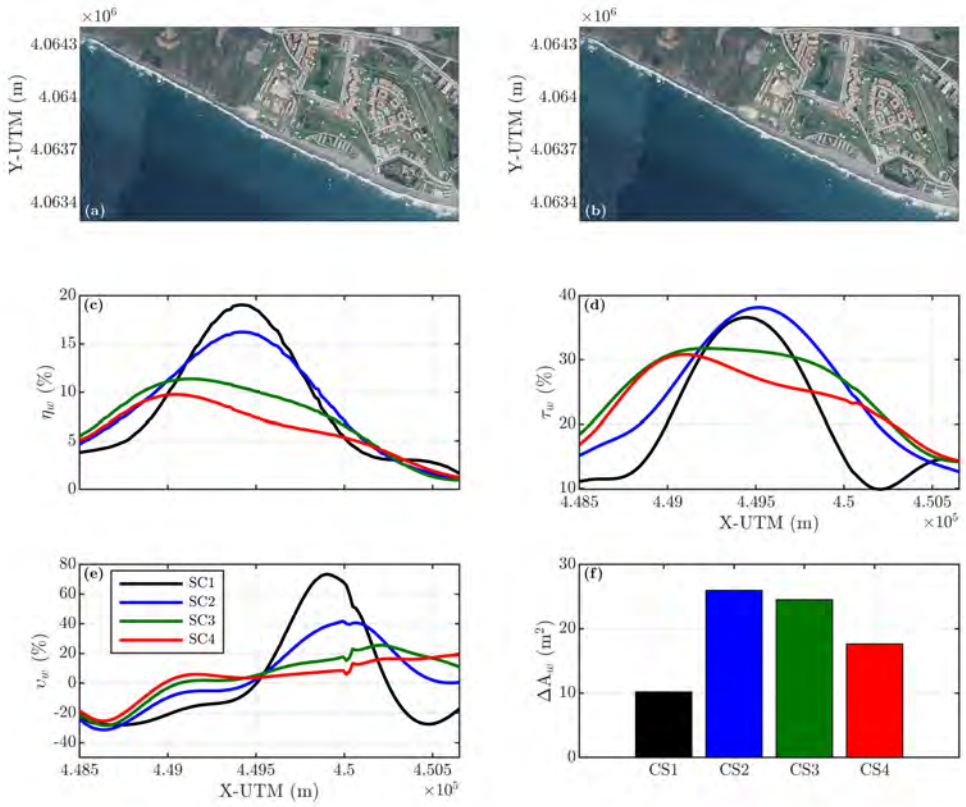

Fig. 5.35 (a,b) Aerial photograph of the beach; (c) η_w (weighted value of η); (d) τ_w (weighted value of τ); (e) υ_w (weighted value of υ); and (f) ΔA_w (weighted value of ΔA) in the four scenarios. Rodriguez-Delgado et al. (2019).

of increased dry beach area occurs for SC2 ($\overline{\upsilon_w} = 4.7\%$), followed by SC3 ($\overline{\upsilon_w} = 4.5\%$), SC4 ($\overline{\upsilon_w} = 3.3\%$) and SC1 ($\overline{\upsilon_w} = 1.8\%$).

Finally, the overall impact on the dry beach surface of Playa Granada is shown in Figure 5.35f, where it is observed that accretion with respect to the baseline dominates for all scenarios. SC1, with the smallest inter-WEC spacing, yields the worst overall performance, with a dry beach surface increase of a mere 10.2 m^2. Conversely, the best results occur in SC2 ($\Delta A_w = 25.9$ m^2), followed by SC3 ($\Delta A_w = 24.5$ m^2). Finally, SC4 shows that when the inter-WEC spacing is increased beyond a certain threshold, the coastal protection performance of the wave farm decreases significantly ($\Delta A_w = 17.6$ m^2).

5.6 Discussion

In this section, the results presented in this chapter are discussed, and the specific conclusions applicable to the study site are described. A more generalised discussion and analysis of the repercussions of this work beyond the study site will be presented in the next chapter. Modifications in the wave climate due to the presence of the wave farm were modelled numerically with a wave propagation model (Delft3D) calibrated and validated for the study area. Wave breaking parameters obtained with Delft3D were used to compute LST rates and apply the one-line model in order to quantify farm-induced changes in the shoreline morphology.

Section 5.3 deals with the effects of a wave farm on wave propagation patterns, longshore sediment transport and shoreline evolution on a gravel-dominated deltaic beach (Playa Granada, southern Spain), which has experienced significant erosion problems in recent years. The results indicate that scenarios 4 and 5 are the most advisable alternatives of wave farm location in terms of coastal protection. The reductions in significant wave height and LST rates are greater under easterly storm conditions: while the alongshore-averaged value of the non-dimensional wave height reduction ($\overline{\eta}$) is 2.3% (0.6%) for scenario 4 (scenario 5) under westerly storms, this rises to 12.4% (16.4%) in the case of easterly storm waves. The maximum non-dimensional alongshore-averaged LST rate reduction under easterly (westerly) storm conditions is obtained with scenario 5 (scenario 4), with reductions of 44.6% (22%).

Considering the number of westerly/easterly and low energy/storm sea states over the last 25 years, scenarios 4 and 5 increase the weighted average dry beach surface in 24.12 m^2 and 25.58 m^2, respectively, with respect to the no-farm situation (scenario 0). The evolution of the dry beach area shows that the wave farm location is a key parameter in preventing negative effects in terms of coastal protection; indeed, only three of the eight scenarios studied generate a weighted increment in dry beach surface with respect to the baseline (no-wave) farm scenario: scenarios 3, 4 and 5. Taking into account both wave resource and coastal protection criteria, scenario 5 is the best option for installing a wave farm.

Section 5.4 has shown the effects of the wave farm layout on the study site. The impact that each scenario has on the significant wave height at breaking and, therefore, on the LST rates and erosion/accretion patterns, which modify the resulting dry beach area, is different depending on the incoming wave direction. Under westerly waves, reductions in significant wave height in the lee of the wave farm are mainly focused on the stretch of beach close to the farm. Thus, scenarios 3 and 4, with a greater number of rows but covering a shorter length of beach, maximise advance in the eastern part of the beach. However, scenarios 1 and 2, with fewer WEC rows but covering a longer stretch, increase the non-dimensional alongshore-averaged shoreline advance, with gains of dry beach area of 16.05 m^2 and 17.43 m^2 with respect to the baseline scenario, respectively. Under easterly waves, advance occurs principally in the western part of Playa Granada, with greater values of shoreline advance than under westerly wave conditions. Again, scenarios 1 and 2 yield higher non-dimensional alongshore-averaged shoreline advances, resulting in an increase of dry beach surface of 35.29 m^2 and 34.46 m^2, respectively.

Taking into account the number of westerly/easterly and low energy/storm sea states during the last 25 years, the best protection provided by scenarios 1 and 2 is confirmed. The weighted dry beach surface difference with respect to the baseline scenario is slightly higher for scenario 2 (25.94 m^2 versus 25.67 m^2), whereas scenarios 3 and 4 yield a lower increase in beach surface (22.9 m^2 and 21.19 m^2, respectively). It follows that, in terms of coastal protection, a wave farm layout with more WEC rows does not perform better, and

the length of beach covered by the wave farm is more relevant as it increases the spread of the wave farm shadow.

Finally, in Section 5.5, the impact on the coast produced by the inter-device spacing of the WECs forming a wave farm has been studied. The results depict that the sea state was found to affect the performance of the dual wave farm. In the case of westerly waves, a smaller inter-WEC spacing results in a more pronounced wake of the farm and, consequently, a more pronounced reduction in the significant wave heights in the surf zone and the LST rates. Conversely, a greater spacing reduces the impact of the farm on the shoreline.

In the case of easterly waves, and due to the position of the wave farm vis-à-vis the beach, the effect of the farm on the beach is more intense, whether it be in terms of significant wave heights in the surf zone or LST rates. The differences between scenarios, less marked than under westerly waves, are as follows. A smaller inter-WEC spacing leads to advance of the shoreline with respect the baseline in a narrow stretch and erosion elsewhere. With greater inter-WEC spacings, this retreat is mitigated, but the concentrated advance is also weaker.

The values of the increase in dry beach area (ΔA_w) show that the best performance is achieved with intermediate inter-WEC spacings, i.e., $2D$ and $3D$ (corresponding to scenarios SC2 and SC3, respectively). Indeed, these scenarios lead to the greater increases in weighted dry beach surface ($\Delta A_w = 25.9$ m^2 and $\Delta A_w = 24.5$ m^2, respectively). SC1, with the smallest inter-WEC spacing (D), results in advance concentrating in a narrow stretch, with significant retreat elsewhere. Finally, SC4, at the other extreme of inter-WEC spacing ($4D$), results in weaker advance and, overall, a weaker gain in dry beach surface than SC2 and SC3. Based on these results, SC2 (inter-WEC spacing, $2D = 180$ m) emerges as the best option in terms of coastal protection among those studied in this section.

The duration was implemented in this research work to identify trends in the shoreline evolution of the coastal system. However, in all the scenarios tested the influence of the duration was limited. Shoreline advance (or retreat) results are linear with the duration in all cases. This is due to the LST rates obtained. LST rates depend on two parameters: (i) the characteristics of the sea state (significant wave height, wave period and mean

wave direction) and (ii) the geometry of the shoreline studied, more specifically, the angle between the shoreline and the incident waves. As the sea states were kept constant along with the duration of the numerical experiment, this part did not change with time. Also, as per the shoreline geometry, Playa Granada is nearly rectilinear in its whole domain except for the regions next to the Guadalfeo river mouth and Punta del Santo. In a rectilinear shoreline, the angle between this and the incident waves does not vary significantly in the short term. Because of that, LST rates are almost constant along with the numerical experiment and therefore, the variation of the position of the shoreline is linear with time.

Playa Granada is a highly altered system as has been described in Chapter 4 with a number of land uses present. It is important to note that the election of a determined location for a wave farm in order to provide coastal protection is a complicated problem that involves many factors and agents. Although as a summary in Section 5.3 the dry beach surface has been used to benchmark the impact of each scenario on the stretch of coast, from Figures 5.13 to 5.16 it is clear that this dry beach surface difference is not equally distributed along the coast. Land uses in Playa Granada may be summary in two big groups: agricultural uses in the west part (up to X-UTM = 4.4925×10^5 m approx.) and recreational uses in the east part. This distribution makes that each scenario affects each use differently.

The distribution of shoreline advance and retreat with respect of the baseline scenario depicted in Figures 5.13 to 5.16 shows that under westerly storms scenarios 1, 2, 7 and 8 do not produce great alterations to the system. However, scenarios 3 and 4 produce advance in the west part, producing a positive impact to the agricultural uses in the study site, whereas scenario 6 produces the opposite: retreat with respect the baseline of the beach part dedicated to agricultural uses and shoreline advance in the area designated to recreational uses. Scenario 5, which is also the best in terms of overall dry beach surface difference, minimise the retreat in both ends and produce an advance of the shoreline in the central part of the beach, affecting both land uses equally. Under easterly waves the behaviour of the system is similar, with each scenario producing different affections to these two groups of land uses.

Attending the wave farm layout (Section 5.4) scenarios 2, 3 and 4 focus the advance of the shoreline with respect the baseline in the east part where recreational uses dominate. However, these scenarios maximise the retreat of the shoreline in the west part of the beach where agricultural uses are found. Scenario 1 for its part, partially avoid the retreat of the shoreline in the agricultural uses area but it also reduces the advance in the area of recreational uses. In this sense the layout of the wave farm could be used to enhance the impact in determined areas.

As stated previously, in the case of the inter-device spacing, scenarios with a lower spacing concentrate the impact in a narrow stretch of beach and the scenarios with a greater spacing spread this impact to a wider stretch. This fact adds a layer of flexibility to the decisions of managers and stakeholders. Related to the configuration of Playa Granada, similar to the conclusions drawn in the previous paragraph. In this case, the four scenarios modelled produce a retreat of the shoreline in the west part of the beach, where agricultural uses dominate. However, this retreat is higher for SC1 and SC2 with a lower spacing. In addition, these scenarios maximise the advance of the shoreline in the east part of the coast, which is mostly dedicated to recreational uses. On the contrary, SC3 and SC4 which depicted the worst overall performance, minimise the retreat in the agricultural land uses area but also minimise the relative advance of the shoreline in the west part of the beach.

The Guadalfeo deltaic coast is a closed system and thus, the only sources of sediments are the river discharge and the sediment transport between the beaches that form the system. Another sign of the many factors involved in the decision can be observed in the impact produced by scenario 7 of the position sensitivity analysis, under easterly waves. In the section dedicated to the baseline results it is observed that easterly storms produce advance of the shoreline with respect the baseline in Playa Granada, this is because under easterly waves the sediment accumulated in Poniente Beach is transported to the west towards Playa Granada. The wave farm modelled in scenario 7 is located just in front of Poniente Beach, reducing the sediment transport at this zone and therefore, reducing the main source of sediments to Playa Granada. In this sense, it is important to note that in a similar manner a wave farm situated in front of Playa Granada would have a similar effect on the adjacent beaches. Salobreña beach situated at the west of Playa Granada is a more isolated

beach in terms of sediments transport due to the river walls present at the Guadalfeo River mouth which prevent most of the sediment transport. Therefore, scenarios 4 and 5 which produce the greater increase of dry beach surface difference at Playa Granada will produce a reduction of dry beach surface at Poniente Beach. However, this fact would help to recover the natural balance of the system as Poniente Beach is overfilled since the Guadalfeo river management has altered the sediment transport dynamic of the beach.

This kind of questions should be answered by designers and stakeholders in the case of a real wave farm project design. The methodology presented at this thesis could help to take decisions in a more informed way, being able to identify the areas affected and characterising the solution based on the specific features of each system. In addition, managers and stakeholders are able to study these parameters to fulfil the requirements of each project. In this sense, not only the alongshore position but the wave farm layout can be calibrated in order to achieve the desired impact on the coast. In the next chapter the main conclusion drawn will be shown, highlighting the main findings of this research.

Chapter 6

Summary and future work

6.1 Conclusions and main findings

Wave energy has received increasing attention in recent years due to its potential and the need for developing carbon-free energies. The repercussions for nearshore hydro- and morphodynamics must be fully understood prior to undertaking any wave farm installation. These effects may be used in coastal areas subjected to erosion to alleviate this problem; in other words, wave farms may have a dual function: carbon-free power production and coastal erosion control. This thesis tries to study the effects of wave farms on gravel-dominated coasts since previous works on this area were focused mainly on sandy beaches. More precisely, three specific objectives were proposed: (i) to study the influence of the alongshore position of the wave farm, (ii) the impact of the layout of the wave farm, and (iii) to address the influence of the inter-device spacing in the coastal protection.

To this end, this thesis investigates the effects of the alongshore location and layout of a wave farm composed by WaveCat wave energy converters (WECs) on a gravel-dominated beach (Playa Granada, southern Spain). Eight scenarios corresponding to alongshore locations were modelled and compared. With the location selected in base of the results of the position sensitivity study, the influence of the layout and more precisely, the number of rows keeping constant the amount of WECs composing the wave farm was analysed by means of four scenarios of wave farm configurations. Finally, four scenarios with different inter-device spacings were modelled and compared. Variations in wave propagation patterns were computed using a spectral wave propagation model (SWAN), longshore

sediment transport rates were assessed and, finally, changes in both the shoreline position and the dry beach surface were obtained by means of a one-line model. Finally, *ad hoc* non-dimensional indicators of the performance of the dual wave farm for coastal erosion control were applied. From the study of these specific objectives, some conclusions may be extracted.

The results of the position sensitivity study indicates that SC5, situated in the east part of Playa Granada, is the most advisable location for the wave farm in terms of coastal protection, increasing the dry beach by 25.58 m^2 per storm on average with respect to the no-farm situation. The wave farm location is a key parameter in preventing negative effects in terms of coastal protection; indeed, it was found that only three of the eight locations studied generated a weighted increase in dry beach surface with respect to the baseline. In the case of the wave farm layout, the best scenario is that composed by two rows of WECs. In this case, the increase in dry beach surface with respect to the baseline scenario is 25.94 m^2, whereas the farms with 3 and 4 rows yield a lower increase in beach surface. Finally, four inter-device spacings were modelled and the best results were obtained for a spacing of 2D, where D = 90 m is the space between the two bows of the WaveCat. This option yields an average increase per storm in dry beach area of 25.9 m^2.

As main findings of this thesis, the research carried out in this work shows that the most important parameter in order to achieve the expected results in terms of coastal protection performance of a dual wave farm is the alongshore position. The significance of the results of the position sensitivity study is that they provide evidence of the critical role played by the longshore position of the farm in determining whether its effects are negative (retreat) or positive (advance). The analysis of the alongshore position effects shows that the location of the wave farm is a key parameter, not only in terms of energy production but also in order to use the wave farm as a coastal management element. Only three locations of a total of eight studied produced a positive impact on the shoreline evolution and consequently on the dry beach area surface. Once the alongshore position is fixed, layout and inter-device spacing may help to improve the obtained results. In the case of the number of rows of the wave farm layout, the results show that those wave farms with a greater number of rows maximise advance with respect the baseline in the stretch of

coast situated just at their lee. However, the wave farms with fewer rows produce a lower local advance just in their lee but extend the impact to a greater extension of the coast. In summary, a wave farm with a greater number of rows does not perform better in terms of coastal protection, as the extension of the stretch of coast covered is more relevant. A similar conclusion can be drawn from the inter-device spacing impact study. Wave farms with a lower inter-device spacing produce higher local peaks of shoreline advance in their lee. On the contrary, wave farms with greater spacing reduce this retreat but the advance is also weaker, affecting the dry beach area difference with respect to the baseline. In this case, the wave farms with an intermediate spacing achieve a balance between these two extremes and stand as the better alternatives.

The use of an LST formulation specifically designed for gravel beaches and the validation of the model improve the accuracy of the results. To this end, it is proved that WECs can reduce erosion in gravel dominated beaches. Gravel beaches are dominant in high latitude areas and steep slopes basins. Moreover, gravel dominated beaches are more common nowadays due to the increasing prevalence of artificial beach nourishments as coastal protection or coastal defence measures, of which a great number use coarser gravel sediments. Therefore, the conclusions obtained in this work have great relevance in relation to the coastal management of these important coastal environments.

Given the prevalence of gravel coastlines worldwide, these findings are relevant in that they open up the possibility of using wave farms not only for carbon-free energy production but also for coastal protection. This methodology, which may be applied to other coastal areas, constitutes a useful tool for the decision-making in the development of a wave farm, which considers not only the potential energy production, but also the repercussion for the nearshore hydrodynamics, longshore sediment transport and shoreline morphology. Although the limitations of this study need to be understood prior the application of this methodology. The case studies analysed do not cover the full range of possibilities, and this research should be continued to explore more combinations of these and other variables involved in the design of a wave farm. Another aspect of note is the characteristics of the beach itself. Playa Granada is a gravel-dominated beach, and the results of this thesis cannot be extrapolated to beaches with different sedimentologies. These results should be

taken as an example of the impact produced by wave farms on gravel dominated beaches. WaveCat is a WEC with particular features and this study was carried out in a particular gravel dominated beach, with a particular geometry, sedimentology and wave climate. However, the relevance of each parameter on the impact of a wave farm on the coast nearshore are valid for wave farm projects in the vicinities of gravel dominated coasts worldwide. Moreover, the methodology applied in this thesis allows to control thoroughly the different aspects that play a role in the shoreline evolution so the results could be adapted for the needs of each project.

It should be noted that, some limitations arise around the methodology followed in this thesis. First of all, as mentioned in the last paragraph only a few sea states have been tested. In this sense, results cannot be fully extrapolated to the long term and the results can only be taken as an assessment in order of magnitude. Besides, WEC survivability is still compromised under storms. The Mediterranean Storms tested in this thesis have lower energy than Atlantic cyclones and most WECs developed at this moment should withstand storms of this magnitude. However, it is important to note that we are modelling a "best case" in which WECs are fully operating under a storm and this is not always the case. Moreover, the grid size sensitivity study showed that some boundary effects are present in the east end. Although, as the results shown, it has little effect on the finer grid where the wave farms are placed, this has to be taken into account.Finally, numerical scheme used for the one-line model is very sensitive to changes of aligment of the coast. Therefore, model accuracy is lower when sudden changes in alignment appear as in the case of Punta del Santo.

Finally, the results show that wave farms may be used as coastal defence elements in gravel dominated coasts, reducing erosion in eroded beaches. This synergy increases the value of wave energy. First, because wave farms provide an alternative tool for coastal protection in coasts at risk such as deltaic coasts with an important economic, social and environmental value. In this sense, wave farms can compete with traditional coastal defence structures such as jetties or groins, as they can also produce carbon-free energy which is becoming more and more important due to the limited existence of fossil fuels and the environmental problems derived from their use. Second, the economic externalities

derived from the coastal protection may be incorporated to wave energy. The benefits accruing from the latter are externalities from the point of view of the wave farm project. It these externalities are internalised by means of appropriate schemes, i.e. if the benefits in terms of coastal protection for the community are transferred, albeit partially, to the wave farm developer in the form of subsidies, tax breaks, or other appropriate incentives, they will make wave energy more competitive vis-à-vis other renewables and thus contribute to its development. However, a number of parameters have to be taken into account in order to maximise the coastal protection of the wave farm. Especially, the alongshore position stands out as a key parameter in order to achieve positive results for coastal management. The methodology proposed in this thesis can be extended easily to other gravel dominated coasts worldwide and in this sense provides a useful tool for coastal managers and designers in this kind of projects, allowing to add an extra value to the wave farm.

6.2 Future research lines

From the results and conclusions extracted in this thesis, a number of future research lines arise. The following research lines may help to further explore the use of wave farms for coastal defence, improving the existing knowledge and the methodology proposed for designing and management purposes:

- In this thesis, the performance of wave farms in terms of coastal defence was explored through the shoreline evolution and dry beach area. However, another key aspect of the coastal defence structures is preventing coastal flooding. In this sense, wave farms, as floating structures, could improve the performance of traditional detached structures like jetties or groins. With this purpose, the methodology described in this paper could be combined with a nearshore sediment transport and mean flow numerical model (for example XBeach), to obtain run-up values and flooded dry beach area.

- In relation to the previous item, the adaptability of wave farms to the future sea-level rise is another key element. In order to provide an effective coastal defence in the

next years, wave farms need to be able to adapt to future scenarios including sea-level rise and the increase of the storminess. Available sea-level rise data provided by the Intergovernmental Panel on Climate Change (2014) could be incorporated to the described methodology to study the influence of the sea-level rise on the results obtained.

- Diverse parameters in the decision-making process of a wave farm project were studied in this thesis. The developing of a unified numerical tool, capable of dealing with the different aspects would be an important improvement for the design process. Artificial intelligence tools such as neural networks have been widely applied in the coastal engineering and energy literature to achieve similar purposes in wind farms (Lin et al., 2013; Ou et al., 2017), OWC systems (López and Iglesias, 2014) and headland-bay beaches (Iglesias et al., 2010).

- Until now, the impacts of wave farms on the coast have been studied at storm scale. Further studies, including the whole life-cycle of the wave farm, would consolidate our knowledge and would contribute to fully understanding the effect of wave farms on the beach situated in their lee. In this sense, simplified models and downscaling techniques could be used to study longer time scales within a reasonable computational effort.

- Finally, economic aspects derived from the synergy between wave energy and coastal protection have not been fully addressed so far. How the economic externalities derived from the coastal management can be incorporated and, more importantly, how they may improve the viability of wave energy still needs further study. Similar studies can be found in the literature for offshore wind farms and their synergies with wave farms in Astariz and Iglesias (2015); Astariz et al. (2015).

References

(1990). *The Progress Of Wave Power Generator In Japan*, volume All Days of *Pacific/Asia Offshore Mechanics Symposium*. ISOPE-P-90-022.

Abanades, J., Flor-Blanco, G., Flor, G., and Iglesias, G. (2018). Dual wave farms for energy production and coastal protection. *Ocean & Coastal Management*, 160:18 – 29.

Abanades, J., Greaves, D., and Iglesias, G. (2014a). Coastal defence through wave farms. *Coastal Engineering*, 91:299–307.

Abanades, J., Greaves, D., and Iglesias, G. (2014b). Wave farm impact on the beach profile: A case study. *Coastal Engineering*, 86:36–44.

Abanades, J., Greaves, D., and Iglesias, G. (2015a). Coastal defence using wave farms: The role of farm-to-coast distance. *Renewable Energy*, 75:572–582.

Abanades, J., Greaves, D., and Iglesias, G. (2015b). Wave farm impact on beach modal state. *Marine Geology*, 361:126–135.

Alonso, R., Solari, S., and Teixeira, L. (2015). Wave energy resource assessment in Uruguay. *Energy*, 93(Part 1):683 – 696.

Anthony, E. J., Marriner, N., and Morhange, C. (2014). Human influence and the changing geomorphology of Mediterranean deltas and coasts over the last 6000 years: From progradation to destruction phase? *Earth-Science Reviews*, 139:336–361.

Aragonés, L., Pagán, J., López, M., and García-Barba, J. (2016). The impacts of Segura River (Spain) channelization on the coastal seabed. *Science of The Total Environment*, 543:493 – 504.

Arena, F., Laface, V., Malara, G., Romolo, A., Viviano, A., Fiamma, V., Sannino, G., and Carillo, A. (2015). Wave climate analysis for the design of wave energy harvesters in the Mediterranean Sea. *Renewable Energy*, 77:125–141.

Astariz, S. and Iglesias, G. (2015). The economics of wave energy: A review. *Renewable and Sustainable Energy Reviews*, 45:397 – 408.

Astariz, S., Perez-Collazo, C., Abanades, J., and Iglesias, G. (2015). Co-located wave-wind farms: Economic assessment as a function of layout. *Renewable Energy*, 83:837 – 849.

Battjes, J. A. and Janssen, J. (1978). Energy loss and set-up due to breaking of random waves. In *Coastal Engineering 1978*, pages 569–587.

Bergillos, R. J., López-Ruiz, A., Medina-López, E., Moñino, A., and Ortega-Sánchez, M. (2018a). The role of wave energy converter farms on coastal protection in eroding deltas, Guadalfeo, southern Spain. *Journal of Cleaner Production*, 171:356 – 367.

Bergillos, R. J., López-Ruiz, A., Ortega-Sánchez, M., Masselink, G., and Losada, M. A. (2016a). Implications of delta retreat on wave propagation and longshore sediment transport - Guadalfeo case study (southern Spain). *Marine Geology*, 382:1–16.

Bergillos, R. J., López-Ruiz, A., Principal-Gómez, D., and Ortega-Sánchez, M. (2018b). An integrated methodology to forecast the efficiency of nourishment strategies in eroding deltas. *Science of The Total Environment*, 613-614:1175 – 1184.

Bergillos, R. J., Masselink, G., McCall, R. T., and Ortega-Sánchez, M. (2016b). Modelling overwash vulnerability along mixed sand-gravel coasts with XBeach-G: Case study of Playa Granada, southern Spain. In *Coastal Engineering Proceedings*, volume 1, page 13.

Bergillos, R. J., Masselink, G., and Ortega-Sánchez, M. (2017a). Coupling cross-shore and longshore sediment transport to model storm response along a mixed sand-gravel coast under varying wave directions. *Coastal Engineering,*, 129:93–104.

Bergillos, R. J., Ortega-Sánchez, M., and Losada, M. A. (2015a). Foreshore evolution of a mixed sand and gravel beach: The case of Playa Granada (Southern Spain). In *Proceedings of the 8th Coastal Sediments*. World Scientific.

Bergillos, R. J., Ortega-Sánchez, M., Masselink, G., and Losada, M. A. (2016c). Morpho-sedimentary dynamics of a micro-tidal mixed sand and gravel beach, Playa Granada, southern Spain. *Marine Geology*, 379:28–38.

Bergillos, R. J., Rodriguez-Delgado, C., Allen, J., and Iglesias, G. (2019). Wave energy converter geometry for coastal flooding mitigation. *Science of The Total Environment*, 668:1232 – 1241.

Bergillos, R. J., Rodríguez-Delgado, C., López-Ruiz, A., Millares, A., Ortega-Sánchez, M., and Losada, M. A. (2015b). Recent human-induced coastal changes in the Guadalfeo river deltaic system (southern Spain). In *Proceedings of the 36th IAHR-International Association for Hydro-Environment Engineering and Research World Congress: http://89.31.100.18/˜iahrpapers/87178.pdf*.

Bergillos, R. J., Rodríguez-Delgado, C., Millares, A., Ortega-Sánchez, M., and Losada, M. A. (2016d). Impact of river regulation on a mediterranean delta: Assessment of managed versus unmanaged scenarios. *Water Resources Research*, 52(7):5132–5148.

Bergillos, R. J., Rodríguez-Delgado, C., and Ortega-Sánchez, M. (2017b). Advances in management tools for modeling artificial nourishments in mixed beaches. *Journal of Marine Systems*, 172:1–13.

Besio, G., Mentaschi, L., and Mazzino, A. (2016). Wave energy resource assessment in the mediterranean sea on the basis of a 35-year hindcast. *Energy*, 94:50–63.

Bjerke, I., Hjetland, E., Tjensvoll, G., and Sjolte, J. (2011). Experiences from field testing with the bolt wave energy converter. In *Proceedings of the 9th European Wave and Tidal Energy Conference (EWTEC11), Southampton, UK*, volume 59.

Boake, C. B., Whittaker, T. J., Folley, M., Ellen, H., et al. (2002). Overview and initial operational experience of the limpet wave energy plant. In *The Twelfth International Offshore and Polar Engineering Conference*. International Society of Offshore and Polar Engineers.

Boccotti, P. (2003). On a new wave energy absorber. *Ocean Engineering*, 30(9):1191–1200.

Booij, N. et al. (2008). Swan technical documentation: Swan cycle iii version 40.72. *Delft University of Technology*.

Boren, B. C., Batten, B. A., and Paasch, R. K. (2014). Active control of a vertical axis pendulum wave energy converter. In *2014 American Control Conference*, pages 1033–1038.

Boström, C., Svensson, O., Rahm, M., Lejerskog, E., Savin, A., Strömstedt, E., Engström, J., Gravråkmo, H., Haikonen, K., Waters, R., Björklöf, D., Johansson, T., Sundberg, J., and Leijon, M. (2009). Design proposal of electrical system for linear generator wave power plants. In *2009 35th Annual Conference of IEEE Industrial Electronics*, pages 4393–4398.

Bozzi, S., Besio, G., and Passoni, G. (2018). Wave power technologies for the mediterranean offshore: Scaling and performance analysis. *Coastal Engineering*, 136:130 – 146.

Brown, S. and Nicholls, R. (2015). Subsidence and human influences in mega deltas: The case of the Ganges–Brahmaputra–Meghna. *Science of The Total Environment*, 527-528:362 – 374.

Buccino, M., Stagonas, D., and Vicinanza, D. (2015). Development of a composite sea wall wave energy converter system. *Renewable Energy*, 81:509–522.

Carballo, R. and Iglesias, G. (2013). Wave farm impact based on realistic wave-WEC interaction. *Energy*, 51:216–229.

Carballo, R., Sánchez, M., Ramos, V., Fraguela, J., and Iglesias, G. (2015). The intra-annual variability in the performance of wave energy converters: A comparative study in N Galicia (Spain). *Energy*, 82:138 – 146.

Carballo, R., Sánchez, M., Ramos, V., Taveira-Pinto, F., and Iglesias, G. (2014). A high resolution geospatial database for wave energy exploitation. *Energy*, 68:572 – 583.

Castelle, B., Marieu, V., Bujan, S., Splinter, K. D., Robinet, A., Sénéchal, N., and Ferreira, S. (2015). Impact of the winter 2013–2014 series of severe Western Europe storms on a double-barred sandy coast: Beach and dune erosion and megacusp embayments. *Geomorphology*, 238:135 – 148.

Chang, G., Ruehl, K., Jones, C., Roberts, J., and Chartrand, C. (2016). Numerical modeling of the effects of wave energy converter characteristics on nearshore wave conditions. *Renewable Energy*, 89:636 – 648.

Charlier, R. H., Chaineux, M.-C. P., Finkl, C. W., and Thys, A. C. (2010). Belgica's antarctic toponymic legacy. *Journal of Coastal Research*, 26(6):1168–1171.

Chozas, J. F. and Soerensen, H. C. (2009). State of the art of wave energy in spain. In *2009 IEEE Electrical Power Energy Conference (EPEC)*, pages 1–6.

Clare, R., Evans, D., and Shaw, T. (1982). Harnessing sea wave energy by a submerged cylinder device. *Proceedings of the Institution of Civil Engineers*, 73(3):565–585.

Clément, A., Babarit, A., Gilloteaux, J.-C., Josset, C., and Duclos, G. (2005). The searev wave energy converter. In *Proceedings of the 6th Wave and Tidal Energy Conference, Glasgow, UK*, volume 29.

Clément, A., McCullen, P., de O. Falcão, A. F., Fiorentino, A., Gardner, F., Hammarlund, K., Lemonis, G., Lewis, T., Nielsen, K., Petroncini, S., Pontes, M.-T., Schild, P., Sjöström, B.-O., Sørensen, H. C., and Thorpe, T. (2002). Wave energy in Europe: current status and perspectives. *Renewable and Sustainable Energy Reviews*, 6:405–431.

Collins, J. I. (1972). Prediction of shallow-water spectra. *Journal of Geophysical Research (1896-1977)*, 77(15):2693–2707.

Contestabile, P., Ferrante, V., and Vicinanza, D. (2015). Wave energy resource along the coast of Santa Catarina (Brazil). *Energies*, 8(12):14219–14243.

Contestabile, P., Iuppa, C., Lauro, E. D., Cavallaro, L., Andersen, T. L., and Vicinanza, D. (2017). Wave loadings acting on innovative rubble mound breakwater for overtopping wave energy conversion. *Coastal Engineering*, 122:60 – 74.

Cornett, A. M. (2008). A global wave energy resource assessment. In *The Eighteenth International Offshore and Polar Engineering Conference*. International Society of Offshore and Polar Engineers.

Cruz, J. (2008). *Ocean wave energy: current status and future prespectives*. Springer Science & Business Media.

Davies, P. G., Cloke, M. S., Major, K. A., Page, D. I., and Taylor, R. J. (1985). Wave energy. the department of energy's r&d programme 1974-1983.

Dawson, D., Shaw, J., and Gehrels, W. R. (2016). Sea-level rise impacts on transport infrastructure: The notorious case of the coastal railway line at Dawlish, England. *Journal of Transport Geography*, 51:97 – 109.

de O. Falcão, A. F. (1999). Owc wave energy devices with air flow control. *Ocean Engineering*, 26(12):1275 – 1295.

de O. Falcão, A. F. (2007). Modelling and control of oscillating-body wave energy converters with hydraulic power take-off and gas accumulator. *Ocean Engineering*, 34(14):2021–2032.

de O. Falcão, A. F. (2010). Wave energy utilization: A review of the technologies. *Renewable and Sustainable Energy Reviews*, 14(3):899 – 918.

de O. Falcão, A. F., Henriques, J. C., and Cândido, J. J. (2012). Dynamics and optimization of the OWC spar buoy wave energy converter. *Renewable Energy*, 48:369 – 381.

Defne, Z., Haas, K. A., and Fritz, H. M. (2009). Wave power potential along the Atlantic coast of the southeastern USA. *Renewable Energy*, 34:2197 – 2205.

D.L. Inman and R. Bagnold (1963). *Litoral processes*. The sea.

European Commission (2007). A European Strategic Energy Technology Plan (Set-Plan): Towards a low carbon future. *Brussels: Commission of the European Communities*.

Falcão, A. d. O. (2000). The shoreline OWC wave power plant at the Azores. In *Proceedings of 4th European Wave Energy Conference*, pages 42–47.

Félix, A., Baquerizo, A., Santiago, J. M., and Losada, M. A. (2012). Coastal zone management with stochastic multi-criteria analysis. *Journal of Environmental Management*, 112:252–266.

Fernandez, H., Iglesias, G., Carballo, R., Castro, A., Fraguela, J., Taveira-Pinto, F., and Sanchez, M. (2012). The new wave energy converter WaveCat: Concept and laboratory tests. *Marine Structures*, 29:58–70.

Fernandez-Diez, P. (2004). Técnicas que aprovechan la energía de las olas. url-http://files.pfernandezdiez.es/EnergiasAlternativas/mar/PDFs/03Olas.pdf.

Foti, E. and Blondeaux, P. (1995). Sea ripple formation: the heterogeneous sediment case. *Coastal Engineering*, 25(3):237 – 253.

Gareev, A. (2011). Analysis of variable pitch air turbines for oscillating water column (OWC) wave energy converters.

Graw, K. (1996). Wave energy breakwaters-a device comparison. In *Proc. Conference in Ocean Engineering, Madras, INDIA*.

Greaves, D. and Iglesias, G. (2018). *Wave and Tidal Energy*. Wiley-Blackwell.

Guanche, R., de Andrés, A., Simal, P., Vidal, C., and Losada, I. (2014). Uncertainty analysis of wave energy farms financial indicators. *Renewable Energy*, 68(Supplement C):570 – 580.

Hammons, T. (2008). Energy potential of the oceans in Europe and North America: tidal, wave, currents, OTEC and offshore wind. *International Journal of Power and Energy Systems*, 28(4):416–428.

Hansen, R. H., Kramer, M. M., and Vidal, E. (2013). Discrete displacement hydraulic power take-off system for the wavestar wave energy converter. *Energies*, 6(8):4001–4044.

He, F. and Huang, Z. (2014). Hydrodynamic performance of pile-supported OWC-type structures as breakwaters: An experimental study. *Ocean Engineering*, 88:618 – 626.

Heath, T., Whittaker, T. J., , and Boake, C. B. (2001). The design, construction and operation of the LIMPET wave energy converter (Islay, scotland) [Land Installed Marine Powered Energy Transformer].

Henderson, R. (2006). Design, simulation, and testing of a novel hydraulic power take-off system for the Pelamis wave energy converter. *Renewable Energy*, 31(2):271 – 283. Marine Energy.

Hoffmann, G. (1987). *Holozänstratigraphie und Küstenlinienverlagerung an der andalusischen Mittelmeerküste*. PhD thesis, Universität Bremen.

Holthuijsen, L., Booij, N., and Ris, R. (1993). A spectral wave model for the coastal zone. ASCE.

Huenteler, J., Niebuhr, C., and Schmidt, T. S. (2016). The effect of local and global learning on the cost of renewable energy in developing countries. *Journal of Cleaner Production*, 128:6 – 21.

Iglesias, G. and Carballo, R. (2011). Choosing the site for the first wave farm in a region: A case study in the Galician Southwest (Spain). *Energy*, 36:5525–5531.

Iglesias, G. and Carballo, R. (2014). Wave farm impact: The role of farm-to-coast distance. *Renewable Energy*, 69:375–385.

Iglesias, G., Carballo, R., Castro, A., and Fraga, B. (2009). Development and design of the WaveCat™ energy converter. In *Coastal Engineering 2008: (In 5 Volumes)*, pages 3970–3982. World Scientific.

Iglesias, G., Diz-Lois, G., and Pinto, F. T. (2010). Artificial intelligence and headland-bay beaches. *Coastal Engineering*, 57(2):176 – 183. Hydrodynamics and Applications of Headland-Bay Beaches.

Intergovernmental Panel on Climate Change (2014). *Climate change 2014: synthesis report*. IPCC Geneva, Switzerland.

Iuppa, C., Cavallaro, L., Foti, E., and Vicinanza, D. (2015a). Potential wave energy production by different wave energy converters around Sicily. *Journal of Renewable and Sustainable Energy*, 7(6):061701.

Iuppa, C., Cavallaro, L., Vicinanza, D., and Foti, E. (2015b). Investigation of suitable sites for Wave Energy Converters around Sicily (Italy). *Ocean Science Discussions*, 12(1).

Jabaloy-Sánchez, A., Lobo, F. J., Azor, A., Martín-Rosales, W., Pérez-Peña, J. V., Bárcenas, P., Macías, J., Fernández-Salas, L. M., and Vázquez-Vílchez, M. (2014). Six thousand years of coastline evolution in the Guadalfeo deltaic system (southern Iberian Peninsula). *Geomorphology*, 206:374–391.

Jennings, R. and Shulmeister, J. (2002). A field based classification scheme for gravel beaches. *Marine Geology*, 186(3):211–228.

Kamphuis, J. W. (1991). Alongshore sediment transport rate. *Journal of Waterway, Port, Coastal, and Ocean Engineering*, 117(6):624–640.

Kamphuis, J. W. (2002). Alongshore transport rate of sand. In *Coastal Engineering Conference*, pages 2478–2490. American Society of Civil Engineers.

Kendon, M. (2015). The UK storms of winter 2013/2014. *Weather*, 70(2):39–40.

Kerr, D. (2007). Marine energy. *Philosophical Transactions of the Royal Society A: Mathematical, Physical and Engineering Sciences*, 365(1853):971–992.

Kirk, R. (1980). Mixed sand and gravel beaches: morphology, processes and sediments. *Progress in Physical Geography: Earth and Environment*, 4(2):189–210.

Kofoed, J. (2002). *Wave Overtopping of Marine Structures: utilization of wave energy*. PhD thesis, Denmark. PDF for print: 191 pp.

Kofoed, J. P., Frigaard, P., Friis-Madsen, E., and Sørensen, H. C. (2006). Prototype testing of the wave energy converter Wave Dragon. *Renewable Energy*, 31:181–189.

Kraemer, D. R., McCormick, M. E., and Ohl, C. O. (2001). Comparison of experimental and theoretical results of the motions of a mccabe wave pump.

Kung, C., Zhang, L., and Chang, M. (2017). Promotion policies for renewable energy and their effects in Taiwan. *Journal of Cleaner Production*, 142:965 – 975.

Liberti, L., Carillo, A., and Sannino, G. (2013). Wave energy resource assessment in the Mediterranean, the Italian perspective. *Renewable Energy*, 50:938–949.

Lin, W., Hong, C., Huang, C., and Ou, T. (2013). Hybrid Control of a Wind Induction Generator Based on Grey–Elman Neural Network. *IEEE Transactions on Control Systems Technology*, 21(6):2367–2373.

Lobo, F., Fernández-Salas, L., I.Moreno, Sanz, J., A.Maldonado, and Medialdea, T. (2005). Large-scale depositional bodies on the shelf around the guadalfeo river, northern margin of the alboran sea, and their relationship with conduits of sediment transport into deeper domains. *Geophysical Research Abstracts*, 7:06291.

López, I., Aragonés, L., Villacampa, Y., and Navarro-González, F. (2018). Gravel beaches nourishment: Modelling the equilibrium beach profile. *Science of The Total Environment*, 619-620:772 – 783.

López, I., Castro, A., and Iglesias, G. (2015a). Hydrodynamic performance of an oscillating water column wave energy converter by means of particle imaging velocimetry. *Energy*, 83:89 – 103.

López, I. and Iglesias, G. (2014). Efficiency of OWC wave energy converters: A virtual laboratory. *Applied Ocean Research*, 44:63 – 70.

López, I., Pereiras, B., Castro, F., and Iglesias, G. (2014). Optimisation of turbine-induced damping for an OWC wave energy converter using a RANS–VOF numerical model. *Applied Energy*, 127:105 – 114.

López, I., Pereiras, B., Castro, F., and Iglesias, G. (2015b). Performance of OWC wave energy converters: Influence of turbine damping and tidal variability. *International Journal of Energy Research*, 39(4):472–483. ER-13-4164.R2.

López, M., Veigas, M., and Iglesias, G. (2015c). On the wave energy resource of Peru. *Energy Conversion and Management*, 90:34 – 40.

López-Ruiz, A., Bergillos, R. J., and Ortega-Sánchez, M. (2016). The importance of wave climate forecasting on the decision-making process for nearshore wave energy exploitation. *Applied Energy*, 182:191 – 203.

López-Ruiz, A., Bergillos, R. J., Raffo-Caballero, J. M., and Ortega-Sánchez, M. (2018). Towards an optimum design of wave energy converter arrays through an integrated approach of life cycle performance and operational capacity. *Applied Energy*, 209:20 – 32.

Losada, M. A., Baquerizo, A., Ortega-Sánchez, M., and Ávila, A. (2011). Coastal evolution, sea level, and assessment of intrinsic uncertainty. *Journal of Coastal Research*, 59:218–228.

Mäki, T., Vuorinen, M., and Mucha, T. (2014). Waveroller one of the leading technologies for wave energy conversion. In *5th International Conference on Ocean Energy*, pages 4–6.

Malmo, O. and Reitan, A. (1986). Development of the kvaerner multiresonant owc. In Evans, D. V. and de Falcão, A. F. O., editors, *Hydrodynamics of Ocean Wave-Energy Utilization*, pages 57–67, Berlin, Heidelberg. Springer Berlin Heidelberg.

Margheritini, L., Vicinanza, D., and Frigaard, P. (2009). SSG wave energy converter: Design, reliability and hydraulic performance of an innovative overtopping device. *Renewable Energy*, 34:1371–1380.

Masselink, G., Russell, P., Blenkinsopp, C., and Turner, I. (2010). Swash zone sediment transport, step dynamics and morphological response on a gravel beach. *Marine Geology*, 274(1):50 – 68.

McCall, R., Masselink, G., Poate, T., Roelvink, J., Almeida, L., Davidson, M., and Russell, P. (2014). Modelling storm hydrodynamics on gravel beaches with XBeach-G. *Coastal Engineering*, 91:231 – 250.

McCormick, M. E. (1974). Analysis of a wave energy conversion buoy. *Journal of Hydronautics*, 8(3):77–82.

Medina-López, E., Bergillos, R., Moñino, A., Clavero, M., and Ortega-Sánchez, M. (2017). Effects of seabed morphology on oscillating water column wave energy converters. *Energy*, 135:659–673.

Millar, D., Smith, H., and Reeve, D. (2007). Modelling analysis of the sensitivity of shoreline change to a wave farm. *Ocean Engineering*, 34:884–901.

Millares, A., Polo, M. J., Moñino, A., Herrero, J., and Losada, M. A. (2014). Bedload dynamics and associated snowmelt influence in mountainous and semiarid alluvial rivers. *Geomorphology*, 206:330–342.

Miller, C. (2004). A brief history of wave and tidal energy experiments in san francisco and santa cruz. *Western Neighborhoods Projects. Western Neighborhoods Project*, 3.

Moñino, A., Medina-López, E., Clavero, M., and Benslimane, S. (2017). Numerical simulation of a simple OWC problem for turbine performance. *International Journal of Marine Energy*, 20:17 – 32.

Moody, G. (1979). The nel oscillating water column: recent developments. In *In: First symposium on wave energy utilization*.

Nørgaard, J. H., Andersen, T. L., and Kofoed, J. P. (2013). Wave Dragon wave energy converters used as coastal protection. In *Coastal Structures 2011: (In 2 Volumes)*, pages 83–94.

Ortega-Sánchez, M., Bergillos, R. J., López-Ruiz, A., and Losada, M. A. (2017). *Morphodynamics of Mediterranean Mixed Sand and Gravel Coasts*. Springer.

Osawa, H., Washio, Y., Ogata, T., Tsuritani, Y., Nagata, Y., et al. (2002). The offshore floating type wave power device "Mighty Whale" open sea tests: Performance of the prototype. In *The Twelfth International Offshore and Polar Engineering Conference*. International Society of Offshore and Polar Engineers.

Ou, T.-C., Lu, K.-H., and Huang, C.-J. (2017). Improvement of Transient Stability in a Hybrid Power Multi-system Using a Designed NIDC (Novel Intelligent Damping Controller). *Energies*, 10(4).

Pagán, J., López, I., Aragonés, L., and Garcia-Barba, J. (2017). The effects of the anthropic actions on the sandy beaches of Guardamar del Segura, Spain. *Science of The Total Environment*, 601-602:1364 – 1377.

Palha, A., Mendes, L., Fortes, C. J., Brito-Melo, A., and Sarmento, A. (2010). The impact of wave energy farms in the shoreline wave climate: Portuguese pilot zone case study using Pelamis energy wave devices. *Renewable Energy*, 35:62–77.

Payo, A., Mukhopadhyay, A., Hazra, S., Ghosh, T., Ghosh, S., Brown, S., Nicholls, R. J., Bricheno, L., Wolf, J., Kay, S., Lázár, A. N., and Haque, A. (2016). Projected changes in area of the Sundarban mangrove forest in Bangladesh due to SLR by 2100. *Climatic Change*, 139(2):279–291.

Pecher, A., Kofoed, J., Le Crom, I., Neumann, F., Azevedo, E. d. B., et al. (2011). Performance assessment of the Pico OWC power plant following the EquiMar Methodology. In *The Twenty-first International Offshore and Polar Engineering Conference*. International Society of Offshore and Polar Engineers.

Pelc, R. and Fujita, R. M. (2002). Renewable energy from the ocean. *Marine Policy*, 26(6):471 – 479.

Pelnard-Considère, R. (1956). Essai de theorie de l'evolution des formes de rivage en plages de sable et de galets. *Les Energies de la Mer: Compte Rendu Des Quatriemes Journees de L'hydraulique, Paris 13, 14 and 15 Juin 1956; Question III, rapport 1, 74-1-10*.

Platts, W. (1979). The development of the wave contouring raft. In *International Conference on Future Energy Concepts*, pages 160–163.

Poate, T., Masselink, G., Davidson, M., McCall, R., Russell, P., and Turner, I. (2013). High frequency in-situ field measurements of morphological response on a fine gravel beach during energetic wave conditions. *Marine Geology*, 342:1 – 13.

Raghunathan, S. (1995). The wells air turbine for wave energy conversion. *Progress in Aerospace Sciences*, 31(4):335–386.

Rodriguez-Delgado, C. (2016). Artificial nourishments on mixed sand and gravel beaches: data analysis and numerical modelling. *University of Granada*, http://hdl.handle.net/10481/45091.

Rodriguez-Delgado, C., Bergillos, R. J., and Iglesias, G. (2019). Dual wave farms and coastline dynamics: The role of inter-device spacing. *Science of The Total Environment*, 646:1241 – 1252.

Rodriguez-Delgado, C., Bergillos, R. J., Ortega-Sánchez, M., and Iglesias, G. (2018a). Protection of gravel-dominated coasts through wave farms: Layout and shoreline evolution. *Science of The Total Environment*, 636:1541 – 1552.

Rodriguez-Delgado, C., Bergillos, R. J., Ortega-Sánchez, M., and Iglesias, G. (2018b). Wave farm effects on the coast: The alongshore position. *Science of The Total Environment*, 640-641:1176 – 1186.

Ross, D. (1995). *Power from the Waves*. Oxford University Press, USA.

Rourke, F. O., Boyle, F., and Reynolds, A. (2009). Renewable energy resources and technologies applicable to Ireland. *Renewable and Sustainable Energy Reviews*, 13(8):1975–1984.

Ruol, P., Zanuttigh, B., Martinelli, L., Kofoed, P., and Frigaard, P. (2011). Near-shore floating wave energy converters: Applications for coastal protection. *Coastal Engineering Proceedings*, 1(32):61.

Rusu, E. (2009). Wave energy assessments in the Black Sea. *Journal of Marine Science and Technology*, 14(3):359–372.

Rusu, E. and Onea, F. (2016). Study on the influence of the distance to shore for a wave energy farm operating in the central part of the Portuguese nearshore. *Energy Conversion and Management*, 114:209–223.

Rusu, E. and Soares, C. G. (2013). Coastal impact induced by a Pelamis wave farm operating in the Portuguese nearshore. *Renewable Energy*, 58:34–49.

Salter, S. H. (1974). Wave power. *Nature*, 249(5459):720–724.

Sánchez-Arcilla, A., García-León, M., Gracia, V., Devoy, R., Stanica, A., and Gault, J. (2016). Managing coastal environments under climate change: Pathways to adaptation. *Science of The Total Environment*, 572:1336 – 1352.

Senechal, N., Coco, G., Castelle, B., and Marieu, V. (2015). Storm impact on the seasonal shoreline dynamics of a meso- to macrotidal open sandy beach (Biscarrosse, France). *Geomorphology*, 228:448 – 461.

Sibley, A., Cox, D., and Titley, H. (2015). Coastal flooding in England and Wales from Atlantic and North Sea storms during the 2013/2014 winter. *Weather*, 70(2):62–70.

Silva, D., Bento, A. R., Martinho, P., and Soares, C. G. (2015). High resolution local wave energy modelling in the Iberian Peninsula. *Energy*, 91:1099–1112.

Smith, H. C., Pearce, C., and Millar, D. L. (2012). Further analysis of change in nearshore wave climate due to an offshore wave farm: An enhanced case study for the wave hub site. *Renewable Energy*, 40(1):51 – 64.

Soomere, T. and Eelsalu, M. (2014). On the wave energy potential along the eastern baltic sea coast. *Renewable Energy*, 71:221 – 233.

Spencer, T., Schuerch, M., Nicholls, R. J., Hinkel, J., Lincke, D., Vafeidis, A. T., Reef, R., McFadden, L., and Brown, S. (2016). Global coastal wetland change under sea-level rise and related stresses: the DIVA Wetland Change Model. *Global and Planetary Change*, 139:15–30.

Stagonas, D., Muller, G., Maravelakis, N., Magagna, D., and Warbrick, D. (2010). Composite seawalls for wave energy conversion: 2D experimental results. In *3rd International Conference on ocean energy*.

Stansby, P., Moreno, E. C., and Stallard, T. (2015). Capture width of the three-float multi-mode multi-resonance broadband wave energy line absorber m4 from laboratory studies with irregular waves of different spectral shape and directional spread. *Journal of Ocean Engineering and Marine Energy*, 1(3):287–298.

Syvitski, J. P. M., Kettner, A. J., Overeem, I., Hutton, E. W. H., Hannon, M. T., Brakenridge, G. R., Day, J., Vörösmarty, C., Saito, Y., Giosan, L., and Nicholls, R. J. (2009). Sinking deltas due to human activities. *Nature Geoscience*, 2(10):681–686.

Taghipour, R., Moan, T., et al. (2008). Efficient frequency-domain analysis of dynamic response for the multi-body wave energy converter in multi-directional wave. In *The Eighteenth International Offshore and Polar Engineering Conference*. International Society of Offshore and Polar Engineers.

Thorpe, T. W. (1992). A review of wave energy. *DTI Report ETSU-R-72*.

Tjugen, K. (1994). Tapchan ocean wave energy project. In *Proc. European Wave Energy Symposium, Edinburgh, Scotland*, pages 265–270.

Torre-Enciso, Y., Marqués, J., and López de Aguileta, L. (2010). Mutriku. lessons learnt. In *3rd International Conference on Ocean Energy*.

Torre-Enciso, Y., Ortubia, I., De Aguileta, L. L., and Marqués, J. (2009). Mutriku wave power plant: from the thinking out to the reality. In *Proceedings of the 8th European wave and tidal energy conference, Uppsala, Sweden*, volume 710, pages 319–329.

USACE (1984). Shore protection manual. *US Army Corps of Engineers, Coastal Engineering Research Center, Vicksburg, MS*, 2.

Valério, D., Beirão, P., and da Costa, J. S. (2007). Optimisation of wave energy extraction with the archimedes wave swing. *Ocean Engineering*, 34(17):2330 – 2344.

van der Westhuysen, A. J., Zijlema, M., and Battjes, J. A. (2007). Nonlinear saturation-based whitecapping dissipation in SWAN for deep and shallow water. *Coastal Engineering*, 54(2):151–170.

Van Rijn, L. C. (2014). A simple general expression for longshore transport of sand, gravel and shingle. *Coastal Engineering*, 90:23 – 39.

Veigas, M. and Iglesias, G. (2014). Potentials of a hybrid offshore farm for the island of Fuerteventura. *Energy Conversion and Management*, 86:300 – 308.

Veigas, M., Ramos, V., and Iglesias, G. (2014). A wave farm for an island: Detailed effects on the nearshore wave climate. *Energy*, 69:801 – 812.

Vicinanza, D., Contestabile, P., and Ferrante, V. (2013a). Wave energy potential in the north-west of Sardinia (Italy). *Renewable Energy*, 50:506–521.

Vicinanza, D. and Frigaard, P. (2008). Wave pressure acting on a seawave slot-cone generator. *Coastal Engineering*, 55(6):553–568.

Vicinanza, D., Margheritini, L., Kofoed, J. P., and Buccino, M. (2012). The SSG wave energy converter: Performance, status and recent developments. *Energies*, 5:193–226.

Vicinanza, D., Nørgaard, J. H., Contestabile, P., and Andersen, T. L. (2013b). Wave loadings acting on overtopping breakwater for energy conversion. *Journal of Coastal Research*, 65(sp2):1669–1674.

Vidal, C., Méndez Fernando, J., Díaz, G., and Legaz, R. (2007). Impact of Santoña WEC installation on the littoral processes. In *Proceedings of the 7th European conference, Porto, Portugal*, pages 11–14.

Viviano, A., Naty, S., Foti, E., Bruce, T., Allsop, W., and Vicinanza, D. (2016). Large-scale experiments on the behaviour of a generalised oscillating water column under random waves. *Renewable Energy*, 99:875 – 887.

Washio, Y., Osawa, H., Nagata, Y., Fujii, F., Furuyama, H., Fujita, T., et al. (2000). The offshore floating type wave power device "Mighty Whale": open sea tests. In *The Tenth International Offshore and Polar Engineering Conference*. International Society of Offshore and Polar Engineers.

Weber, J. (2012). Wec technology readiness and performance matrix–finding the best research technology development trajectory. In *Proceedings of the 4th International Conference on Ocean Energy, Dublin, Ireland*, volume 17.

Weber, J., Mouwen, F., Parish, A., and Robertson, D. (2009). Wavebob — research & development network and tools in the context of systems engineering. In *Proceedings of the Eighth European Wave and Tidal Energy Conference, Uppsala, Sweden*, pages 416–420.

Weinstein, A., Fredrikson, G., Parks, M. J., and Nielsen, K. (2004). Aquabuoy - the offshore wave energy converter numerical modeling and optimization. In *Oceans '04 MTS/IEEE Techno-Ocean '04 (IEEE Cat. No.04CH37600)*, volume 4, pages 1854–1859 Vol.4.

Whittaker, T., Collier, D., Folley, M., Osterried, M., Henry, A., and Crowley, M. (2007). The development of oyster—a shallow water surging wave energy converter. In *Proceedings of the 7th European wave and tidal energy conference*, pages 11–14.

Whittaker, T., Stewart, T., Raghunathan, S., and Curran, R. (1995). Implications of operational experiences of the islay owc for the design of wells' turbines. In *Proceedings of the 2nd European Wave Energy Conference, Lisbon, Portugal, Nov*.

Yemm, R. (1999). The history and status of the pelamis wave energy converter. In *Wave power–Moving towards commercial viability", IMECHE Seminar, London, UK*.

Zanuttigh, B. and Angelelli, E. (2013). Experimental investigation of floating wave energy converters for coastal protection purpose. *Coastal Engineering*, 80:148–159.

Zodiatis, G., Galanis, G., Nikolaidis, A., Kalogeri, C., Hayes, D., Georgiou, G. C., Chu, P. C., and Kallos, G. (2014). Wave energy potential in the Eastern Mediterranean Levantine Basin. An integrated 10-year study. *Renewable Energy*, 69:311–323.